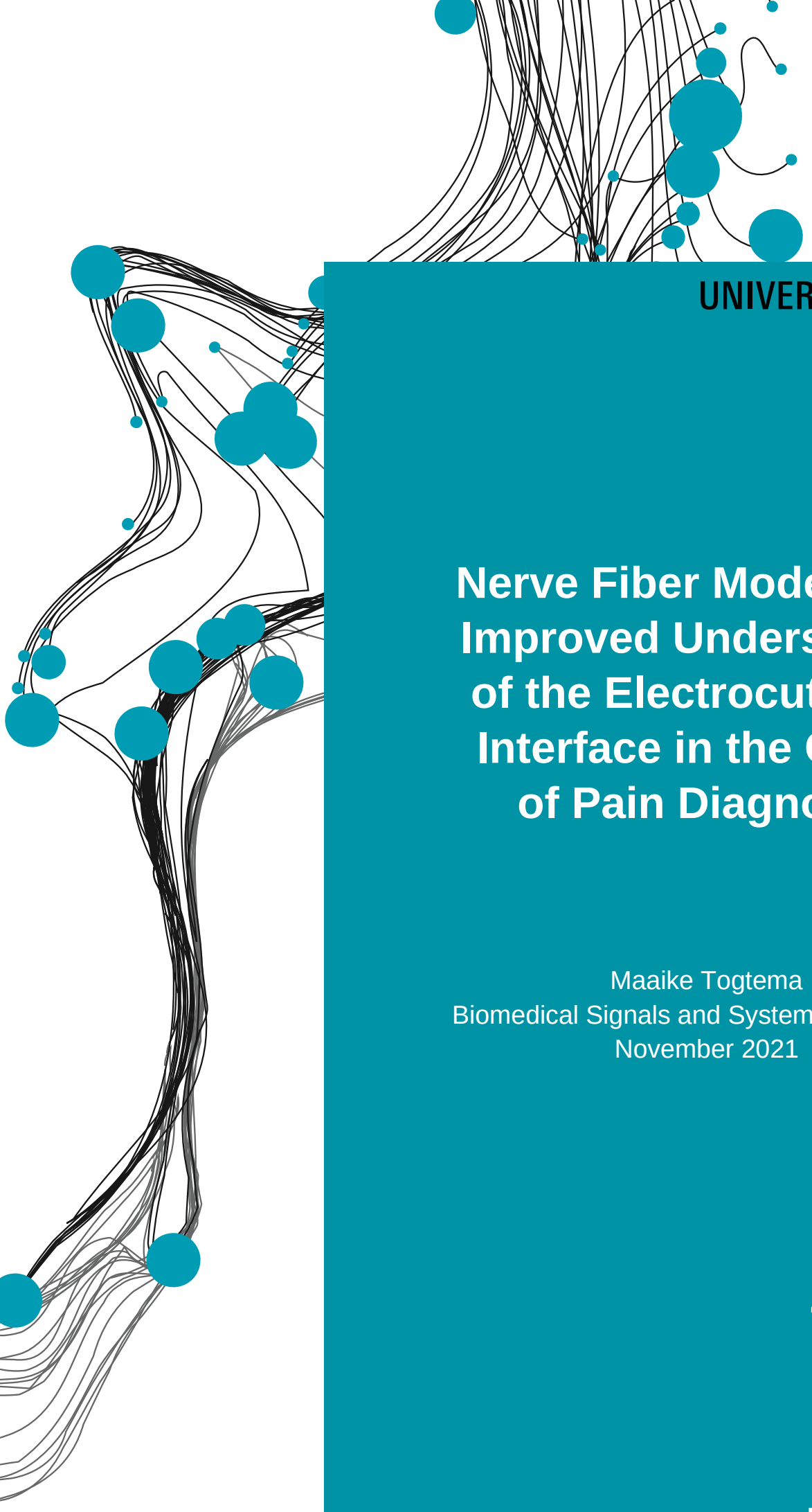

UNIVERSITY OF TWENTE.

Nerve Fiber Modelling for Improved Understanding of the Electrocutaneous Interface in the Context of Pain Diagnostics

Maaike Togtema
Biomedical Signals and Systems, NSP-team
November 2021

Examination commitee:
Dr. ir. J.R. Buitenweg
N. Jansen M.Sc.
Dr. ir. J. Rouwkema

Biomedical Engineering
University of Twente

ABSTRACT

In order to understand chronic pain for possible treatment improvement or early detection, it is of importance to know the underlying structures and neural pathways involved. The nociceptive system regulates pain in the human body and can be (selectively) activated with the use of electrical stimuli given by electrodes attached on the skin surface. To give better insight in the electrocutaneous interface, specifically on nerve fiber level, nerve fiber modelling could be an option. This research aimed at validating a mathematical model of the skin-electrode interface containing touch related Aβ-fibers and nociceptive Aδ-fibers. The mathematical model consists of a 2D volume-conduction model in COMSOL using FEM and a stochastic branching fiber model in MATLAB. The model was validated using the results presented by Morch2011a [1]. The mean threshold ($\pm$ SEM) calculated by the model ranged between 2.0 ± 0.01 to $2.7 \pm 0.01 mA$ for Aβ and 5.5 ± 0.04 to $7.6 \pm 0.03\ mA$ for Aδ for electrode diameter sizes ranging from 0.2 to 20 mm. These results were a factor 7 for Aβ and a factor 12 for Aδ higher compared to the articles findings. Consequently, a reason as to why the data differed had to be found. All the (model) steps described in the article were checked and for parameters that were not described (in detail) the effect on the mean threshold was investigated. This concluded no clear source for the discrepancy in data. In addition, another 2D FE model of a single needle IES electrode was made and simulations were carried out to investigate whether penetration depth of the needle in the skin influenced Aβ and Aδ activation. Preferential activation of Aδ was observed where Aβ thresholds were 1.4 to 1.8 times higher when the needle tip resided in the epidermis, resembling results found in literature. Furthermore, an increase of needle depth in the skin model presented an increase in Aδ threshold. The results of this research taken together leads to a contradiction with respect to the validation of the mathematical model where is concluded that more research is required, including other validation steps.

SAMENVATTING (DUTCH ABSTRACT)

Om chronische pijn te begrijpen voor mogelijke verbetering van behandelingen of eerdere diagnose, is het van belang om de onderliggende structuren en zenuwbanen te herkennen. Het nociceptieve systeem reguleert pijn in het menselijk lichaam en kan (selectief) worden geactiveerd met behulp van elektrische prikkels die worden gegeven door elektrodes die op het huid oppervlak zijn bevestigd. Om beter inzicht te krijgen in de electrocutane interface, specifiek op zenuwvezel niveau, zou het modelleren van zenuwvezels een optie kunnen zijn. Dit onderzoek was gericht op het valideren van een wiskundig model van de huid-elektrode interface met tastgerelateerde Aβ vezels en nociceptische Aδ vezels. Het wiskundig model bestaat uit een FEM 2D-volume geleidings model in COMSOL en een stochastisch vertakkend vezel model in MATLAB. Het model is gevalideerd met behulp van de resultaten gepubliceerd door Morch2011a [1]. De gemiddelde drempelwaarde ($\pm$ SEM) berekend door het model varieerden van 2.0 ± 0.01 tot $2.7 \pm 0.01 mA$ voor Aβ en 5.5 ± 0.04 tot $7.6 \pm 0.03 mA$ voor Aδ voor elektrode diameters van 0.2 tot 20 mm. Deze resultaten waren een factor 7 voor Aβ en een factor 12 voor Aδ hoger in vergelijking met de bevindingen van het artikel van Morch et al. [1]. Een reden waarom de data niet overeenkwam moest worden gevonden. Alle (model)stappen die in het artikel beschreven stonden zijn gecontroleerd en voor parameters die niet (in detail) zijn beschreven is gekeken naar het effect op de gemiddelde vezel drempel. Hieruit werd geconcludeerd dat er geen duidelijke bron is voor de discrepantie in de gegevens. Daarnaast is een ander 2D FE-model van een naald IES-elektrode gemaakt en zijn er simulaties uitgevoerd om te onderzoeken of de penetratiediepte van de naald in de huid de activering van Aβ en Aδ vezels beïnvloed. Preferentiële activering van Aδ werd waargenomen waar Aβ-drempels 1.4 tot 1.8 keer hoger waren wanneer de punt van de naald zich in de epidermis bevond, wat redelijk overeenkomt met resultaten beschreven in de literatuur. Bovendien zorgde een toename van de diepte van de naald in het huidmodel voor een toename van de Aδ-drempel. De resultaten van dit onderzoek leiden tot een tegenstrijdigheid met betrekking tot de validatie van het wiskundige model, waar wordt geconcludeerd dat meer onderzoek nodig is, inclusief andere validatiestappen.

LIST OF ACRONYMS AND SYMBOLS

Acronyms

AP Action Potential

CNS Central Nervous System

FE Finite Element

FEM Finite Element Modelling

IES Intra-epidermal Electrical Stimulation

LEP Laser-Evoked Potentials

ODE Ordinary Differential Equation

PW Pulse Width

SC Stratum Corneum

SD Standard Deviation

SEM Standard Error of the Mean

Symbols and Constants

A_{node} = Surface Area of Nodal Gap $[cm^2]$
C_m = Membrane Capacitance $[S]$
c_m = Membrane Capacitance p. unit area; $30.4e-3\ [S/cm^2]$
d = Diameter Fiber **without** myelin $[\mu m]$
D = Diameter Fiber **with** myelin $[\mu m]$
d_n = Needle Depth [mm]
G_m = Membrane Conductance $[F]$
g_m = Membrane Conductance p. unit area; $2e-6\ [F/cm^2]$
I_m = Membrane Current $[mA]$
I_s = Stimulation Current $[mA]$
l = Nodal Width; $4\ [\mu m]$
L = Internode Length $[mm]$
ϕ = Angle zr-plane
R = Resistance $[\Omega]$
r = Radius $[mm]$

σ = Electrical Conductivity $[S/mm]$
σ_i = Axoplasm Conductivity; $9.909e-4$ $[S/mm]$
θ = Angle xy-plane
U_{crit} = Critical Potential; 50 $[mV]$
U_e = Extracellular Potential $[mV]$
U_m = Membrane Potential $[mV]$
V_n = Cut-off Potential; $\Delta 20$ $[mV]$
V_r = Resting membrane potential; -70 $[mV]$

List of Figures

List of Tables

Contents

1 INTRODUCTION

1.1 Motivation

Chronic pain is a hard problem to solve and remains a physical and mental burden for people that deal with chronic pain on a daily basis [5]. The definition of chronic pain is a pain that persists when it is past the healing phase after an injury [6]. Diabetes mellitus, back pain, or after cancer/chemotherapy treatments are examples where chronic pain can surface [7]. With respect to treatment, only in a limited number of patients the pain is moderately reduced [5]. It is said that certain processes in the central nervous system are disturbed due to damaged neural pathways, causing an increased sensitivity to (non) painful stimuli [8, 9].

The sensation of pain in a human body is regulated by the nociceptive system, consisting of nerve fibers such as Aδ and unmyelinated C-fibers. However, other types of nerves are also present in the skin, such as Aβ fibers associated with touch [2]. To better understand and prevent pain, insight in the pathways and mechanisms associated with the nociceptive system is required. In this research the focus is on the peripheral receptors, therefore Aδ- and C-fibers are of interest. Possibilities to selectively characterize the nociceptive system include laser stimuli [10, 11] and electrical stimuli [12–14]. Electrical stimuli is where this research focuses on.

Electrodes attached on the skin can deliver electrical stimuli and are advantageous due to high temporal resolution and the ability to selectively activate nociceptors. Several types of electrodes exist. Examples are the regular patch electrode [15], pin electrode [14], or Intra-Epidermal Stimulation (IES) electrode [13, 16]. It is essential to choose an electrode type that is capable of selectively activating the nociceptive fibers for proper interpretation of the obtained results. Research suggests that the IES electrode is more suitable for the activation of nociceptive fibers [13, 14, 16]. The IES electrode consists of a small needle that penetrates the outer skin layer (stratum corneum), eliminating the high resistance boundary it needs to overcome. Due to this, the electrode is able to create a concentrated potential field that reaches up to the epidermis, mainly activating the fibers located there (Aδ and C-fibers). Although with higher stimulation currents, other fiber types could be activated as well [13].

At the University of Twente, the BSS-NSP group developed an IES electrode which consists of a silicon top with 5 needles attached [17]. When the electrode is placed on the skin a slight pressure is applied to ensure the needles penetrate the stratum corneum. The electrode is fixed on the skin and held in place by use of tape. It is of importance to know whether elements introduce an uncertainty in the validity of the data after carrying out measurements with this particular electrode. One example is the variation in needle angle. Another is the depth of the needle in the skin. When the IES electrode is attached to the skin a variation of penetration depth of the needle(s) is suspected since the amount of pressure applied is not consistent. Therefore the effect of penetration depth on the activation of Aβ- and Aδ-fibers is investigated.

Therefore nerve fiber modelling could be a suitable option to give insight into what happens on

nerve-fiber level, specifically how the nociceptive system can be best stimulated. Existing types or even new designs of electrodes can be modelled as well, where simulations with a nerve fiber model can explain the activation profile of an electrode. Other parameters can be investigated such as if the penetration depth of a needle electrode has an effect on the activation of nociceptive and other fibers.

McNeal et al. [4] mathematically describes a simple myelinated fiber and has become a widely accepted manner for describing axons and their membrane dynamics. Various studies have been conducted that include nerve fiber modelling in their research [1,15,18–20]. Morch et al. [1] describes a finite element (FE) model of the skin-electrode interface and a stochastic fiber model containing branching Aδ- and Aβ-fibers. Motogi et al. [18] and Poulsen et al. [15, 19] carried out simulations with a model for the IES electrode and investigated the size of the potential field and the range in which nerve fibers are activated. The research that is carried out and described in this report aims at validating an already existing branching nerve fiber model with the use of Morch et al. [1] and using this model further to run simulations with an FE model of an IES electrode.

1.2 Goals

There are two main goals of this research.
1. Create a branching nerve fiber model and a skin-electrode interface with FEM, and validate the model with the use of Morch2011a [1]. After validation, simulations with the model are carried out.
A second goal is set.
2. Investigate the effect the penetration depth of a single needle of the IES electrode used by the BSS-NSP group at the University of Twente has on the activation of Aδ- and Aβ-fibers with the use of nerve fiber modelling.

1.3 Report Organization

The first step is a literature study to obtain information about the central nervous system with focus on the nociceptive part (Aδ- and C-fibers) and fibers associated with touch (Aβ). Methods to activate the (nociceptive) fibers are briefly mentioned with the focus electrical stimuli done by electrodes. Different electrode types that are available are mentioned and which nerve fibers they (selectively) activate, supported by literature. Then nerve fiber models of the electrocutaneous interface are studied and how the various components are translated to mathematical functions. This is described in Chapter 2. The next step is creating a model of the skin-electrode interface and possible additions to an existing stochastic branching nerve fiber model, and validate the mathematical model. The validation is done with the use of the results of the article by Morch et al. [1]. A 2D finite element model of the skin-electrode interface is created in COMSOL and the stochastic fiber model of the Aδ- and Aβ-fibers in MATLAB is already available within the BSS-NSP team of the University of Twente. After validation, a 2D FE model of a single needle IES electrode is made in COMSOL. Chapter 3 describes these steps in detail. The results of the validation and simulations with the models are shown in Chapter 4 and are analysed. Since the results of the simulations were not as expected, extra steps are taken, described in the second part of the Chapter, 4.2. Chapter 5 discusses the results of the validation and reasons as to why the results deviated from expectations, while also discussing the surprising results for the IES electrode simulations. At last Chapter 6 states the conclusion of this research followed up by recommendations for possible future studies.

2 BACKGROUND

This chapter contains the background for this research, including similar research found in literature. To understand (chronic) pain, it is important to know the different types of nerves involved, how these signals originate and how to measure these signals in the human body. Specifically the nociceptive system is of importance. This is described in the first section. The second section contains information about ways to activate the nociceptive system (selectively), with a focus on electrical stimulation. The last section contains mathematical modelling of (passive) nerve fibers, available fiber and skin models and finite element modelling.

2.1 Somatosensory System

The main function of nerve fibers is to transfer signals in the human body. These signals could be to activate a muscle, to transport visual information to the brain, sense touch or to sense pain. In this research the focus is on nerves that facilitate touch and nerves that facilitate pain (which is called the nociceptive system).

2.1.1 Types of Nerves

Sensory afferent nerve fibers transport electrical signals throughout the body, usually over 'long' distances, to deliver sensory information to the central nervous system (CNS) [2, Chapter 9]. To improve propagation time, these fibers are often myelinated. The myelin sheath, made up of proteins and lipids, functions as an insulator, reducing current leaking out of the membrane. A more in depth explanation about electrical signals follows in subsection 2.1.2.
Axons that facilitate pain and touch are located in the skin. Two skin types are distinguished: glabrous and hairy skin. Figure 2.1 portrays the various layers of a glabrous skin type (found in among others the hand palm and fingertips). The outer skin layer is called the stratum corneum. Then follow the epidermis, dermis and subcutaneous layer (or hypodermis). Hairy skin distinguishes itself from glabrous skin because it contains i.a. hair follicles, located in the dermis and epidermis [21, Chapter 5]. In hairy skin the nerve fiber endings are differently distributed, namely denser around the hair follicles, compared to a regular distribution in the glabrous skin [22].

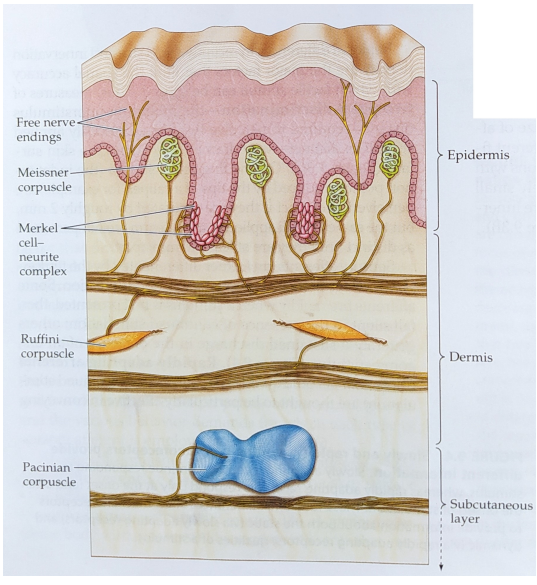

Figure 2.1: Skin layers in the fingertip with a variety of nerves; Adopted from D. Purves [2], Figure 9.5

Fibers that are sensitive to touch are called Aβ afferents, or Aβ fibers. Aβ-fibers are thick myelinated fibers (axon diameter between $6-12\mu m$) that terminate in the dermis and have a relatively fast conduction velocity between $35-75 m/s$ [2, Chapter 9]. Aβ afferents include various receptor types such as Merkel, Meissner, Pacinian and Ruffini cells, each responding to a specific stimuli [2, Chapter 9]. Proprioceptors or muscle activation related fibers are also present in the skin, but are outside the scope of this research.

Nerve fibers that respond to noxious stimuli, and therefore involved in pain sensation, are called nociceptors and consist of less or even unmyelinated fibers, divided into Aδ- and C-fibers. The Aδ-fibers have less myelin compared to Aβ-fibers, and lose their myelin when crossing the dermo-epidermal junction, terminating as free nerve endings in the epidermis. C-fibers are completely unmyelinated, and thus thinner, and also terminate in the epidermis. Due to the lack of myelin, C-fibers conduct signals slower compared to Aδ, with conduction velocities less than $2\ m/s$. Aδ fibers have conduction velocities of $5-30\ m/s$, dividing pain pathways in two categories: slow or fast [2, Chapter 10]. This research focuses on the nociceptive Aδ fibers and touch-related Aβ fibers.

2.1.2 Electrical Signals and Ion Channels

A constant negative potential between -40 to $-90\ mV$ (depending on type of nerve) is maintained across the membrane of a nerve fiber, called the resting membrane potential. Due to active transporters in the membrane (i.a. sodium-potassium pump), a difference in ion concentration outside (extracellular) compared to inside the axon (intracellular) is kept [2, Chapter 2]. The important ions involved are sodium (Na^+), potassium (K^+), calcium (Ca^{2+}) and chloride (Cl^-) [3, Chapter 2]. When an equilibrium of ion transport is reached, the membrane potential is in a stable state (resting membrane potential) and can be calculated by the Goldman-Hodgkin-Katz equation [2, Chapter 2] (which is an extension of the Nernst equation [3, Chapter 2]):

$$E_m = \frac{RT}{F} ln \frac{P_K[K^+]_{out} + P_{Na}[Na^+]_{out} + P_{Cl}[Cl^-]_{in}}{P_K[K^+]_{in} + P_{Na}[Na^+]_{in} + P_{Cl}[Cl^-]_{out}} \tag{2.1}$$

With E_m the potential across the membrane in $[V]$, for an axon typically $-70\ mV$ as resting membrane potential [23]. R, T and F represent the ideal gas constant in $[J/K/mol]$, the temperature in $[K]$ and Faraday's constant in $[C/mol]$, respectively. P_{ion} is the selectivity for the specific ion in $[m/s]$ and $[ion]_{in}$ and $[ion]_{out}$ represent the ion concentration inside and outside the membrane in $[mol/m^3]$.

When a stimulus is applied, a change in membrane potential is observed. Section 2.2 explains the different types of stimuli in more detail. For now a proper stimulus results in voltage-gated ion channels to open and close, generating an action potential, used to transport electrical signals along an axon [2, Chapter 4]. Figure 2.3 describes such a response. The membrane potential becomes more positive, depolarising, and when a certain threshold value is reached, an action potential, or spike, occurs. After the action potential, the membrane becomes more negative over time and an after hyperpolarisation happens. The stimulus size does not influence the amplitude of the action potential, only the frequency [2, Chapter 2].

An action potential is generated along the axon at the nodes of Ranvier, which can be described as a gap in the myelin of an axon, seen in Figure 2.2. Conduction velocity is improved by a great degree since the action potential jumps from node to node [2, Chapter 3].

As mentioned before, an action potential occurs when a certain voltage threshold is reached. However, it is difficult to determine a solid number, whereas it is more a region. Therefore the

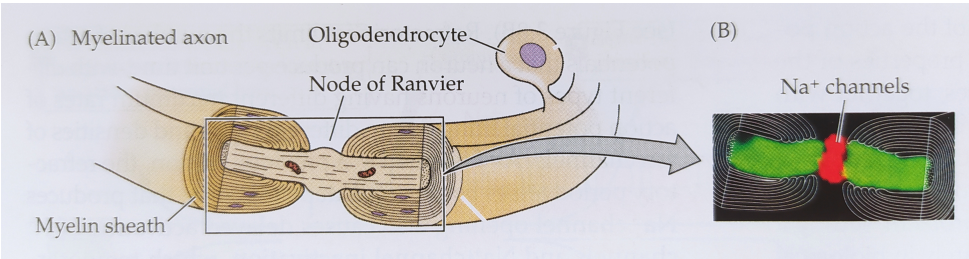

Figure 2.2: A myelinated axon with a node of Ranvier; Adopted from D. Purves [2], Figure 3.11

current threshold (minimal amplitude of injected current of infinite duration needed for an action potential to occur) is used, also called the rheobase [3, Chapter 1]. So whenever threshold is mentioned later on, the minimal stimulation current (usually in [mA]) to elicit an action potential is meant. A strength-duration curve shows the rheobase, since it depicts the relation between the duration of a stimulus and stimulus strength. Usually when the pulse duration increases, the threshold decreases. Another well known parameter is chronaxie, which describes the pulse duration needed to elicit an action potential with twice the rheobase, useful to define neuron excitability.

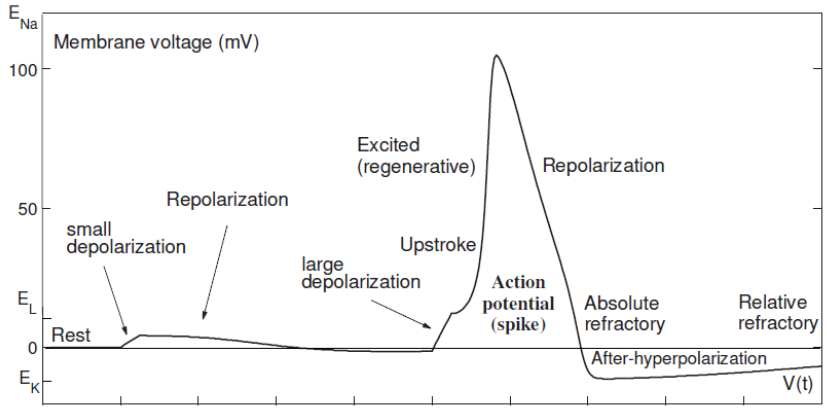

Figure 2.3: Representation of a single action potential. Adopted from E. Izhikevich [3]; Figure 2.14

2.1.3 Gain Control Mechanisms

The information discussed above mainly focuses on the receptors of the somatosensory system in cutaneous areas. However, the somatosensory system, including the nociceptive system, consist of larger pathways, to the spinal cord and leading up all the way to the brain [2, Chapter 10]. This research mainly focuses on the peripheral sensitisation, yet the other mechanism involved are briefly mentioned here. [24].

There are three main levels of neural integration [21, Chapter 13]:
1. Receptor level (sensory receptors, such as Aβ and Aδ fibers)
2. Circuit level (processing in ascending pathways e.g. spinal cord and dorsal horn)
3. Perceptual level (processing in cortical sensory areas in the brain)

Treede et al. [24] describes gain control mechanisms in order to understand the body's nociceptive system. These mechanisms start at receptor level in the periphery, to the spinal cord

where the brainstem also has influence. and ends at higher centers of the brain (at the cortex), all involved in pain processing.

2.2 Activation of Nociceptive System

Nociceptors respond to thermal, chemical and mechanical stimuli. When a stimulus is received as painful it has reached the pain threshold [2, Chapter 10]. This mechanism of 'pain' is set in motion because the stimulus applied can be potentially damaging or harmful for the human body. Which is also the reason why nociceptors do not, or barely adapt to a constant stimulus, protecting the body's structures [21, Chapter 13].
The area of the skin over which a stimulation results in a change in action potentials is called receptive field. The density of fibers is of great influence on the size of receptive field [2, Chapter 9]. Areas such as the hand palm or sole of the foot have a high fiber density, associated with a small receptive field, making it relatively easy to locate the origin of stimulus [2, Chapter 9].

Methods to stimulate the nociceptive system experimentally are: Laser stimuli [11,25], Mechanical stimuli [26] and Electrical stimuli [1, 11, 13, 16, 17, 27, 28, 28, 29].

2.2.1 Stimulation

Various methods to selectively stimulate the nociceptive system have been investigated and are described by literature.

Stimulation through heating of the skin by use of a laser elicits Laser Evoked potentials (LEP) and has been proven to be highly efficient for selectively activating the nociceptive system [11, 16, 25]. The advantage of this method is that it imitates a natural stimulation, unlike electrical stimulation which is discussed later on. However, disadvantages with laser stimulation arise as well. Due to the use of an expensive powerful laser high temperatures are reached locally, meaning stimulation on the same location for longer periods of time is not possible without damaging or burning the skin. A different location is necessary, which calls for variation in structure [11].

Another widely used option is activation of fibers with the use of electrodes. Advantages compared to the use of a laser are the equipment being rather cheap and an easy setup. However, the stimulus applied is artificial, neglecting certain pathways [25].

Despite the unnatural nature of the stimulus, this research focuses on stimulation with the use of electrodes. A wide choice of electrodes is available to investigate and measure nerve signals of which several types are discussed in subsection 2.2.2.

Electrodes consist of a cathode and anode, where the cathode is negative and the anode positive, and apply a stimulation current in the form of a pulse that changes the extracellular potential in the skin. Various types of stimulation pulses are described in literature, each chosen with their desired effects. Used in this research and also by Morch et al. [1] is a single constant current pulse, or rectangular pulse. Rectangular pulses in combination with regular electrode types such as the patch electrode stimulate the larger Aβ-fibers first compared to the smaller Aδ [30]. Therefore to selectively activate the nociceptive system other stimulation protocols have been developed. A slow rising pulse is used by Hugosdottir et al. [14] where a linear, exponential and bounded exponential pulse shape were chosen to investigate the effect on activation of nociceptive fibers.

2.2.2 Electrode Types

The various electrodes mentioned below have their own typical characteristics with respect to design, preferential fiber innervation, (perception) threshold and research application which is called upon below:

- Patch electrode (i.e. Ambu®neuroline 700) [15]
- Pin electrode (or high frequency stimulation electrode) [14, 15, 27]
- Intra-epidermal electrical stimulation (IES) electrode [13, 15–17]
- Planar concentric electrode [11, 15, 29]
- Planar array electrode [15, 28]
- BiModal electrode [31, 32]

The **patch electrode**, or also known as the regular Ag-AgCl electrode, has a gel that connects tissue and electrode. It typically generates a large electrical field in the skin, activating large diameter nerve fiber types such as Aβ-fibers. This leaves the patch electrode unfavorable for pain research, since it is not selective for nociceptive fibers [14]. Moreaux et al. reported non-painful thresholds of $2.9 \pm 0.9\ mA$ (mean $\pm$ standard deviation (SD)) measured on the calf and $1.5 \pm 0.3 mA$ on the posterior part of the hand with a rectangular pulse of 50 μs. Kaube et al. [29] used a conventional normal electrode in their experiments, measuring on the right forehead, and found thresholds between 10 to 15 mA being perceived as slightly painful.
A **pin electrode** consists of small pin needles, positioned in a circular shape with around a larger circle. The needles serve as cathodes while the larger circle functions as a concentric anode. Due to the use of small needles, a more concentrated, smaller potential field is generated, compared to the regular patch electrode [14, 27]. This is beneficial for nerve endings located in superficial skin layers, such as the epidermis, and therefore suited for activating nociceptive fibers. Poulsen et al. [15] measured on the volar forearm and identified a rheobase of $0.107\, mA$ (median) whereas Hugosdottir et al. [14] reported a rheobase of $0.06\ mA$.
The **IES electrode** consists of a small needle that penetrates the upper skin layer, the stratum corneum. Just as the pin electrode, the IES electrode is able to generate a concentrated potential field, therefore able to mainly activate Aδ- and C-fibers [13, 16]. A study by Inui et al. [16] confirmed electrical stimulation by means of a needle electrode where non-painful stimulation thresholds of $0.9 \pm 0.1\, mA$ on the hand and $1.0 \pm 0.2\, mA$ on the upper arm (mean $\pm$ SD) with a stimulus pulse of 0.5 ms were reported. Mouraux et al. [13] used capsain and a nerve fiber block in their experiment to determine selectivity and were able to exclusively activate Aδ fibers. When a stimulation current twice as high was applied, Aβ fibers were activated, losing its selectivity for the nociceptive system [13].
The **planar concentric electrode** by Kaube et al. [29] consist of a small metal cathode located in the center with a concentric anode around. Due to the minimal distance between cathode and anode, a high current density is produced, able to preferentially activate nociceptive fibers [29]. Sensory and pain thresholds of $0.34 \pm 0.19\, mA$ and $0.54 \pm 0.19\, mA$ were reported and increased to $1.34 \pm 0.29\ mA$ after Aδ and C-fibers were blocked by local anaesthesia where light touch was still felt. The electrode was placed on the right forehead.
The **planar array electrode** has interconnected square cathodes with on each side a rectangular anode. Hugosdottir et al. [28] used a planar array electrode with 12 cathodes and skin cooling to investigate if the excitability of fibers changed. They concluded that the perception threshold decreased for slowly increasing pulses of long duration when the skin was cooled [28].
The **bimodal electrode** consists of five needles and four flat electrodes, where the needles activate Aδ-fibers (as mentioned before) and the flat discs activate Aβ-fibers [31], making it suitable for nociceptive and tactile sensation [32]. A sensation threshold of $0.66 \pm 0.37\, mA$ (mean $\pm$ SD) was reported for the needle electrode and $2.82 \pm 1.12\ mA$ for the disc electrode with a square-wave pulse of 0.21 ms [32].

Thus in order to selectively activate the nociceptive system with electrical stimulation, a preferred electrode design is one that generates a concentrated potential field, reaching the superficial skin layers like the epidermis where Aδ- and C-fibers terminate, yet keeping the stimulation current low enough to prevent activation of Aβ-fibers located in the dermis.

2.3 Mathematical models

Accepted methods to mathematically describe a nerve fiber with its membrane dynamics and how to model the cutaneous interface are discussed in this section.

2.3.1 Cable Theory

A (myelinated) nerve fiber can be described by an electrical network, seen in Figure 2.4, where Figure 2.4b illustrates a more detailed representation, including the various voltage-gated ion channels specific to sodium (Na^+), calcium (Ca^{2+}), potassium (K^+) and chloride (Cl^-).

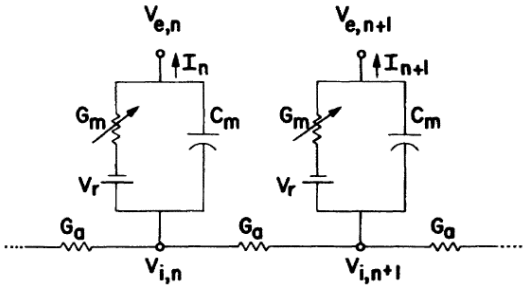

(a) Adopted from McNeal et al. [4], Figure 1

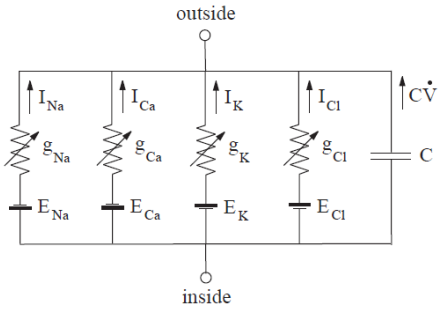

(b) Adopted from E. Izhikevich [3], Figure 2.3

Figure 2.4: Representation of the membrane of a nerve fiber as an electrical network

McNeal et al. [4] describes a passive nerve fiber model that is widely accepted. In between the nodes of Ranvier (depicted by $V_{i,n}$) the internodal conductance (G_a) is calculated with:

$$G_a = \frac{\pi d^2}{4\rho_i L} \tag{2.2}$$

The membrane capacitance (C_m) is given by:

$$C_m = c_m \pi d l \tag{2.3}$$

And membrane conductance (G_m):

$$G_m = g_m \pi d l \tag{2.4}$$

With d ($[cm]$) the axon diameter (without myelin), ρ_i ($110\ \Omega \cdot cm$) the axoplasm resistivity, L ($[cm]$) the internode length, l the nodal gap and c_m ($2\ \mu F/cm^2$) and g_m ($30.4\ mmho/cm^2$) the membrane capacitance and conductance per unit area, respectively. V_r ($-70\ mV$) is modelled as a battery, representing the resting membrane potential. The internodal distance and axon diameter are proportional to fiber diameter D, given by $L/D = 100$ and $d/D = 0.7$ [4]. Where fiber diameter describes the axon diameter without myelin. The nodal gap is a constant ($2.5\ \mu m$ for all diameters), where its surface area is calculated with:

$$A_{node} = \pi d l \tag{2.5}$$

2.3.2 Membrane Dynamics

The membrane dyncamis presentend by Mcneal et al. [4] allow to calculate the membrane potential V_n ($[mV]$) at the nodes of Ranvier:

$$\frac{dV_n}{dt} = \frac{1}{C_m}[G_a(V_{n-1} - 2V_n + V_{n+1} + V_{e,n-1} - 2V_{e,n} + V_{e,n+1}) - G_m V_n] \tag{2.6}$$

Where $V_n = V_{i,n} - V_{e,n} - V_r$, with V_i the intra-cellular potential, V_e the extracellular potential and V_r the resting membrane potential. The initial conditions of $V_n(0) = 0$ for all n, where n is the node number. The external membrane potential (V_e) is modelled as a current point source with the assumption that the electrical potential outside the fiber is determined only by the stimulus current and not influenced by tissue structures around it:

$$V_e = \frac{I}{4\pi r} \tag{2.7}$$

McNeal et al. [4] assumes that the myelin sheath act as a perfect insulator, meaning there is no loss of electrical charge. In a real situation there is however leakage of current. A representation of the simple mylinated nerve fiber as described by McNeal et al. [4] is depicted in Figure 2.5 where the point source representing the cathode is located above node 0 with a distance of 1 mm. Nodes 1, -1 are an even distance apart from node 0 located on the left and the right side. The same goes for nodes 2, -2, 3, -3 and so on. A fiber diameter of $20\ \mu m$ was used with an internode length of $2\ mm$.

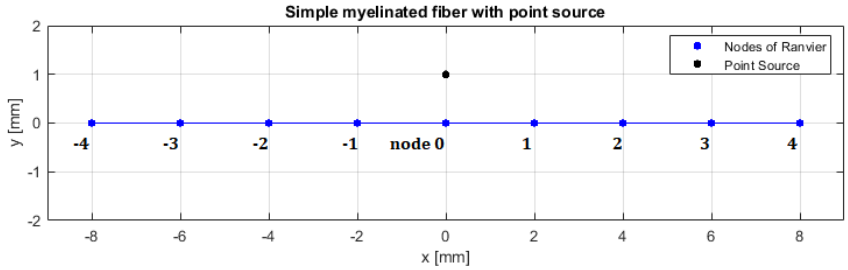

Figure 2.5: Representation of the morphology of the simple myelinated fiber described by McNeal et al. [4] with a fiber diameter of $D = 20\ \mu m$ and a current point source with $I_s = -0.1\ mA$

Besides the use of a current point source, the external membrane potential can also be modelled by the use of finite element modelling, discussed in the next subsection.

2.3.3 Finite Element Modelling of the Electrocutaneous Interface

The extracellular potential an electrode creates in the various skin layers can be modelled by the use of finite element modelling where the skin-electrode interface is comprised of a number of elements. Inside these elements the extracellular potential is calculated with a predetermined shape function [33]. A higher order shape function equals a greater computation time due to the increase of complexity of the equations for each element. Several studies have used FEM in their research where programs such as COMSOL are a common choice.

Morch et al. [1] describes a 2D model of the glabrous skin that is axial symmetric and represents the volar forearm. The various skin layers (stratum corneum, epidermis, dermis and hypodermis) are portrayed as rectangles with the densest mesh at the cathode boundaries since it is expected that the inward current generated by the stainless steel cathode is highest here. Their model consists of 30,000 elements, because beyond this amount the electrical potential

showed no change. Poulsen et al. [15] adopted the model described by Morch et al. [1] and developed it further to compare various electrode designs and their effect on fiber activation. 2D or 3D FE models, depending on electrode configuration, were created and validated. The intra-epidermal, pin, planar concentric, planar array and patch electrode were modelled. Tigerholm et al. [20] used the volume-conduction model described by Morch et al. [1] as well and modified it to their own research. Besides a regular patch electrode, a pin electrode with 15 pins was modelled. Their FE model with the pin electrode created a larger potential field in the stratum corneum and epidermis compared to their FE model of the patch electrode. An FE model of the sole of the foot is presented by Frahm et al. [12], their model consisting of 7 layers: bone marrow, cortical bone, muscle, fate, dermis, epidermis and stratum corneum, respectively.

Besides the skin-electrode interface represented by the volume-conduction model, a mathematical model consist of a second part where nerve fibers are modelled. McNeal et al. [4] was already mentioned above, however other research that contains models of nerve fibers is mentioned in the next subsection.

2.3.4 A-Beta and A-Delta Fiber Models

Model parameters to describe nerve fiber properties are required, likewise for skin layer thickness or values to represent fiber and skin conductivity. In literature several studies report fiber models used in their research and argue the choice in morphology (axon diameter (with and without myelin), internode length, nodal length, fiber density and fiber location). Tigerholm et al. [20] modelled a single Aβ with a diameter of $9\ \mu m$ and a single Aδ fiber with a diameter of $3.5 \mu m$ to represent an entire fiber population. This model was adopted by Poulsen et al. [15, 19] and used it in their research. Frahm et al. [12] models a population of 3000 Aβ and 300 Aδ fibers. Likewise as Morch et al. [1] who simulated a population of 2300 Aβ and 1000 Aδ fibers on a 10 by 10 skin area. Tanaka et al. [34] even modelled Aδ fibers where fiber diameter inside a population was varied. These studies take the stochastic nature of nerve fibers into account.

The model properties mentioned above are based on research where nerve fiber biopsies are studied. Nolano et al. [35] studied glabrous skin biopsies of the finger tip to determine nerve fiber density, fiber diameter and internode length of Aβ-fibers. Whereas Provitera et al. [22] studied nerve fibers in glabrous and hairy skin to determine internodal length, nodal length and fiber diameter of myelinated fibers.

Other fiber properties widely used in literature include membrane capacitance and conductance and resting membrane potential. Hodgkin and Huxley [36] determined these parameters with the use of a giant squid axon [36], whereas Frankenhaeuser et al. [23] extracted these parameters (membrane capacitance and conductance, and resting membrane potential) from a toad.

2.3.5 Active Nerve Fiber Model

Additionally, voltage-gated ion channels can be modelled, describing an active nerve fiber. Wesselink et al. [37] describes and models an active nerve fiber. Two types of gates are identified: active (open channel) and inactive (closed channel), where gating variables describe the probability in which state the channel is. The Hodgkin-Huxley model is a widely accepted model of a giant squid axon and uses persistent K^+, transient Na^+ and a leak current [36]. The Frankenhaeuser-Huxley equations describe the membrane dynamics of a myelinated fiber of a toad [23].

2.4 Implications

Selective activation of the nociceptive system is necessary in order to investigate (chronic) pain. Research shows that preferential activation is achieved with electrodes that create a concentrated potential field, only reaching the superficial skin layers up to the epidermis (where Aδ and C-fibers terminate), provided that low stimulation currents are used. Mathematical modelling of the cutaneous interface can therefore be useful to investigate various electrode types and the effect on the activation of the nociceptive system.
A mathematical model consist of two parts:
1. A model of the skin-electrode interface where finite element modelling proves a useful tool because various electrode types can be created and skin properties can be modelled. However, assumptions are made, simplifying the model, where for example skin layers are portrayed as rectangles or cylinders.
2. A nerve fiber model, where membrane dynamics are described by equations based on McNeal et al. [4] to describe a passive fiber, or if an active fiber model is needed, Wesslink et al. [37] provides research. Studies where a single fiber is modelled exist, whereas a population of fibers captures the random morphology of nerve fibers.

This research aims at the validation of a mathematical model that describes the electrocutaneous interface using the results presented by Morch et al. [1] of a passive fiber model, modelling touch related Aβ and nociceptive Aδ fibers. This mathematical model can then be seen as a base and be used for further research. Other electrode types can be investigated, which is the second aim, where an FE model of the IES electrode is designed and investigated whether the needle depth in the skin influences Aβ and Aδ threshold.

3 METHODS

The chapter is divided into 4 parts. The first describes the mathematical model and its characteristics. This consist of the volume-conduction model representing the skin-electrode interface and the stochastic fiber model where branching nerve fibers are created. All model properties are given. The second part is the validation of the mathematical model and describes the different parameters that are chosen. The article by Morch et al. [1] is used as a means of validation. The third part describes the simulations that are carried out with the model. The last and fourth part is the needle electrode (IES), where the FE model to validate the penetration depth, adjustments to the stochastic fiber model, and the simulations that are carried out are discussed.

3.1 Volume-conduction Model

3.1.1 Skin Properties

A finite element model that is 2D axisymmetric is created in COMSOL Multiphysics 5.4 to represent the various skin layers. Four layers are modelled as separate rectangles on top of each other (and are expanded to cylinders in the 3D model). The layers represent the stratum corneum, epidermis, dermis and hypodermis, respectively. Each have their properties, such as thickness, electrical conductivity and mesh size, described in Table 3.1. Note that the electrical conductivity in the epidermis and dermis depend on direction, written as {x,y,z}. The thickness, radius and electrical conductivity are adopted from Morch et al. [1,38–46]. The mesh consists of free triangular elements and is created for each skin layer with the maximum and minimum element sizes stated in Table 3.1. These values are chosen to ensure a fine enough mesh for the calculation of the extracellular potential at the location of the nodes of the nerve fibers. A quadratic shape function is set to calculate the potential inside a single mesh element. Table 3.1 shows a section of the 2D COMSOL model where the mesh is densest in the stratum corneum and epidermis layer. The model with a cathode of 6 mm diameter contains $4.24923 \cdot 10^5$ elements.

Table 3.1: Electrical properties, size measurements and mesh sizes of the various skin layers in the FE model

Skin Layers	Thickness [mm]	z-coordinate	Radius [mm]	Electrical Conductivity [S/m]	Mesh properties [mm]	
					Maximum Element size	Minimum Element size
Stratum Corneum	0.029	-0.029	50	2.0e-5	0.04	1e-4
Epidermis	0.06	-0.089	50	{0.95, 0.95, 0,15}	0.01	1e-4
Dermis	1.3	-1.389	50	{2.57, 2.57, 1.62}	0.04	1e-4
Hypodermis	5	-6.389	50	0.02	0.1	1e-4

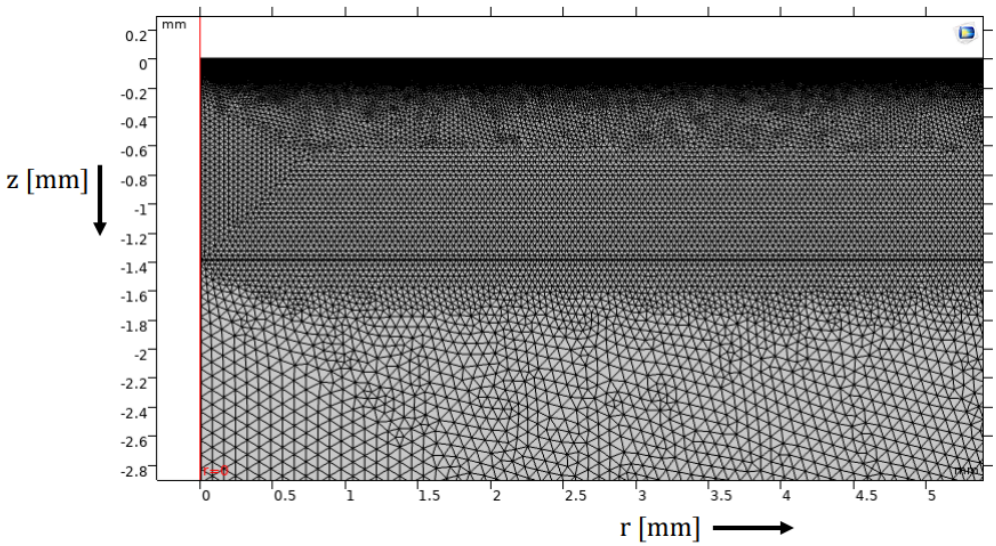

Figure 3.1: Visualization of the mesh of the COMSOL model, presenting the stratum corneum, epidermis and dermis layers, respectively

3.1.2 Electrode Properties

The electrode is modelled as a line segment located on top of the stratum corneum to represent a cathode with an inward current of $-1\,mA$. The lower boundary of the hypodermis is set as a ground, while the other outer boundaries are electrically insulated. Various electrode sizes are chosen, stated in Table 3.2. The extracellular potential is calculated in COMSOL by means of a stationary study, solving the following equation:

$$\nabla(-\sigma\nabla V_{FE} + J_e) = 0 \tag{3.1}$$

With σ the electrical conductivity in $[S/m]$, V_{FE} the calculated electrical potential by the finite element model in $[V]$ and J_e the externally generated current density in $[A/m]$. It takes 32 seconds to solve the COMSOL model.

Table 3.2: Cathode diameters in [mm]

Electrode Diameter [mm]
0.2
0.9
1.5
2
4
6
8
10
12
16
20

3.2 Stochastic Fiber Model

The stochastic model that creates the Aβ- and Aδ-fibers is made in MATLAB 2018b. The fiber's origin point (first node of Ranvier) is chosen randomly (uniformly distributed) in a skin area of 10 by 10 mm, which represent the x- and y-coordinates. The z-coordinate of the first node of Ranvier is for all fibers equal and is the lower boundary of the hypodermis, located at $-6.389\,mm$, also seen in Figure 3.2. From here on the fibers are built up in a straight line with an angle. The angle is chosen randomly from an interval, $[0, \pi/10]$ for the zr-plane (ϕ), and $[0, 2\pi]$ for the xy-plane (θ) [1]. When the fibers enter the dermis layer, there is a possibility of branching. This is set to a probability of 10% at each node [22, 35, 47]. When branching occurs, it always results in two branches being created with an angle chosen randomly the same manner the angle at the origin point of the fiber is determined. Each of the fiber types have different properties with respect to branching, fiber diameter and internode distance, and are discussed below.

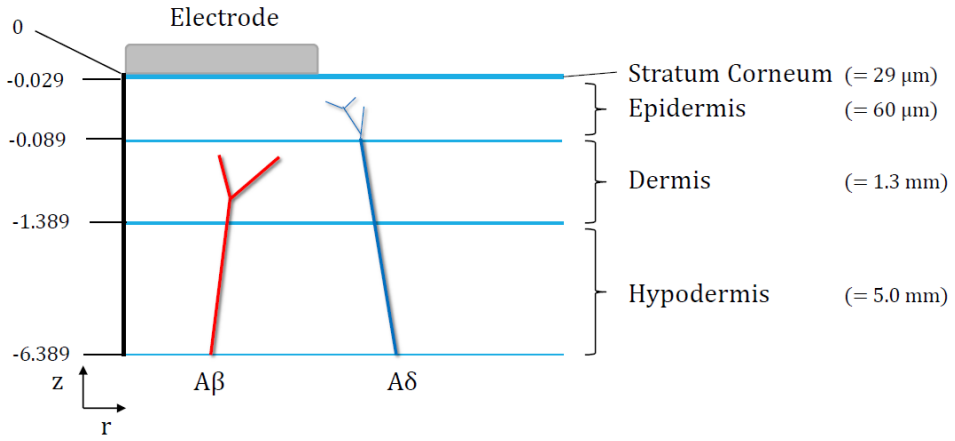

Figure 3.2: Modelled skin layers with their z-coordinate in [mm] on the left and their thickness on the right. Aβ (red) terminates in the dermis and Aδ (blue) terminates in the epidermis, losing its myelin when crossing the dermo-epidermal junction

3.2.1 A-Beta Properties

The properties for Aβ fibers are seen in Table 3.3. The diameter of an Aβ fiber is set to $9\,\mu m$ [48] (with myelin). Without myelin the fiber is $6.3\,\mu m$, with the axon ratio of 0.7 adopted from McNeal et al. [4]. The distance between the nodes is 900 μm and calculated with the ratio of internodal space to fiber diameter: $L/D = 100$ [4]. The nodal width is $4\mu m$ [22]. As stated before, when the Aβ fiber enters the dermis skin layer, there is a possibility of branching at each node of Ranvier, which is 10% [22, 35]. If this occurs, the diameter of the Aβ fibers is reduced with a factor 0.98 [22, 35]. The internode distance also reduces, since these depend on each other. The Aβ fiber terminates in the dermis as well. The termination point is chosen at random between all possible termination points to keep the internode distance equal.

Table 3.3: An overview of Aβ fiber properties

Aβ fiber Properties	Values
Diameter Aβ (D)	9 [µm]
Diameter Aβ without myelin (d)	0.7*D = 6.3 [µm]
Internode Distance Aβ (L)	100*D = 900 [µm]
Nodal Width (l)	4 [µm]
Shrink factor after branch	0.98

3.2.2 A-Delta Properties

An overview of the properties for Aδ fibers is seen in Table 3.4. The diameter of Aδ fibers is smaller and set to $4\,\mu m$ [49]. The diameter of the fiber without myelin is $2.8\,\mu m$ [4]. The distance between the nodes is $400\,\mu m$ [4] and the nodal width is also $4\,\mu m$ [22]. The Aδ fibers are able to branch [47] after entering the dermis with a probability of 10% at each node of Ranvier, and the diameter is reduced with a factor 0.95 if this occurs [1]. When the Aδ fibers cross the dermo-epidermal junction they lose their myelin. This is modelled by reducing the diameter to $1\,\mu m$ and the internode distance to $4\,\mu m$ [49]. The Aδ fiber terminates in the epidermis, chosen randomly between all possible termination points to keep the internode distance equal.

Table 3.4: An overview of Aδ fiber properties

Aδ fiber Properties	Values
Diameter Aδ (D)	4 [µm]
Diameter Aδ without myelin (d)	0.7*D = 2.8 [µm]
Diameter Aδ AFTER entering epidermis	1 [µm]
Internode Distance Aδ (L)	100*D = 400 [µm]
Internode Distance Aδ AFTER entering epidermis	4 [µm]
Nodal Width (l)	4 [µm]
Shrink factor after branch	0.95

Aδ-fibers cross the dermo-epidermal junction and lose their myelin in the process as mentioned above. Several options on how to model it are explored to investigate the effect of varying internode length and the placement of a node on or above the dermo-epidermal junction of the FE model and how this translates to the threshold of the fiber. The diameter (D_{cross}) and internode length (L_{cross}) of the cross-over part are varied, depicted by the red line in Figure 3.3. The 5 options given in Figure 3.3 are investigated by studying the effect on threshold values with the use of simple Aδ fibers (no angle, no branching). With respect to crossing the dermo-epidermal junction, options C and D place a node directly on the border of the dermis and epidermis. Options A, B and E first cross it, and place a node 5% (options A and B) or 1% (option E) in the epidermis layer. As for fiber diameter, option A and C have a diameter that is reduced by 5%. The other options have a fiber diameter that remains equal. After entering the epidermis, the diameter and internode length become the same for all options, $D = 1\ \mu m$ and $L = 4\ \mu m$ respectively.

Option A	Option B	Option C	Option D	Option E
$D_{cross} = 0.95 * D_{dermis}$	$D_{cross} = D_{dermis}$	$D_{cross} = 0.95 * D_{dermis}$	$D_{cross} = D_{dermis}$	$D_{cross} = D_{dermis}$
$L_{cross} = 1.05 * z_{diff}$	$L_{cross} = 1.05 * z_{diff}$	$L_{cross} = z_{diff}$	$L_{cross} = z_{diff}$	$L_{cross} = 1.01 * z_{diff}$

$With\ z_{diff} = z_{epidermis} - z_{last\ node\ dermis}$

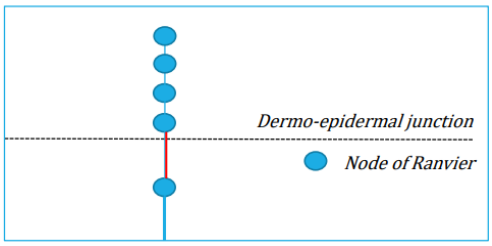

Figure 3.3: Table with various options to cross the dermo-epidermal junction for Aδ fibers that are explored where the red part of the Aδ-fiber is varied

3.2.3 Membrane Properties

The nerve fiber is built up in segments. Each segment has its own properties such as difference in diameter (after branching or crossing the dermo-epidermal junction), internal response matrix that consist of the internal resistance, and nodal surface area. An Aβ fiber that does not branch consist of only 1 segment, yet an Aδ fiber that does not branch consists of 3 segments: 1) segment in the hypodermis and dermis, 2) transition from dermis to epidermis, and 3) segment in the epidermis. This makes the Aδ fiber more complicated to model. It is crucial that these segments are combined correctly.

Table 3.5 contains membrane properties such as the axoplasm conductivity (σ_i), membrane capacitance per unit area (c_m) and the membrane conductance per unit area (g_m), adopted from McNeal et al. [4], as well as the equations to calculate membrane conductance (G_m) and capacitance (C_m). The internal resistance is calculated with equation 3.2 and is derived from equation 2.2 where $G_a = \frac{1}{R_a}$.

$$R_a = \frac{L}{0.25\sigma_i \pi d^2} \tag{3.2}$$

Eventually the membrane potential at the nodes is calculated with equation 2.6, where the elements of the fiber between the nodes are non-conducting. The ordinary differential equation is solved by the MATLAB function *ode23s*, since this particular ODE solver runs most efficient with respect to computation time [50]. The external potential U_e is extracted from the finite element model in COMSOL. Since the model is 2D axisymmetric, it has r,z-coordinates, whereas the fiber model in MATLAB has x,y,z-coordinates. The coordinates at the nodes of a fiber are therefore transformed from 3D ($n(x, y, z)$) to 2D ($n(r, z)$) as follows:

$$r = \sqrt{x^2 + y^2} \tag{3.3}$$

A linear relation between the stimulation current I_s and the extracellular potential U_e is assumed. The resting potential V_r of the membrane is set to $-70\,mV$. Since it is a passive fiber model, an action potential occurs when the membrane potential at at least one of the nodes of the nerve fiber exceeds a difference of $20\,mV$, leading to a critical potential of $U_{crit} = -50\,mV$ [4].

Table 3.5: An overview of membrane properties and stimulus pulse width

Other Model Parameters and Constants	Values
Skin Area	10 x 10 = 100 [mm^2]
Angle range (zr-plane; xy-plane)	{0, π/10}; {0, 2π}
Axoplasm conductivity (σ_i)	9.909e-4 [S/mm]
Membrane capacitance/unit area (c_m)	2e-6 [F/cm^2]
Membrane conductance/unit area (g_m)	30.4e-3 [S/cm^2]
Branch probability	10%
Resting Potential (V_r)	-70 [mV]
Cut-off Potential (V_n)	Δ20 [mV]
Pulse Width	1 [ms]

3.2.4 Stimulus

The input stimulus is a cathodic stimulation, done with a single constant current pulse with a pulse width (PW) of 1 ms.

3.3 Validation of Mathematical Model

The model is validated to determine its correctness and if can be used for further simulations. Since the model is based on Morch et al. [1], the article's results are used as a means of validation. The mathematical model consists of two separate parts. The FE model of the electrode and skin in COMSOL, where the calculation of the extracellular potential takes place, discussed in 3.1. And the stochastic fiber model in MATLAB for the creation Aδ- and Aβ-fibers, discussed in 3.2.

3.3.1 Current Density

The magnitude of the current density (A/m^2) created by the FE model is extracted from COMSOL. In vertical direction below the center of the cathode (at $r = 0\ mm$) and in horizontal direction at the dermo-epidermal junction (at $z = 89\ \mu m$) for various electrode sizes (Table 3.2).

3.3.2 Activation Function

The second order spatial derivative of the potential (V/mm^2) is calculated in the vertical direction, again at the dermo-epidermal junction (at $z = -89\ \mu m$), using the activation function for unmyelinated fibers [51], given by equation 3.4:

$$S = \frac{d^2U_e}{dx^2} = \frac{(U_{e,n-1} - 2U_{e,n} + U_{e,n+1})}{\Delta x^2} \tag{3.4}$$

3.3.3 Impedance

The electrode-skin impedance is determined with equation 3.5 and calculated for a stratum corneum (SC) thickness of $29\ \mu m$, $0.1\ mm$, $0.3\ mm$ and $1\ mm$ for various electrode sizes.

$$R = \frac{U_{e,s}}{I_s} \tag{3.5}$$

With R the resistance in Ω, $U_{e,s}$ the potential at the electrode-skin boundary in V, extracted from COMSOL, and I_s the stimulation current, equal to $-1\ mA$.

3.3.4 Convergence Studies

The dimensions (hypodermis thickness and radial extent) and mesh size of the FE model are investigated by means of convergence studies to determine whether the chosen values are justified. For each of these the electrical potential U_e is used as the investigative parameter.

For mesh size, COMSOL settings for fine, extra fine and extremely fine mesh are used, as well as the mesh parameters given by Poulsen et al. [15] for the planar concentric electrode, and the mesh parameters given in Table 3.1. An overview of the exact parameters can be found in Figure A.1. For radial extent, various radii of the model (50, 60, 75, 100 and 110 mm) are explored. The external potential directly underneath the center of the electrode (at $r = 0\ mm$) and at the edge of the skin area (at $r = \sqrt{5^2 + 5^2} \approx 7.1\ mm$) in vertical direction is calculated for mesh size and radial extent for a stimulation current of $I_s = -1\ mA$.
For varying hypodermis thickness (5, 10, 20, 30 and 50 mm) the difference in external potential (dU_e) underneath the center of the electrode (at $r = 0\ mm$) and at the edge of the skin area (at $r \approx 7.1\ mm$) are determined. The area of interest is at the dermo-epidermal junction at $z = -89\ \mu m$. The external potential is calculated at the nodes of a simple Aδ fiber.

3.4 Simulations & Data Analysis

Simulations are run for populations of 10, 20, 50, 100 and 200 Aβ- and Aδ-fibers for electrode sizes depicted in Table 3.2. This is in total carried out a number of 5 times to investigate the variation between population of fibers and their size. Another larger simulation with 2300 Aβ- and 1000 Aδ-fibers is done in order to replicate the simulations performed by Morch et al. [1].

The results of the simulations are shown as the mean threshold with standard error of the mean (SEM) for different electrode sizes. For the larger simulation of 2300 Aβ- and 1000 Aδ-fibers the density of nerve-endings and mean termination depth with SEM are determined and a certain percentage of the lowest threshold of fibers is taken and shown as mean threshold with SEM. Percentages of 0.1%, 0.3%, 1%, 3%, 10% and 30% of the lowest threshold of Aβ and Aδ are chosen.

Boxplots of the threshold values of the various fiber populations for different electrode sizes are shown to give insight in the spread of the data and variation between populations.

3.5 Validation Penetration Depth

The model specifications for the IES electrode are mentioned first, followed by the simulations that are carried out and the data analysis afterwards.

3.5.1 Volume-conduction model

A 2D axisymmetric model of the skin and electrode is designed in COMSOL Multiphysics 5.4. The properties of the skin layers are stated in Table 3.1, as well as the mesh size that is used. The electrode consists of a single needle with the dimensions of the 5-needle IES electrode created by the BSS-NSP group at the University of Twente [17].

Figure 3.4 shows the geometry of the needle with a radius (r) of 0.025 mm and a length (l) of 0.2 mm. The needle tip angle is 2α and calculated as follows:

$$\alpha = tan^{-1}(\frac{r}{l}) \tag{3.6}$$

Since the model is in 2D and axisymmetric, the electrode is modelled as a right-angled triangle, with the horizontal axis r and vertical axis z. The right angle denoted by point 3 in Figure 3.4 is located in the center and has coordinates $(0, 0)$. Point 1 is the needle tip and has coordinates $(0, -d_n)$, with d depicting penetration depth of the needle in the skin. And last, point 2, the needle edge that connects with the skin and given by $(d_n \cdot tan(\alpha), 0)$. The line connecting point 1 and 2 (hypotenuse side) is simulated as a cathode, using a terminal in COMSOL. Its length depends on the penetration depth of the needle as it is the side of the needle that connects with the skin.

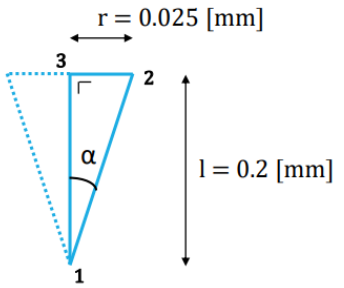

Figure 3.4: Needle geometry of the IES electrode, with 2α the needle tip angle

Figure 3.5 gives a representation how the 'needle' is modelled, where the blue line depicts the cathode. The mesh is densest in the stratum corneum and epidermis layer. The model with maximum penetration depth of the needle contains 425632 elements. The extracellular potential is calculated with the COMSOL model using equation 3.1. It takes 31 seconds to solve the model.

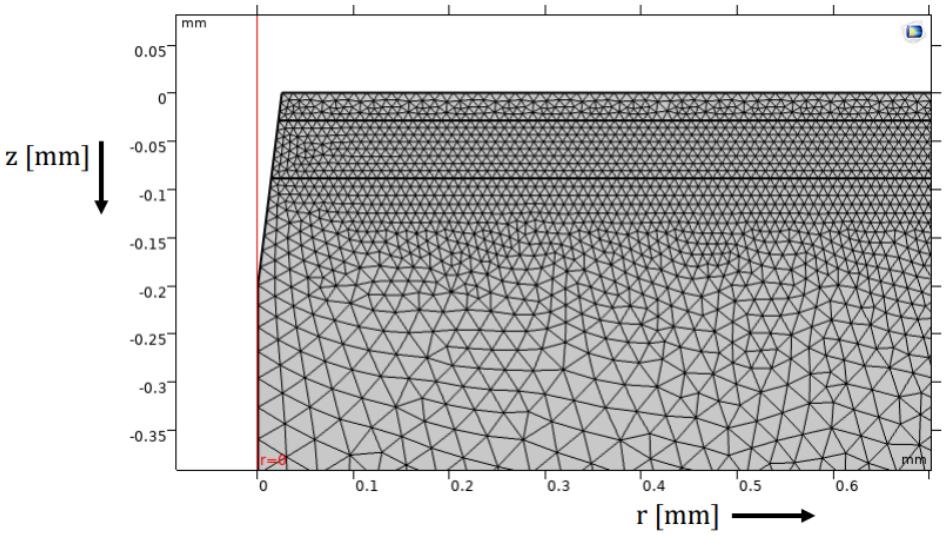

Figure 3.5: Visualization of the mesh of the IES COMSOL model; Including stratum corneum, epidermis and dermis skin layer. The needle is modelled as a cathode (blue line) and has maximum penetration depth ($d_{n,max} = 0.2\ mm$)

Current Density

The magnitude of the current density (A/m^2) created by the FE model is extracted from COMSOL. In vertical direction below the center of the cathode (at $r = 0\ mm$) and in horizontal direction at the dermo-epidermal junction (at $z = -89\ \mu m$).

Electrical Potential

The electrical potential (in V) in a straight line underneath the needle tip of the various FE models is extracted from COMSOL as well.

3.5.2 Stochastic Fiber Model

The stochastic fiber model in MATLAB, discussed in Subsection 3.2, is used and expanded. The needle penetrates the stratum corneum (and epidermis and dermis, depending on needle depth) and since the Aδ-fibers terminate in the epidermis, there is a chance the fibers coincide with the needle. Therefore it is checked whether the next node of the fiber coincides with the needle or not. When this occurs the last node of the fiber outside the needle boundaries becomes the fiber's termination point to prevent needle interference. Figure 3.6 gives a representation of the fibers within the FE model. No needle interference is noticed.

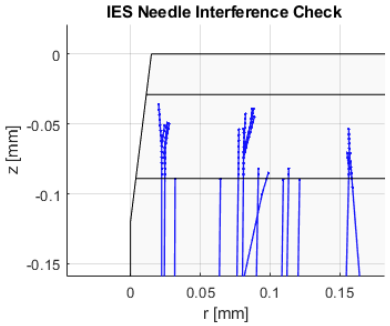

Figure 3.6: Fibers within the FE model of the IES electrode; $d_n = 0.12\ mm$

To validate the model, the threshold of Aδ and Aβ are compared with literature [13, 18, 19].

3.5.3 Simulations & Data Analysis

A study is performed to determine the effect of penetration depth of the needle on the innervation of Aδ- and Aβ-fibers. 3 Aβ-fibers and 1 Aδ-fiber are simulated, the ratio based on the amount of fibers used by Morch et al. [1]. The fibers' origin point is at coordinates (r, z). Where z is randomly chosen between $[(L - 6.389), -6.389]\ mm$, with L the internode length of the specific fiber type to ensure more variation in termination depth, especially for Aβ. r is set as a fixed point, $r = 0.5 mm$. From there on the fiber follows a straight line with an angle of $\theta = \pi$ and $\phi = [0, \pi/36]$, randomly chosen. These (fixed) properties are set to ensure the fibers to grow near the needle (tip) since IES electrodes have a concentrated potential field, hence a small region of interest [19]. For all the penetration depths that are investigated a new population is created, due to the chance of interference with the needle tip. To take variation between populations into account the simulations are repeated 50 times.
The minimum penetration depth of the needle is set to $d_{n,min} = 0.005\ mm$ and the maximum is $d_{n,max} = 0.2\ mm$. A set of needle depths in between is chosen and depicted in Table 3.6. Stimulation is done with a constant current pulse of 0.21 ms [17].

Table 3.6: Penetration depths of the needle in the skin [mm]

Penetration Depths [mm]
0.005
0.01
0.02
0.04
0.08
0.12
0.16
0.2

To evaluate the results, the mean threshold with SEM of the fibers (in mA) of all simulations are shown as well as boxplots of the threshold for each of the penetration depths that are investigated. The current density and potential field the FE model creates for the various needle depths are also determined.

4 RESULTS

The results of the validation of the model are presented first, containing the comparison with the results reported by Morch et al. [1] and McNeal et al. [4]. Since the results are not as expected, the mathematical model is analysed again and certain aspects that could cause the difference in results are investigated. Then the results of the simulations on the IES electrode where penetration depth of the needle on the activation of Aδ and Aβ fibers is investigated, are given.

4.1 Validation of Mathematical Model

4.1.1 Current Density

The current density of the electrode-skin model is determined and extracted from COMSOL. Figure 4.1a.A and 4.1a.B show the current density in vertical direction (z-direction) directly under the center of the electrodes at $r = 0\ \mu m$, and in horizontal direction at the dermo-epidermal junction at $z = -89\ \mu m$, respectively. The smaller the electrode diameter, the higher the generated current per square meter is under the center of the electrode. Also the transition from dermis to hypodermis is seen clearly at a depth of 1.389 mm where the current density has dropped significantly. In the hypodermis the current density becomes gradually lower. The current reaches its peak value at the edge of the electrode, seen in Figure 4.1a.B, which is highest for the smallest electrode. The current density of the FE model presented by Morch et al. [1] is seen in Figure 4.1b.A and 4.1b.B where agreement between both FE models in terms of current density is observed.

4.1.2 Activation Function

The second order spatial derivative of the potential at the dermo-epidermal junction in vertical direction is shown in Figure 4.1a.C. At the electrode edges the potential density is the highest, with again for the smaller electrodes a higher potential compared to the larger electrodes. Figure 4.1b.C shows the results given by Morch et al. [1] for the activation function.

4.1.3 Impedance

The electrode-skin impedance is calculated for various stratum corneum (SC) thicknesses ($29\mu m$, $0.1mm$, $0.3mm$ and $1mm$), and depicted in Figure 4.2a. For a larger SC thickness, the resistance is higher. A higher stimulation current is needed for thicker SC layers to reach the underlying skin layers, which is as expected. For all SC thicknesses is seen with increasing electrode size, the resistance becomes lower. Figure 4.2b shows the electrode-skin impedance of the FE model presented by Morch et al. [1].

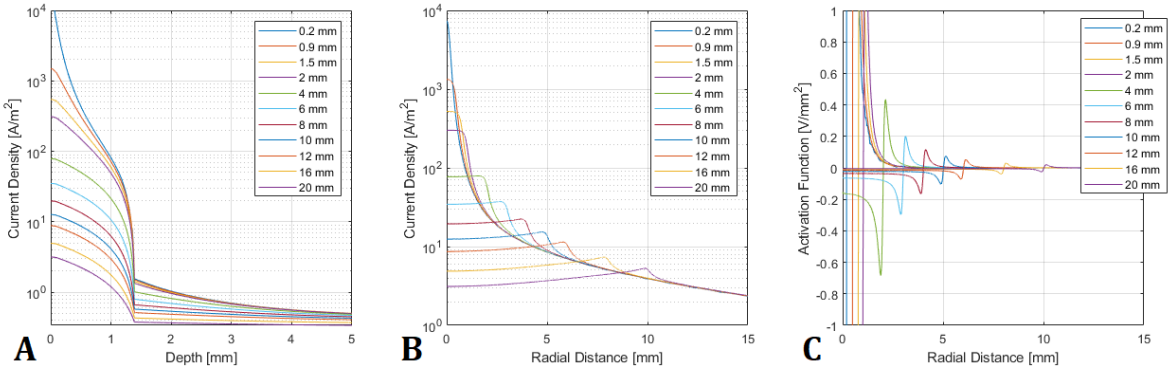

(a) FE models with varying electrode diameter

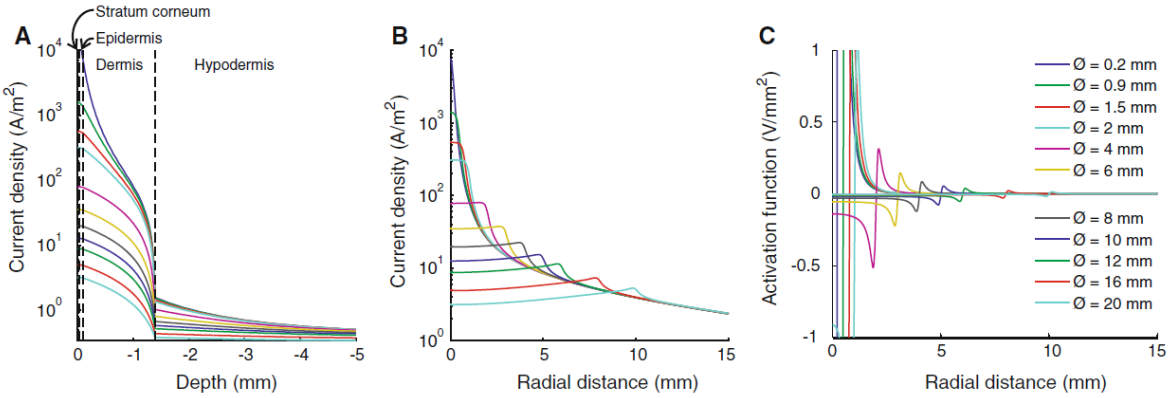

(b) Adopted from Morch et al. [1], Figure 3

Figure 4.1: The current density of the finite element model in **A)** vertical direction (at $r = 0\ \mu m$) and **B)** horizontal direction (at $z = -89\ \mu m$) respectively, and **C)** The second order spatial derivative of the potential in vertical direction on the dermo-epidermal junction (at $z = -89\ \mu m$) for various electrode diameters

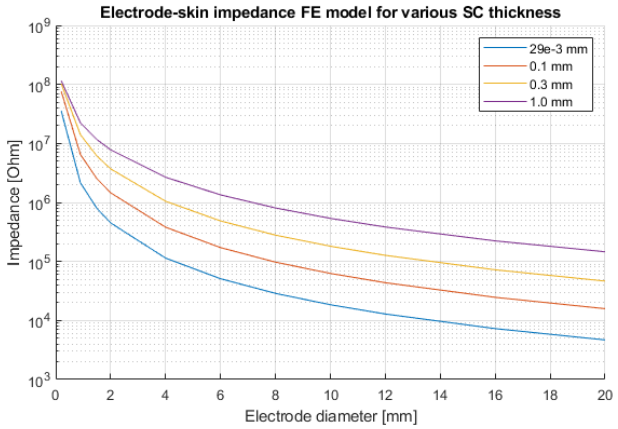

(a) FE models with varying stratum corneum thickness

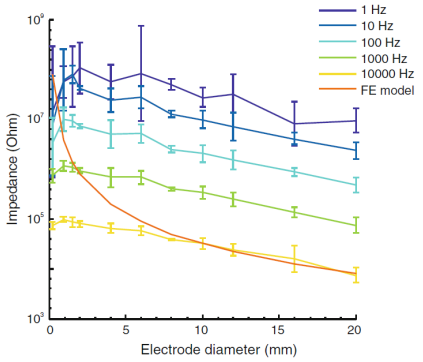

(b) Adopted from Morch et al. [1], Figure 4

Figure 4.2: The electrode-skin impedance (in Ω) of the FE models with varying SC thickness and the FE model presented by Morch et al. [1] (orange line)

4.1.4 Membrane Dynamics

The membrane potential at the nodes of Ranvier is calculated with equation 2.6. Figures 4.3a and 4.3b show the membrane current (I_m) and potential (U_m) of a simple myelinated nerve fiber with a diameter of $20\ \mu m$. A mono-polar electrode with a constant current pulse of 0.1 ms is used. On node 0 a depolarization of the membrane is observed, also seen on nodes 1 and -1 after $70\ \mu s$. The other nodes produce a hyperpolarisation. The membrane current in Figure 4.3b shows for node 0 a fast decrease, even though the input signal is a constant current pulse. For node 1 and -1 the current becomes positive, but for all the other nodes the current remains negative. Figure 4.3c and 4.3d depict the results reported by McNeal et al. [4]. Agreement in both the membrane potential and membrane current is observed.

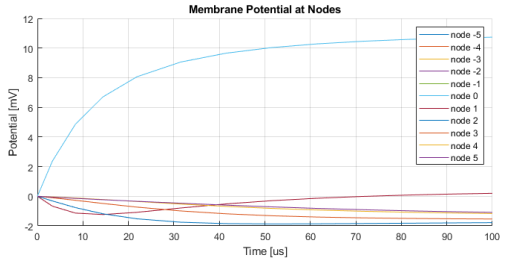

(a) U_m

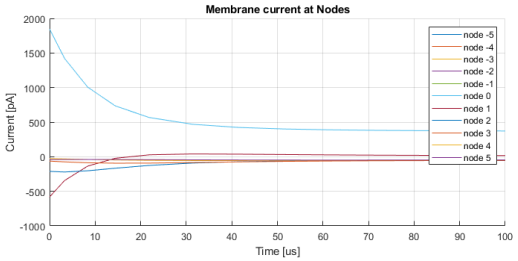

(b) I_m

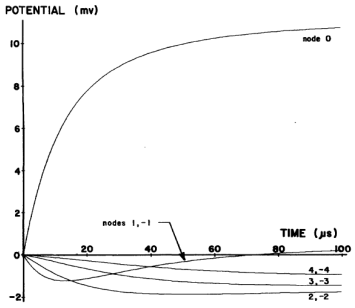

(c) Adopted from McNeal et al. [4], Figure 2

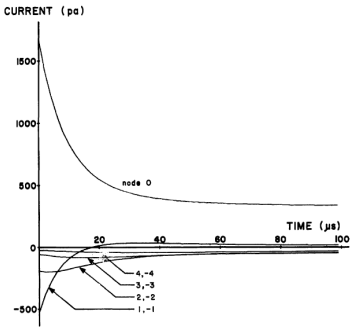

(d) Adopted from McNeal et al. [4], Figure 3

Figure 4.3: Membrane dynamics for a simple myelinated nerve fiber described by McNeal et al. [4]. Stimulation is done with a constant current pulse of $-0.1\ mA$ for 0.1 ms, created by a point source; The potential on the y-axis is corrected for the resting membrane potential of $-70\ mV$

4.1.5 Morphology of Fibers

The morphology of 3 Aβ- (nr. 2,4 and 5) and 3 Aδ-fibers (nr. 1, 3 and 6) are depicted in Figure 4.4. The fibers' origin point (xy-coordinates) is chosen at random (uniform distribution) within a 10 by 10 mm area which is seen in the figure. The fibers are placed within the set grid of [-5, 5] and follow a straight line with a random angle, depicted in the figure as well. The properties of the fibers, such as internode length and diameter, are consistent with the properties described in Figure 3.3 and 3.4. Additionally, the branching of the fibers is in the correct skin layer, which is in the dermis for Aβ and dermis and epidermis for Aδ, just as the termination points are (dermis for Aβ and epidermis for Aδ). And last, the connection of the different segments a fiber consists of is correctly done by the model too.

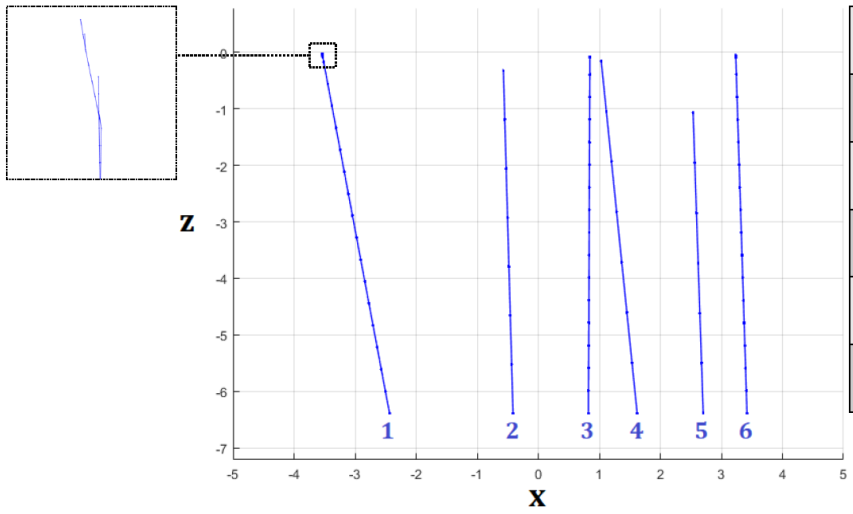

1.	Aδ	[-2.4 , 1.1 , -6.389] [14° , 136°]
2.	Aβ	[-0.4 , 1.6 , -6.389] [16° , 95°]
3.	Aδ	[0.8 , 0.4 , -6.389] [0.3° , 44°]
4.	Aβ	[1.6 , -0.8 , -6.389] [8° , 132°]
5.	Aβ	[2.7 , -1.5 , -6.389] [10° , 260°]
6.	Aδ	[3.4 , 3.3 , -6.389] [2° , 189°]

(a) xz-view

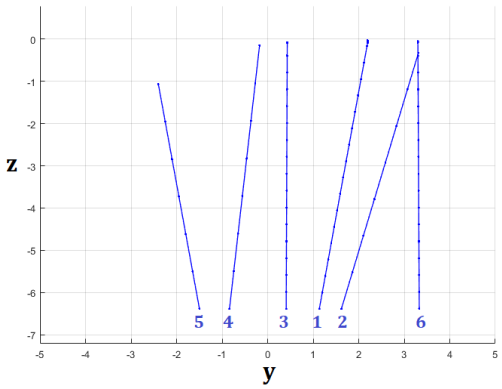

(b) yz-view

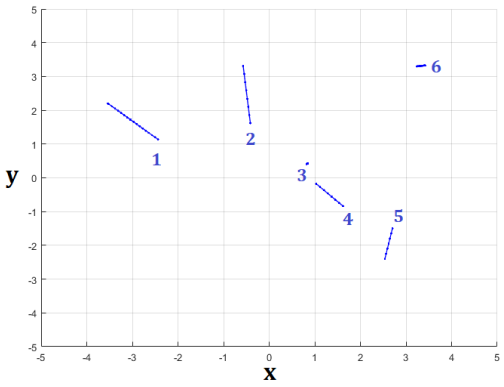

(c) xy-view

Figure 4.4: Stochastic fibers built in MATLAB with origin coordinates [x, y, z] in mm and begin-angle [ϕ, θ] in degrees

4.1.6 Simulations

Mean Threshold

The simulation with 2300 Aβ- and 1000 Aδ-fibers resulted in a mean threshold with SEM for varying electrode diameters as given in Figure 4.5. In each plot a percentage of fibers with the lowest threshold is selected, ending with 100% of the population in Figure 4.5g.

For the complete 100% population (Figure 4.5g), the threshold of Aβ-fibers varies between 2.0 ± 0.01 and $2.7 \pm 0.01\ mA$ for different electrode sizes, whereas for Aδ-fibers the mean threshold is significantly higher. Around $5.5 \pm 0.04\,mA$ for smaller electrode sizes and up to $7.6 \pm 0.03\,mA$ for the largest one with a diameter of 20 mm. The Aβ-fibers had a nerve-ending density of 24.4 per mm^2 at a mean termination depth of $609.7 \pm 9.1\ \mu m$. Aδ-fibers had a density of 25.19 nerve endings per mm^2 at a mean termination depth of $53.0 \pm 0.3\ \mu m$. Figure 4.7 illustrates the nerve-endings for Aβ (red dots) and Aδ (blue dots). It is seen that Aδ terminates in the epidermis and the Aβ fibers in the dermis. The termination points seem normally distributed, apart from termination depth for Aβ which is confined to two regions in the dermis.

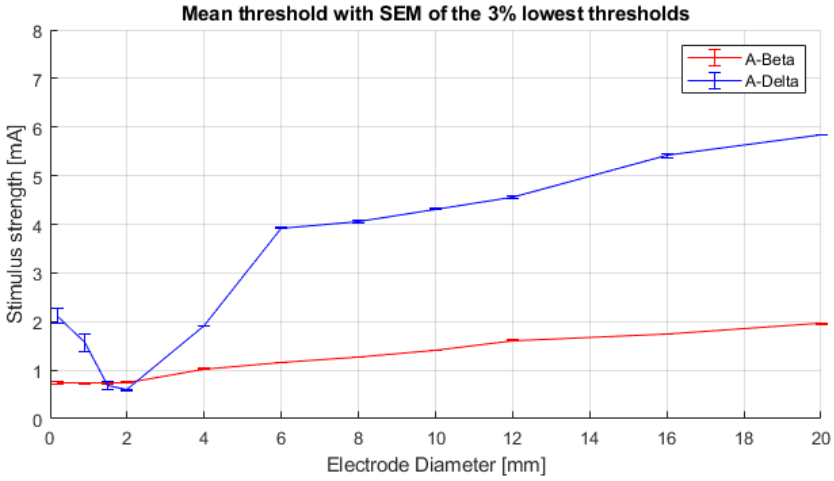

(a) 3%

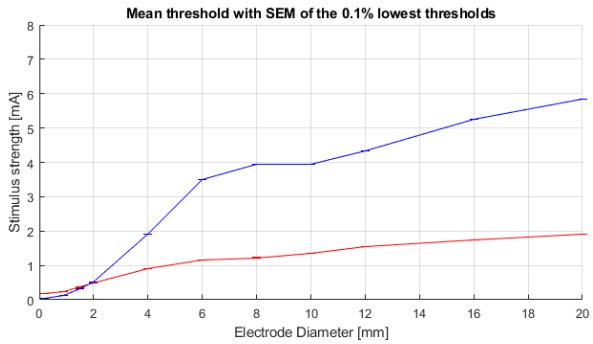

(b) 0.1%

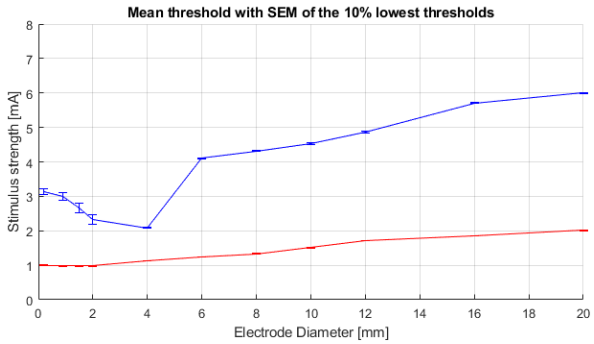

(c) 10%

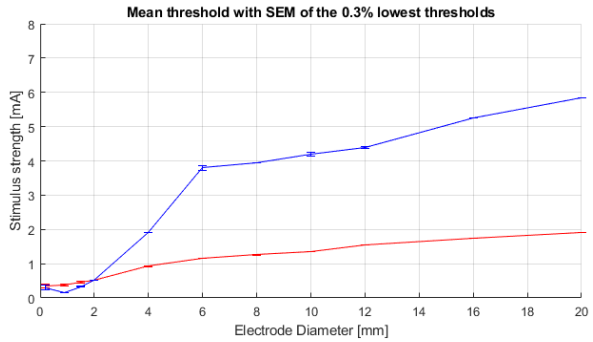

(d) 0.3%

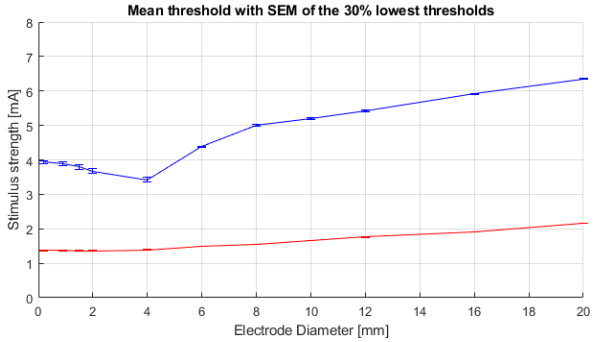

(e) 30%

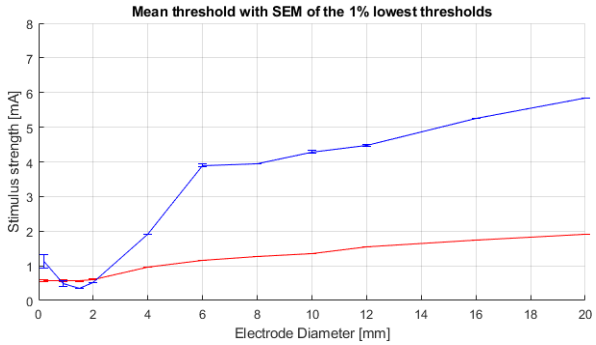

(f) 1%

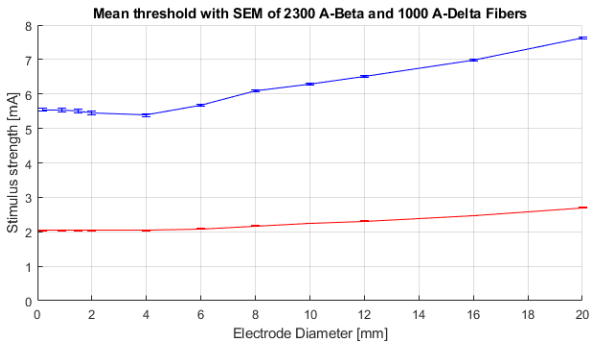

(g) 100%

Figure 4.5: Mean threshold with SEM for varying electrode diameters. A percentage of fibers with the lowest threshold is given in each figure, taken from a population of 2300 Aβ (red) and 1000 Aδ fibers (blue)

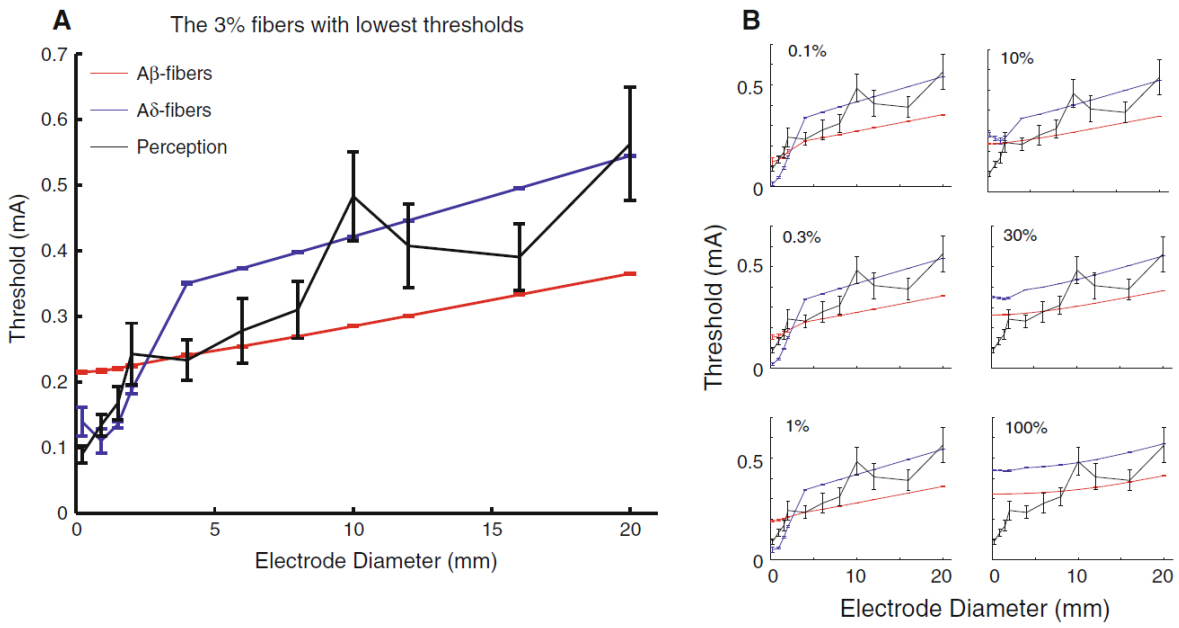

Figure 4.6: Mean threshold with SEM; Adopted from Morch et al. [1], Figure 5

For the percentages of lowest threshold of $0.1\%, 0.3\%, 1\%$ and 3% (seen in Figures 4.5b, 4.5d, 4.5f and 4.5a, respectively) the threshold of Aδ-fibers becomes lower than the threshold of Aβ for an electrode with diameter of 2 mm. The 0.3% and 0.1% Aδ fibers even show a lower mean threshold than Aβ for electrode diameters $\leq 2\ mm$. To continue on the Aδ-fibers, it is seen that the threshold increases more rapidly compared to the Aβ fibers for electrode diameters $> 2\ mm$. Figure 4.6 shows the results reported by Morch et al. [1] and it is observed that the mean threshold with SEM does not agree for a similar size population of 2300 Aβ- and 1000 Aδ-fibers.

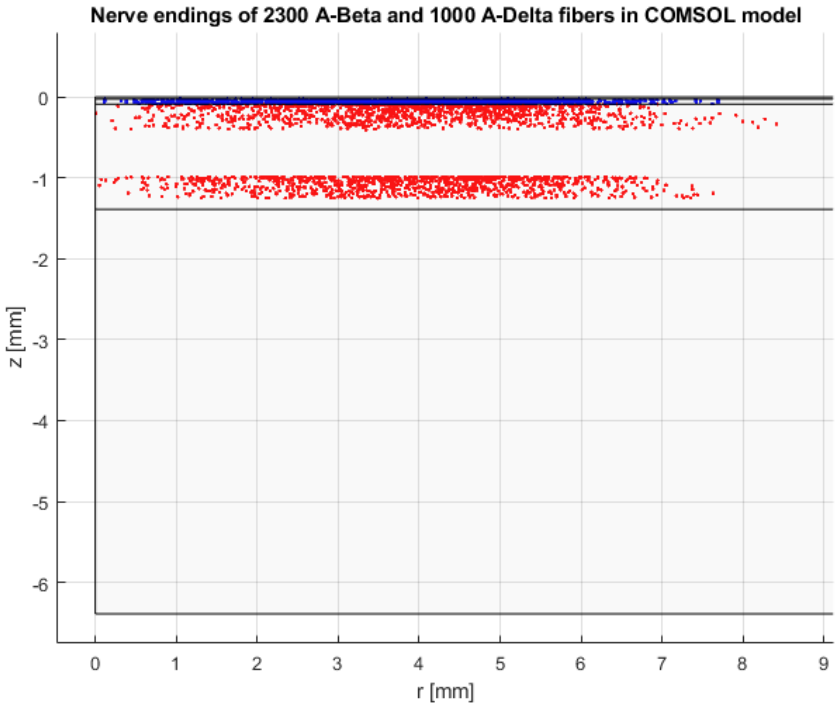

Figure 4.7: Termination points of 2300 Aβ (red) and 1000 Aδ (blue) fibers

Boxplot of Threshold

The spread of the fibers becomes more pronounced in a boxplot since all the threshold values are taken into account. A larger spread of threshold values is observed for Aδ compared to the spread of threshold values for Aβ, seen in Figure 4.8 which shows the boxplots of the threshold for five different populations containing 50 fibers of Aβ and 50 fibers Aδ. For the Aβ-fibers the variation between populations is minimal. The median (depicted by the black line) is around the same threshold value for all five different populations for an electrode diameter of 4 mm or smaller (namely $2\,mA$). For larger electrode diameters the median starts to vary. For Aδ fibers the median is around the same threshold value for all electrode diameters, except for the fourth population where the median is $5\,mA$ for the electrode diameters of 6 mm and lower (instead of $6\,mA$).

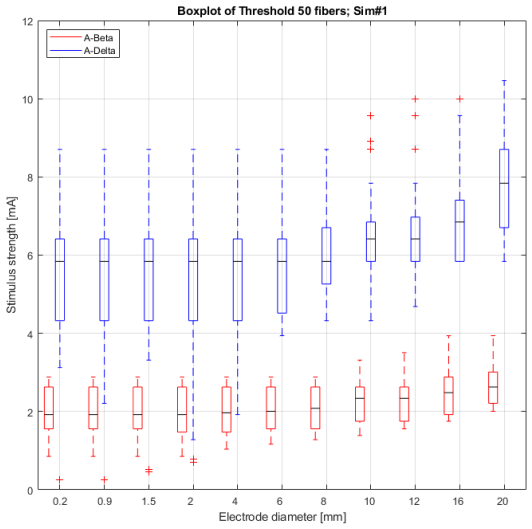

(a) Sim#1

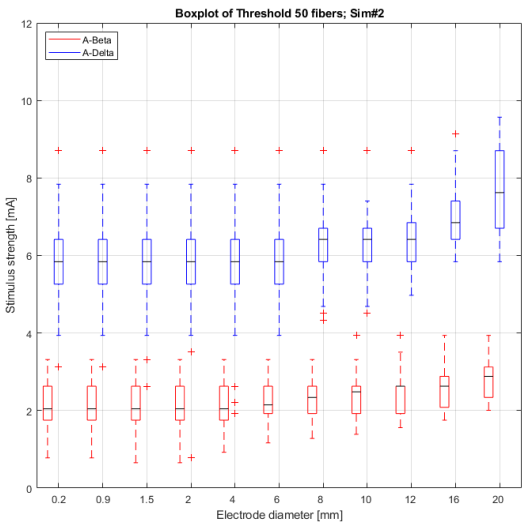

(b) Sim#2

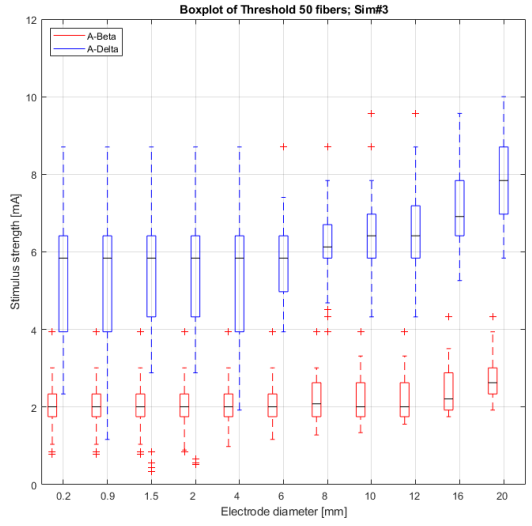

(c) Sim#3

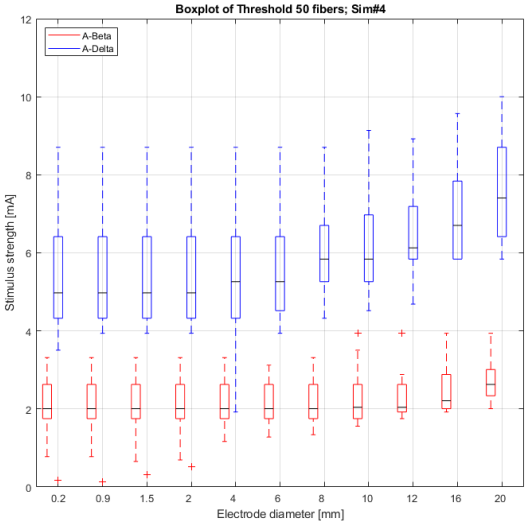

(d) Sim#4

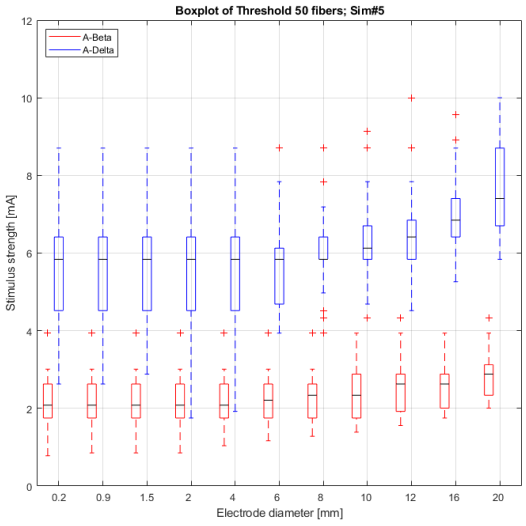

(e) Sim#5

Figure 4.8: Boxplots of the threshold of Aβ (red) and Aδ (blue) fibers for five different populations containing 50 fibers of each type

4.2 Exploration of Discrepancies in the Mathematical Model

The validation steps taken above show different results, especially for the mean threshold, compared to the data reported by Morch et al. [1]. Therefore volume-conduction model as well as the stochastic fiber model are reassessed, described in this section. Since a vast amount of simulations is carried out, the amount of fibers sufficient for the simulations is investigated first.

4.2.1 Amount of Fibers

Simulations with populations of 10, 20, 50, 100 and 200 Aβ- and Aδ-fibers are done and for each fiber the stimulation current needed to elicit an action potential is calculated. Figure 4.9 shows the mean threshold with SEM for each of the populations for various electrode sizes. The mean threshold of the different population sizes are similar to one another and show only a small variation. Therefore a population of 50 fibers is said to be sufficient to carry out further simulations.

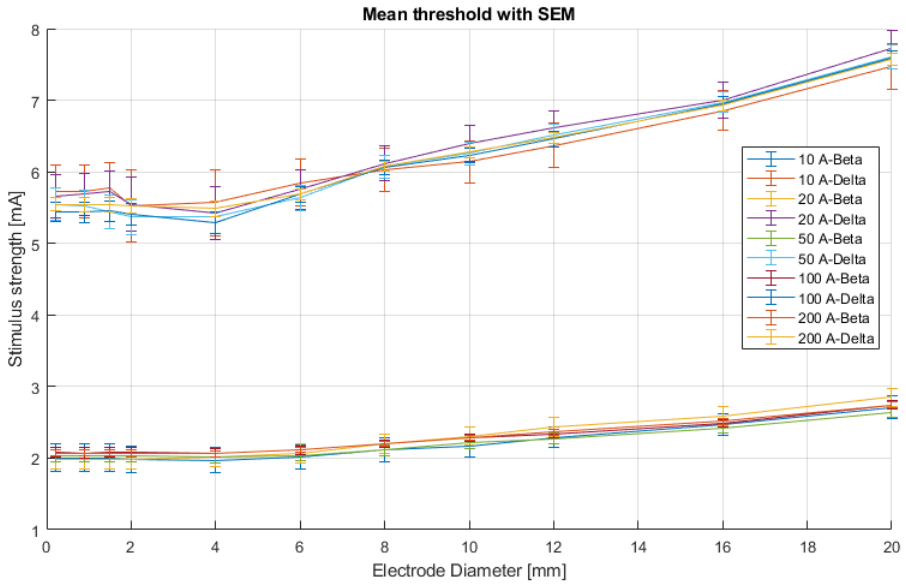

Figure 4.9: The mean threshold with SEM for various electrode sizes and population sizes of Aβ- and Aδ-fibers

4.2.2 Convergence Studies

The electrical potential is calculated for several FE models where radial extent and mesh size is varied, the results seen in Figure 4.10. The external potential at the edge of the skin area is lower compared to the potential at the center of the electrode, which is expected. For the various mesh sizes the potential in vertical direction at the center and at the edge follow the same line, suggesting an agreement in potential. However, for the various radii, a difference in potential is seen. The FE models with radius $\geq$ 60 mm show a less negative potential compared to the radius of 50 mm. The difference in potential between the various radii becomes less with increasing model depth.

The slope of the external potential in vertical direction for varying hypodermis thickness is seen

in Figure 4.11. Both at the center and edge of the skin area the slope follows the same line for all hypodermis thicknesses up until a depth of $800\ \mu m$ (located in the dermis), where the potential starts to differ after.

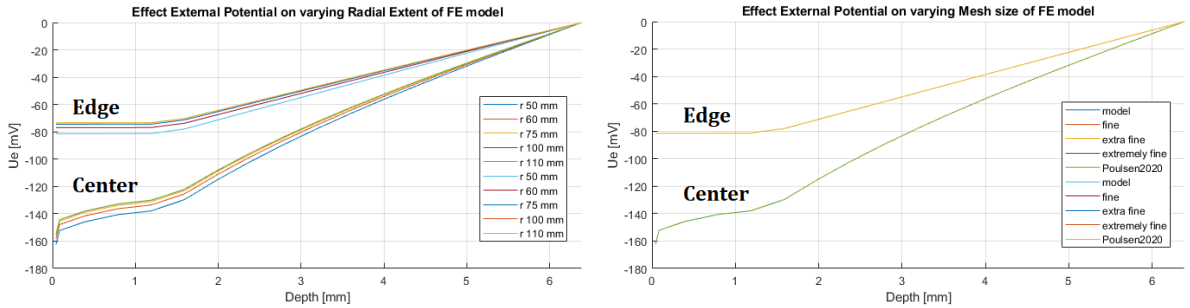

(a) Radial Extent (b) Mesh size

Figure 4.10: External Potential U_e in mV calculated by the FE model in vertical direction at the center (at $r = 0\ mm$) and at the edge (at $r \approx 7.1\ mm$) for varying radii and mesh sizes

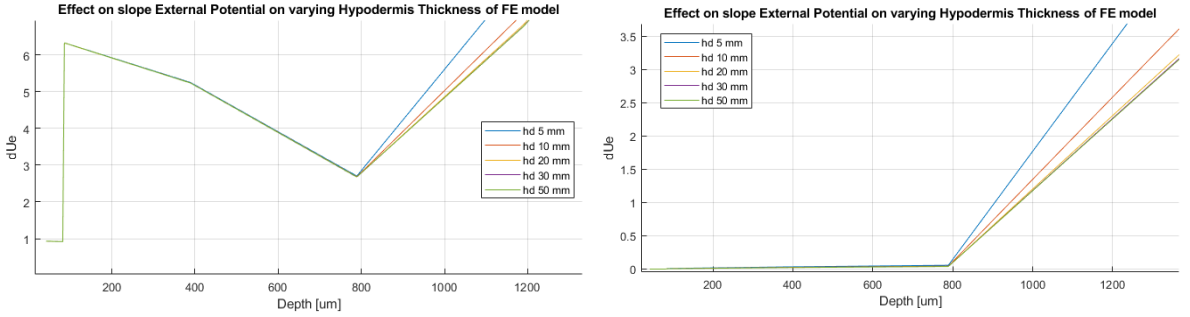

(a) Center (b) Edge

Figure 4.11: External potential difference in vertical direction for varying hypodermis thickness at the center ($r = 0\ mm$) and at the edge at ($r \approx 7.1\ mm$)

Figure 4.12 shows the effect of an increasing hypodermis thickness and radial extent on the current density and activation function. The current density and activation function for the variation in radial extent follows the same line for the given radii. The variation of hypodermis thickness however, shows a difference in current density in vertical direction at $r = 0\ mm$, the center of the electrode, after a depth of 1.389 mm, which is the transition from dermis to hypodermis. The current density (B) and the activation function (C) in Figure 4.12a at the dermo-epidermal junction appear different for the FE model with a hypodermis thickness of 50 mm. Compared to the other FE models a higher current density and a lower activation function is observed.

4.2.3 Shape Function

The electrical potential within a mesh element is calculated by the use of a predetermined shape function. The effect of the choice of shape function on the current density and activation function is seen in Figure 4.13. A quadratic and cubic shape function are used on an FE model with electrode diameter of 4 and 6 mm. The current density in both vertical and horizontal direction shows no difference between a quadratic and cubic shape function. The activation function shows agreement, except the peak values at the edges of the electrodes. These are lower for the cubic shape function compared to the quadratic shape function for both electrode sizes. The change in shape function also causes a difference in computation time. The computation time went from 30 s to 133 s.

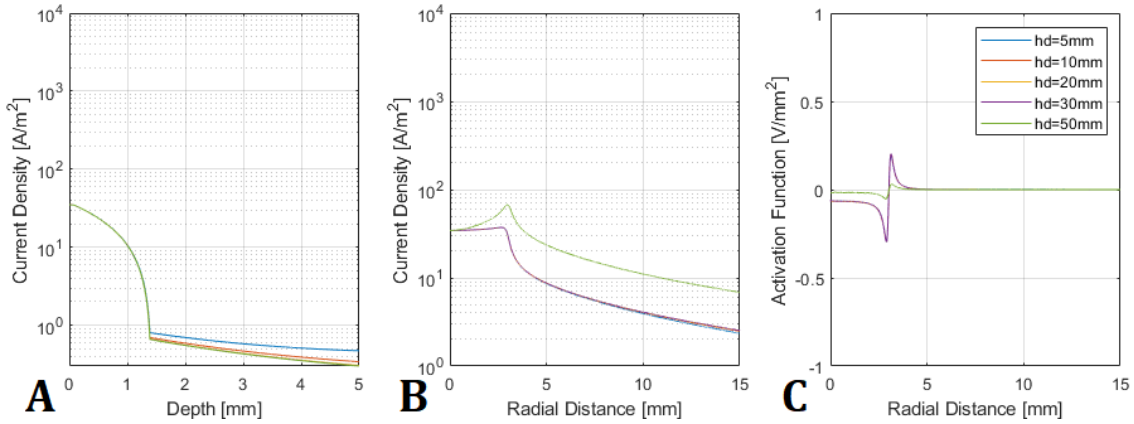

(a) Variation of hypodermis thickness (5, 10, 20, 30, 50 mm)

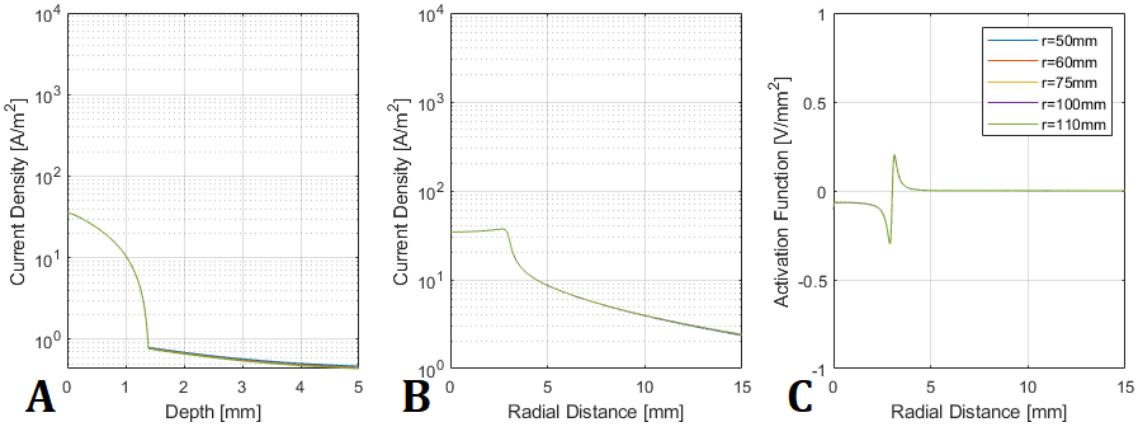

(b) Variation of Radial Extent (50, 60, 75, 100, 110 mm)

Figure 4.12: The current density in **A)** vertical direction (at $r = 0\ \mu m$) and in **B)** horizontal direction (at $z = -89\ \mu m$), and **C)** the activation function in vertical direction (at $z = -89\ \mu m$), respectively. An electrode diameter of 6 mm is used

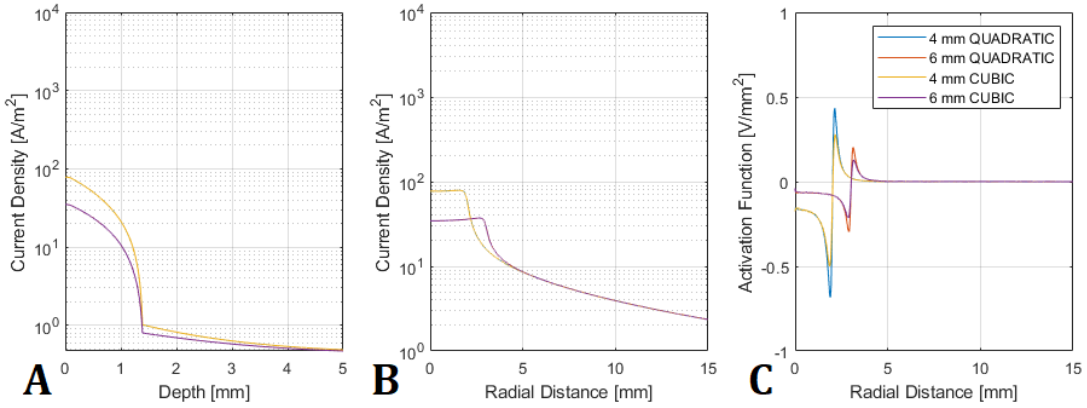

Figure 4.13: The current density in **A)** vertical direction (at $r = 0\mu m$) and in **B)** horizontal direction (at $z = -89\ \mu m$), and **C)** the activation function in vertical direction (at $z = -89\ \mu m$), respectively, for an FE model with electrode diameter of 4 mm and 6 mm. A quadratic and a cubic shape function are used

4.2.4 Placement of Fibers in FE Model

The mathematical model combines the volume-conduction model in COMSOL where the extracellular potential is calculated (U_e) and the stochastic fiber model in MATLAB where the nerve fibers are built and the membrane potential (U_m) is calculated. Eventually the threshold in mA is determined, giving information about the stimulation current needed to elicit an action potential. Figure 4.14 illustrates the Aβ- and Aδ-fibers. Node-coordinates are transformed from 3D to 2D with equation 3.3, and are seen inside the 2D FE model. All the fibers originate from the lower boundary of the hypodermis at $z = -6.389\ mm$ and are located withing the FE model boundaries.

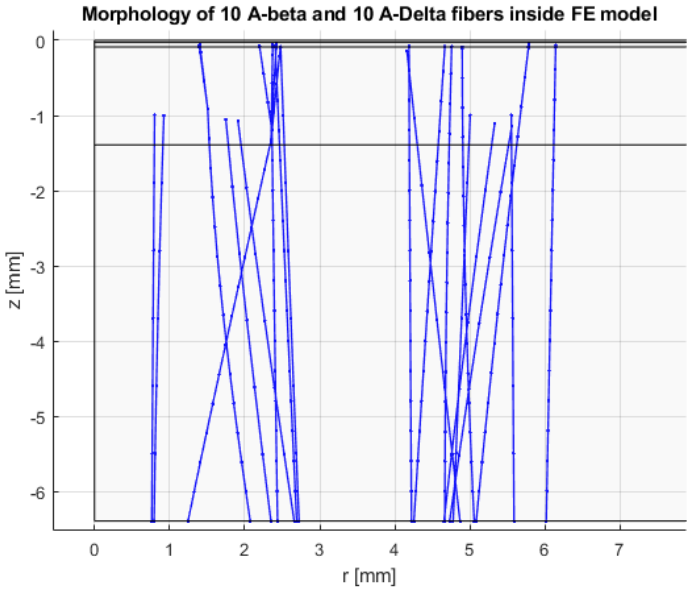

Figure 4.14: Morphology of 10 Aβ and 10 Aδ fibers inside the FE model

4.2.5 Model Thickness

The membrane potential at the nodes at $t = 1\,ms$ of a simple Aβ-fiber (no branching, no angle), located underneath the center ($r = 0\ mm$) and at the edge ($r = 3\ mm$) of a 6 mm diameter electrode is seen in Figure 4.15. Figure 4.15a and 4.15c use an FE model with a hypodermis thickness of 5 mm, whereas Figure 4.15b and 4.15b are made with an FE model with a hypodermis thickness of 50 mm. For the simple Aβ-fiber located under the center of the electrode with a stimulation current of $0.5\ mA$, a maximum depolarisation is seen on the node closest to the electrode (node 7 and 58, respectively, at $z = -0.089\ mm$), which is expected. However, on the nodes located at the lower boundary of the hypodermis, a hyperpolarisation is observed. In the case of the model used in Figure 4.15a, the hyperpolarisation at node 1 almost equals the depolarisation at node 7, a difference of $6.4\ mV$ and $7.9\ mV$, respectively, from the resting membrane potential of -$70\ mV$. When the hypodermis thickness is increased to 50 mm, a hyperpolarisation is still observed, a deviation of $2.2\ mV$ from resting membrane potential. The maximum depolarisation on the node closest to the electrode is $5.6\,mV$ for the FE model with a 50 mm hypodermis. The hyperpolarisation that is observed has decreased for the model with a thicker hypodermis. Yet the (maximum) depolarisation at the node closest to the electrode has decreased as well, from $7.9\ mV$ to $5.6\ mV$, with the same stimulation current.

The membrane potential for a simple Aβ fiber located at the edge of the electrode at $r = 3\,mm$ is seen in Figure 4.15c and 4.15d. The maximum depolarisation seen with a stimulation current

of $0.5\ mA$ is, at node 7, $4.2\ mV$ for a hypodermis thickness of 5 mm, and at node 58, $3.4\ mV$ for a hypodermis thickness of 50 mm. The maximum depolarisation at the edge is less compared to the maximum depolarisation when the fiber is located underneath the center of the electrode. For the model with a hypodermis thickness of 5 mm, the node where the maximum depolarisation occurs shifted from node 8 to node 7.

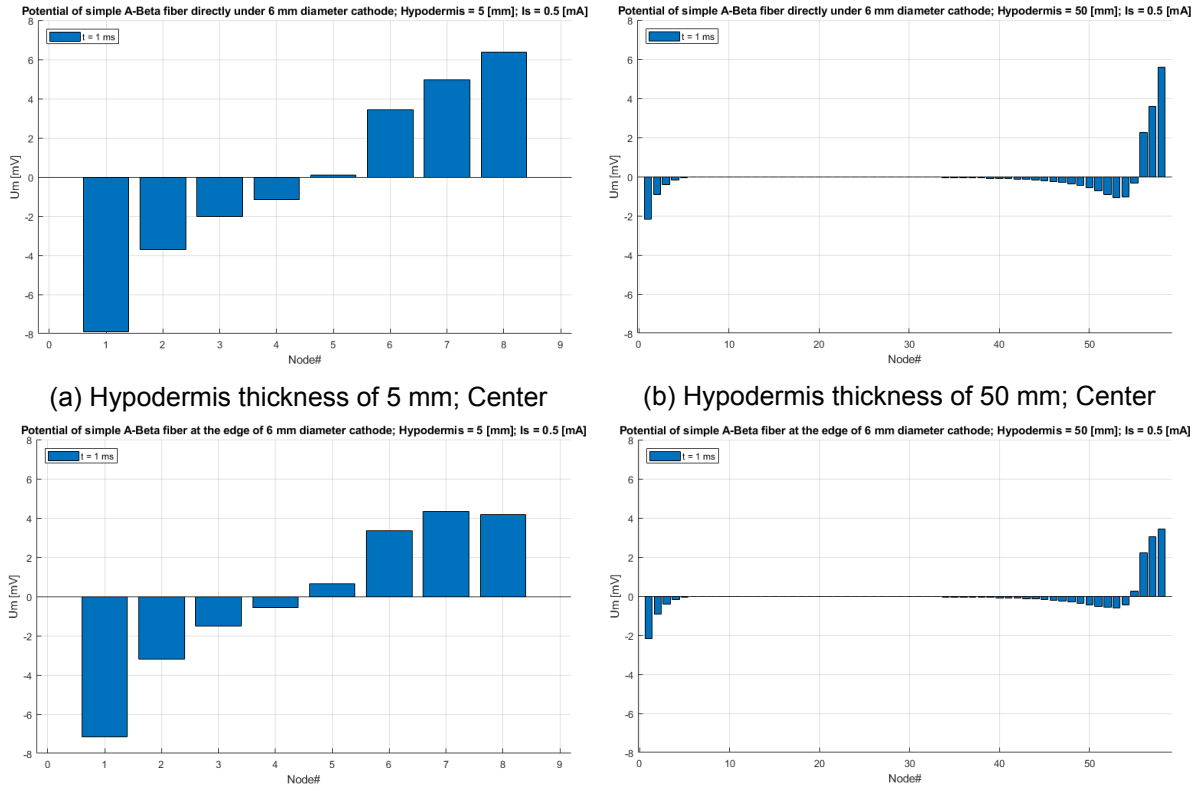

(a) Hypodermis thickness of 5 mm; Center

(b) Hypodermis thickness of 50 mm; Center

(c) Hypodermis thickness of 5 mm; Edge

(d) Hypodermis thickness of 50 mm; Edge

Figure 4.15: Membrane potential deviation from V_r at $t = 1\ ms$ for a simple Aβ fiber directly under the center of a 6 mm diameter cathode with $I_s = -0.5 mA$. The last 7 nodes of both fibers are at the same xyz-coordinates. Hyperpolarisation is observed at the nodes closest to, or on the lower boundary of the hypodermis. The membrane potential on the y-axis is corrected for a resting membrane potential of $-70\ mV$

4.2.6 Dermo-Epidermal Junction

Simple Aδ-fibers with the various options to cross the dermo-epidermal junction are constructed, described in Figure 3.3. The simple Aδ fibers are placed at $r = 0, 1, 2, 3, 4$ and $5\ mm$, illustrated with the numbers 1 to 6 in Figure 4.16. The table in Figure 4.16 shows the threshold values in mA for each option and fiber number. An FE model with an electrode size of 6 mm is used. The overall results show that moving the fiber away from the center of the electrode results in an increase of threshold value, meaning a higher stimulation current is needed to elicit an action potential, which is expected. For fiber 4, 5 and 6, located on the edge and beyond the electrode, the threshold values for all options are equal. The only difference is seen for fibers 1 to 3 that are located underneath the 6 mm diameter electrode. Option C and D result in the highest threshold values, whereas A and B give the lowest. Option E shows for $r = 0$ and $1\,mm$ similar threshold values as for option A and B, and at $r = 3\ mm$, which is exactly underneath the edge, it shows the same threshold value as option C and D.

Options →

#Fiber ↓	A	B	C	D	E
1	3.9404	3.9404	4.3249	4.3249	3.9404
2	3.9404	3.9404	4.3249	4.3249	3.9404
3	3.9404	3.9404	4.3249	4.3249	4.3249
4	5.8386	5.8386	5.8386	5.8386	5.8386
5	6.1269	6.1269	6.1269	6.1269	6.1269
6	6.7036	6.7036	6.7036	6.7036	6.7036

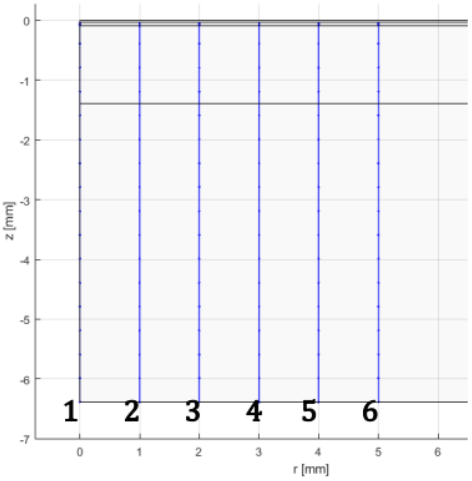

Figure 4.16: Threshold values of simple Aδ fibers given in [mA], placed at various r, and built with different cross-over options. Calculated with FE model with an electrode diameter of 6 mm.

4.2.7 Introduce Erroneous Values

As mentioned before the results of the mean threshold do not agree with the results presented by Morch et al. [1]. Therefore specific model parameters are deliberately adjusted to investigate the effect on the mean threshold. The parameters that are changed, introducing an error, are: The *surface area of the nodal gap* (A_{node}), *resistance* (R), *membrane capacitance per unit area* (c_m), *membrane conductance per unit area* (g_m), *axoplasm conductivity* (σ_i) and *critical value for an action potential* (U_{crit}).

Figure 4.17.A contains the mean threshold with SEM for populations of 50 Aβ- and 50 Aδ-fibers where an error is introduced. The resistance (normally calculated with equation 3.2) is calculated with $R_{i,error} = \frac{L_i}{2.5\sigma_i \pi d^2}$, and results in a lower mean threshold for Aδ (orange line) and Aβ (blue line) compared to the results seen in Figure 4.9 with a factor 0.3.

The surface area nodal gap error is $A_{node,error} = \pi(0.5d)l$ (normally calculated with equation 2.5) and likewise results in a lower threshold for Aβ (yellow line) and Aδ (purple line). Compared to the resistance error the decrease of mean threshold is not of the same magnitude, yet it is a factor 1.5 lower compared to the mean threshold presented in Subsection 4.1.6.

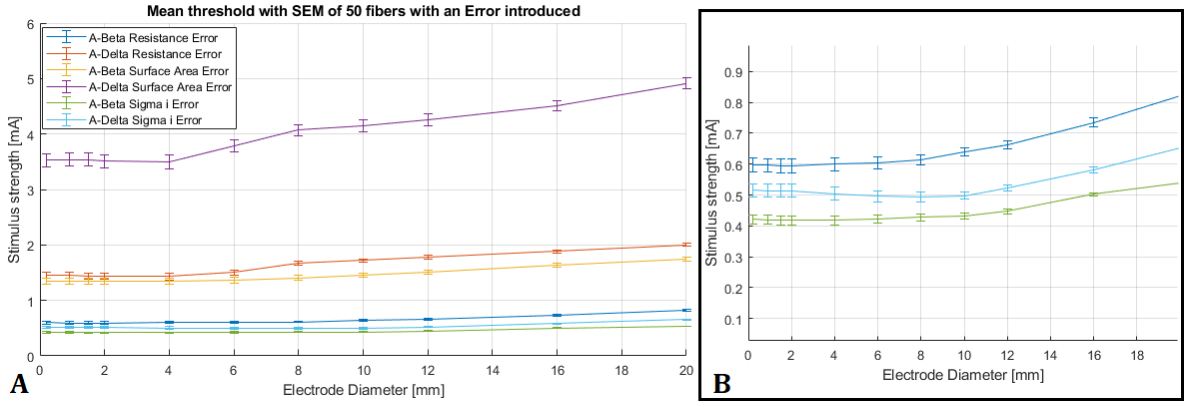

Figure 4.17: Mean threshold with SEM for populations of 50 Aβ and 50 Aδ fibers with an error introduced in the resistance, surface area of the nodal gap and axoplasm conductivity

The axoplasm conductivity error produces the lowest mean threshold compared to the other parameter errors. A σ_i of $9.1\ S/mm$ is implemented (instead of $9.1e{-}4\ S/mm$). Figure 4.17.B highlights the mean threshold values for Aβ (green line) and Aδ (cyan line) and shows a factor 5 and 11 lower mean thresholds, respectively.

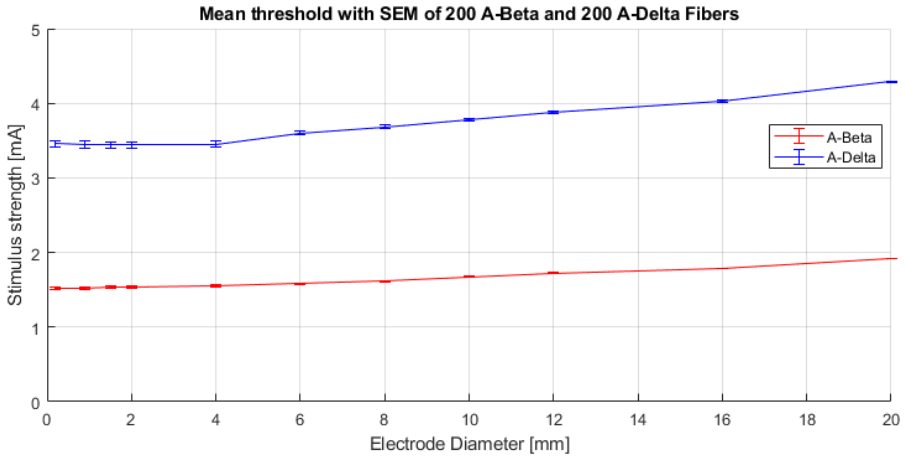

Figure 4.18: Mean threshold with SEM for a population of 200 Aβ- and Aδ fibers. If the membrane potential exceeds a difference of $20\ mV$ (depolarisation **and** hyperpolarisation) an AP happens

As mentioned in Subsection 4.2.5 a hyperpolarisation is observed on the nodes closest to the lower hypodermis border. Normally an action potential is registered when the membrane potential exceeds a difference of $20\ mV$ due to the depolarisation of the membrane. To introduce an error, an action potential can also occur due to a hyperpolarisation of the membrane that exceeds a difference of $20\ mV$ from resting membrane potential. Figure 4.18 shows the result of this error. Compared to Figure 4.9, the mean threshold has become lower, a decrease of a factor 1.4 for Aβ and a factor 1.2 to 1.7 for Aδ depending on electrode size.

4.3 Validation Penetration Depth

4.3.1 Volume-conduction model

Current Density

The current density of the FE model for the IES electrode with varying needle depth is seen in Figure 4.19.A and 4.19.B. The current density differs slightly under the needle tip, yet shows no difference in the dermis and hypodermis anymore. At the dermo-epidermal junction the current density in horizontal direction shows a slight difference for the various needle depths in the first 0.5 mm radial distance, and follows the same line for all needle depths after.

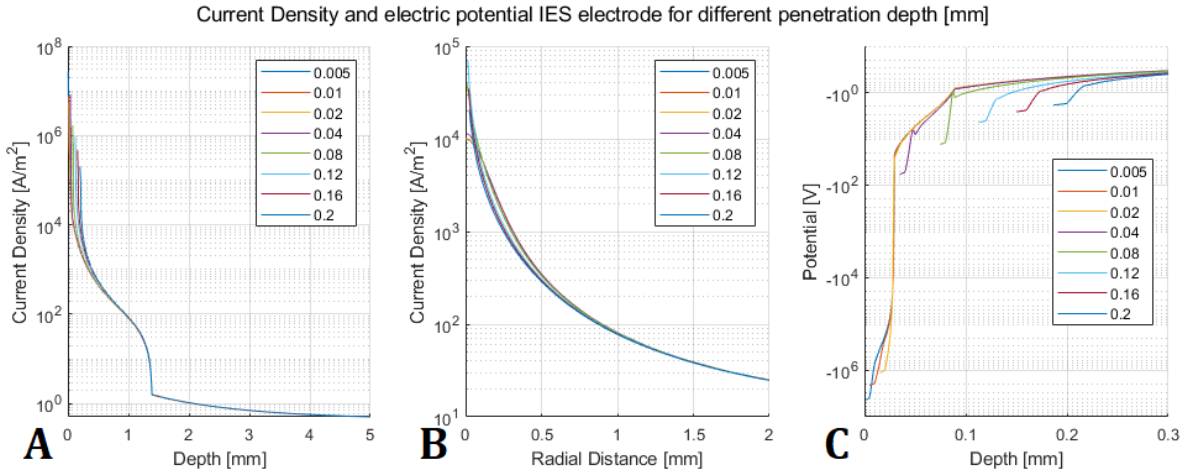

Figure 4.19: The current density of the FE model for the IES electrode in **A)** vertical direction under the needle tip (at $r = 0\ \mu m$) and in **B)** horizontal direction at the dermo-epidermal junction (at $z = -89\ \mu m$) for various needle depths. **C)** The electrical potential in a straight line underneath the needle tip

Electrical Potential

The electrical potential of the FE models with varying needle depth is seen in Figure 4.19.C. The potential data begins at different depths, equal to the penetration depth of the needle, which is expected. There's a slight difference in potential noticeable in the first part of the potential data for the various needle depths, but quickly follow the same line after.

4.3.2 Model Thickness

The membrane potential at the nodes of a simple Aβ and Aδ fiber (no angle, no branching) at $t = 1\,ms$ is given in Figure 4.20. Both fibers originate at (r, z) coordinates $(0, -6.389)$ and follow a straight line up, terminating at $z = -0.089\,mm$ for Aβ and $z = -0.042\,mm$ for Aδ. A stimulation current (I_s) of $-0.01\,mA$ is used. The simple Aβ fiber has a maximum depolarisation of $3.0\,mA$ on the node closest to the needle tip. Besides the depolarisation, a small hyperpolarisation of $0.2\ mA$ is seen. For the Aδ fiber, the last node is located directly under the needle tip ($d_n = 0.04\ mm$). Therefore a depolarisation of $235.7\ mA$ at this node is observed. In turn there is barely any hyperpolarisation visible, which is $0.07\ mA$.

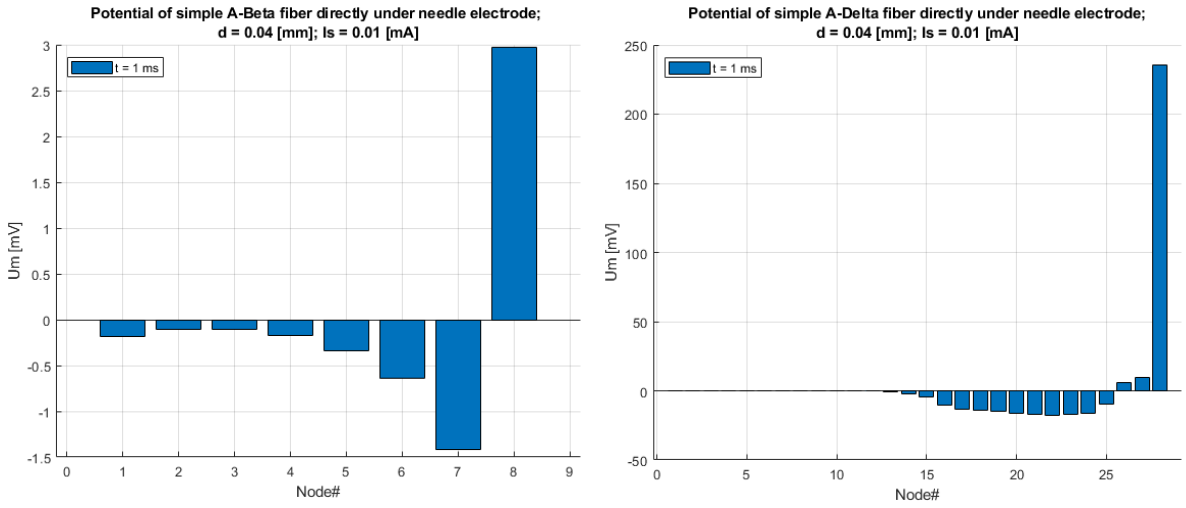

(a) Aβ (b) Aδ

Figure 4.20: Membrane potential deviation from V_r at $t = 1\ ms$ for a simple Aβ and Aδ fiber directly under the needle tip with penetration depth $d_n = -0.04\ mm$ with stimulation current of $-0.01\ mA$. The membrane potential on the y-axis is corrected for a resting membrane potential of $-70\ mV$

4.3.3 Simulations

50 simulations with each 3 Aβ-fibers and 1 Aδ-fiber were carried out, where for each depth of the needle electrode a new population of fibers was made. The results are given below.

Morphology and Termination of Fibers

The morphology of 6 Aβ- and 2 Aδ-fibers is illustrated in Figure 4.21a. The origin angle that determines in which direction the fibers grow results in growth towards the needle. The figure also shows the Aβ fibers terminating in the dermis and Aδ fibers terminating in the epidermis.

The fiber-endings are depicted in Figures 4.21b to 4.21i. The Aβ-fibers (indicated by the red dots) terminate in the dermis and spread out nicely over the area $r = 0$ to $0.5\ mm$. For the Aδ-fibers (indicated by the blue dots) a similar spread is seen. Overall the Aδ-fibers terminate in the epidermis, however for all needle depths, aside from $d_n = 0.005$ and $0.04\ mm$, varying between 1 to 5 Aδ nerve endings are located in the dermis. Except for the maximum needle depth of $0.2 mm$, where a significant higher amount of Aδ nerve endings terminate in the dermis.

Mean Threshold

The mean threshold with SEM for varying penetration depth of the needle electrode of 50 simulations with 3 Aβ-fibers and 1 Aδ-fiber is shown in Figure 4.22. The mean threshold for Aδ is below the mean threshold for Aβ, except at maximum needle depth of $0.2\ mm$ where the mean threshold is almost equal, namely $0.59 \pm 0.073\ mA$ for Aδ and $0.59 \pm 0.014\ mA$ for Aβ. It is also seen that the threshold of Aδ increases for an increasing penetration depth of the needle electrode, apart from a depth of $0.005\ mm$ where the needle barely resides in the stratum corneum. There a mean threshold of $0.4 \pm 0.059\ mA$ is found.

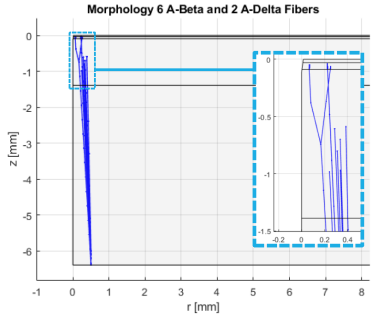

(a) Morphology of 6 Aβ and 2 Aδ with $d_n = 0.04\,mm$

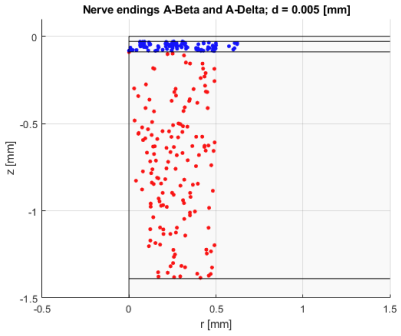

(b) $d_n = 0.005\,mm$

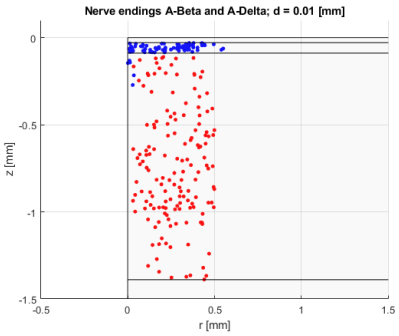

(c) $d_n = 0.01\,mm$

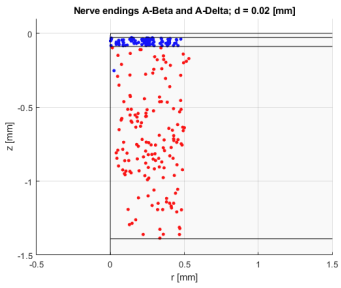

(d) $d_n = 0.02\,mm$

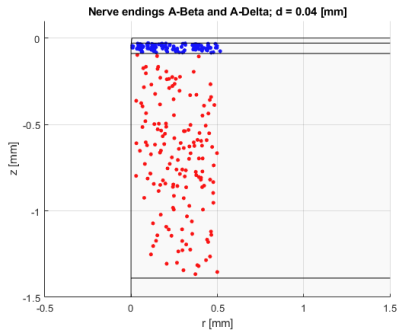

(e) $d_n = 0.04\,mm$

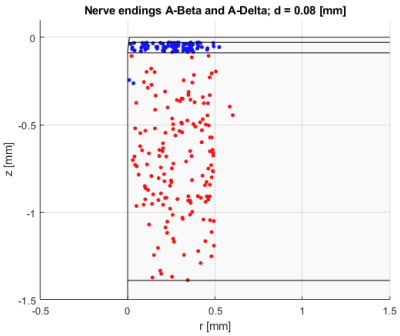

(f) $d_n = 0.08\,mm$

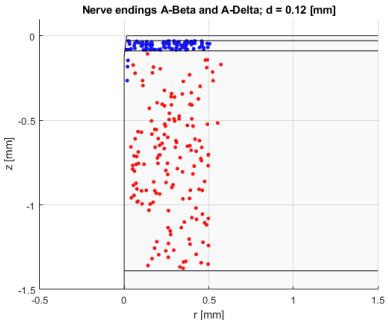

(g) $d_n = 0.12\,mm$

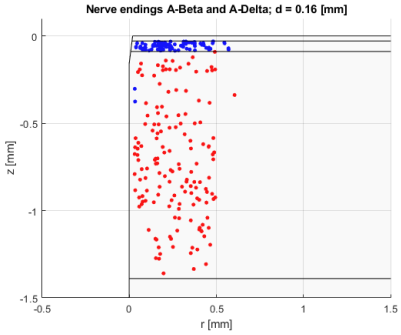

(h) $d_n = 0.16\,mm$

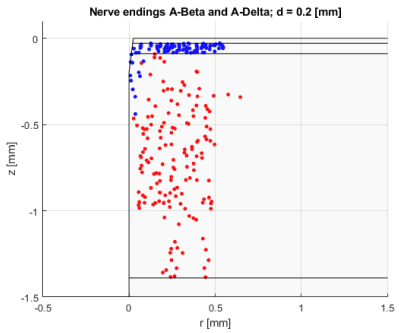

(i) $d_n = 0.2\,mm$

Figure 4.21: **(a)** Morphology of fibers and **(b - i)** the termination points of Aβ (red) and Aδ (blue) fibers inside the various volume-conduction models with different penetration depths of the needle electrode

Boxplot of Threshold

The boxplots of the threshold for the 50 simulations with 3 Aβ-fibers and 1 Aδ are seen in Figure 4.23. A wider spread in threshold values for the Aδ fibers compared to the Aβ is observed, yet overall the threshold for Aδ is below the threshold of Aβ. The median of Aβ is around $0.7\,mA$, whereas the median of Aδ varies between 0.1 and $0.4\,mA$.

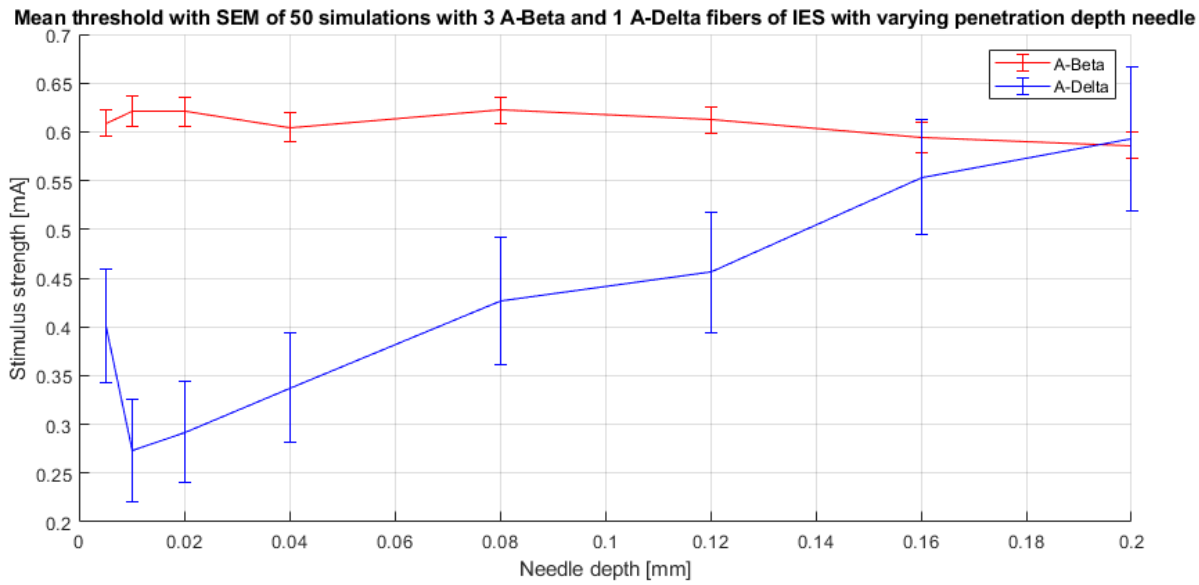

Figure 4.22: Mean threshold with SEM of 50 simulations with 3 Aβ and 1 Aδ fiber for varying penetration depth of the needle electrode

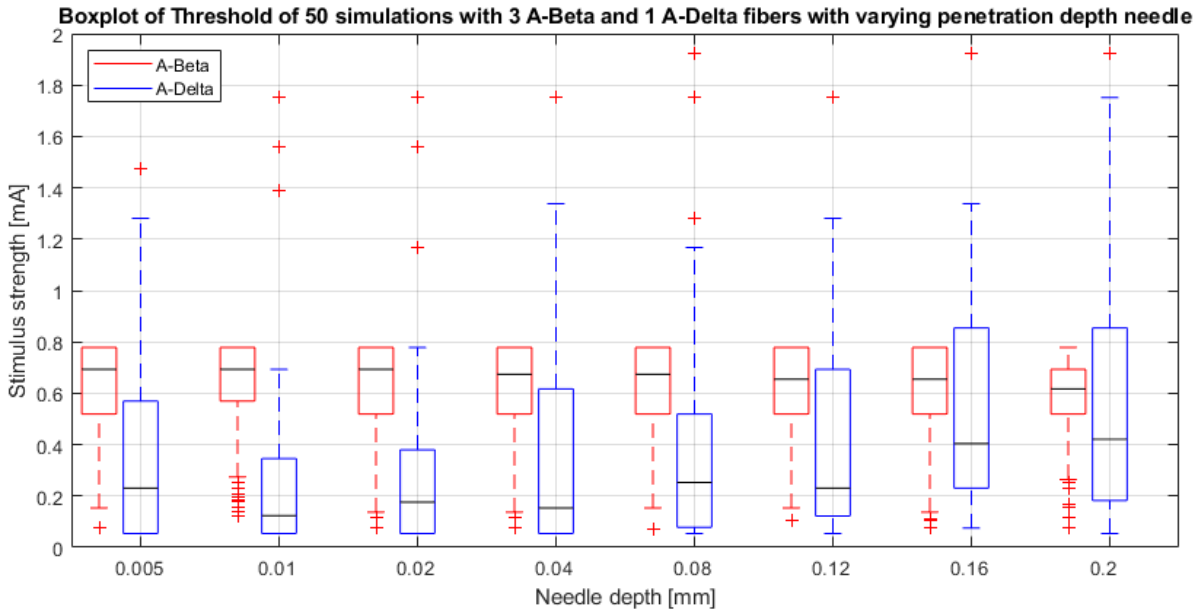

Figure 4.23: Boxplot of the threshold of 50 simulations with 3 Aβ and 1 Aδ fiber for varying penetration depths of the needle electrode

5 DISCUSSION

5.1 Model Validation

The results of the mathematical model described in Chapter 4 are compared with the results described in the article by Morch et al. [1] and discussed below. Similarities and specifically the disagreements are discussed to find a reason for the deviating results for the mean threshold where possible reasons behind those disagreements are explored.

5.1.1 Similarities

Current Density

The current density created by the FE model in COMSOL, seen in Figure 4.1a.A and 4.1a.B, seems to coincide with the current density of the finite element model described by Morch et al. [1], depicted in Figure 4.1b.A and 4.1b.B. This suggests there is an agreement in the spread of the stimulation current by both volume-conduction models.

Membrane Dynamics

The membrane dynamics of the stochastic branching nerve fiber model described by Morch et al. [1] are based on the equations presented by McNeal et al. [4] where the membrane potential and membrane current of a simple myelinated fiber is calculated. Morch et al. [1] extends the simple myelinated fiber to a branching Aβ and Aδ nerve fiber where parameters such as fiber diameter, internode length, branching and origin point with an angle are set. Whether these parts are set up accurately was investigated in different components.

First a simple myelinated fiber as described by McMeal et al. was created. Figure 4.3 shows a successful replication of the membrane potential (4.3a) and the membrane current (4.3b) of this simple myelinated nerve fiber, with the results of McNeal et al. [4] depicted in Figure 4.3c and 4.3d. This proves that the foundation of the membrane dynamics described by equation 2.6 is implemented correctly.

However, more complex branching fibers with specific diameter and internode length properties are created in the model used during this research. So the second step is to inspect these. Figure 4.4 shows the morphology of the fibers where the fiber's diameter and internode length coincide with the properties described by Morch et al. [1]. The Aβ and Aδ fibers terminate in the correct skin layer, which are the dermis and epidermis, respectively. However, variation in certain parameters is present since these are chosen randomly (uniform distribution) from a set range. These parameters are the xy-coordinates for fiber placement, branching, fiber origin angle and the fiber's termination point. Examination showed that these parameters fall in the preset range, and therefore a correct implementation of fiber morphology is stated.

So according to the results discussed above, the theory and calculations where the membrane dynamics are based on (McNeal et al. [4]) seem to be implemented correctly, similarly the branching nerve fiber properties described by Morch et al. [1].

5.1.2 Disagreements

Activation Function

The second order spatial derivative seen in Figure 4.1a.C certainly shows similarities with the results described by Morch et al. [1], yet the peaks at the edges of the various electrode sizes appear to be a fraction higher compared to Figure 4.1b.C, that shows the results of the activation function by Morch et al. [1]. Especially the negative peaks, where for an electrode diameter of 4 mm the value is $-0.68\,V/mm^2$, compared to $-0.5\,V/mm^2$ reported by Morch et al. [1].
This could be explained by the following two differences. First, a difference in mesh size, since the mesh parameters were not stated explicitly in the article by Morch et al. [1] (only a mention of 30,000 elements [1]). Although an adjustment in mesh properties (denser and coarser mesh) gave the same result for the external potential (U_e), as seen in subsection 4.2.2, Figure 4.10b, deeming the mesh as a highly unlikely reason. A second explanation could be the choice of shape function in the FE model. As described in subsection 4.2.3 and seen in Figure 4.13.C., there is a small effect on the peaks of the activation function. The FE models with electrode diameters of 4 and 6 mm that use a cubic shape function replicate the activation function for these same electrode diameters described by Morch et al. [1]. So there is a small difference in activation function found where the choice of shape function plays a role. Yet the shape function cannot explain the deviating threshold results since a slightly higher activation function was found whereas the deviating threshold results suggest a lower activation function which is discussed later on.

Electrode-skin Impedance

The electrode-skin impedance of the FE model was calculated for various SC thicknesses, described in Figure 4.2a, and compared with the results presented by Morch et al. [1]. The electrode-skin impedance of the FE model with an SC thickness of $29\,\mu m$ (used in this research to carry out the simulations), disagrees with the impedance Morch et al. [1] describes. The electrode-skin impedance for an FE model with SC thickness of $0.1\,mm$ also disagrees with Morch et al. [1]. The impedance that Morch et al. [1] reports is located in between the FE models with SC thickness of $29\,\mu m$ and $0.1\,mm$, where an SC of $29\mu m$ has a lower impedance and an SC of $0.1\,mm$ a higher impedance compared to Morch et al. [1]. The article does not explicitly state the SC thickness of the FE model used for the electrode-skin impedance calculations, though it seems unlikely to have chosen a different stratum corneum thickness as stated in the model parameters.

So there is an impedance mismatch. What this means for the FE model and how the effect would be noticeable in the threshold data is discussed here. The electrode-skin impedance is calculated with equation 3.5. The resistance (R) is lower in the model, which leaves two possibilities. The stimulation current I_s is higher, or the potential at the electrode-skin boundary is lower. Since the current density of the FE model matches the current density described by Morch et al. [1], it is said that the stimulation current is equal. Which leaves the option of the potential at the electrode-skin boundary being lower. As an effect, the overall extracellular potential would also be lower. Therefore the difference in electrode-skin impedance could pose as a reason why the mean threshold data does not agree with Morch et al. [1].

The FE model discussed above shows no clear reason why the data results of the mean threshold are different compared to what Morch et al. [1] reports. The membrane dynamics and fiber morphology from the stochastic fiber model and size, conductivity and current density from the FE model were implemented correctly and agree with Morch et al. [1]. The activation function shows a slight difference in peaks, possibly caused by choice in shape function, yet cannot explain the difference in result. The inability to replicate the skin-electrode impedance reported by Morch et al. [1] remains a question since the source is not found. The combination of FE model and stochastic fiber model produces the (mean) threshold values of the simulated fibers and is therefore discussed below.

Threshold

The amount of fibers simulated by Morch et al. [1] were 2300 Aβ- and 1000 Aδ-fibers (in order to generate a density of 59.0 Aβ nerve endings per mm^2 and 163 Aδ nerve endings per mm^2 which is discussed in the next subsection). Therefore a simulation with the exact same amount of fibers was run to truly compare results. The simulation resulted in mean thresholds that were roughly a factor 7 for Aβ and a factor 12 for Aδ higher, seen in Figure 4.5g. On a 10 by 10 mm skin area with the electrode located in the center, the mean threshold ranges from 2.0 ± 0.01 to $2.7 \pm 0.01\ mA$ for Aβ and 5.5 ± 0.04 to $7.6 \pm 0.03\ mA$ for Aδ, depending on electrode size. This disagrees with the findings described by Morch et al. [1], where the mean threshold values are between 0.3 and $0.4\ mA$ for Aβ and 0.42 to $0.62\ mA$ for Aδ of electrode sizes ranging from 0.2 to 20 mm in diameter. An explanation for the difference in mean threshold results needs to be found and is explored here.

Morch et al. [1] reports data that shows a selection of percentages of the lowest threshold, seen in Figure 4.6, to compare the simulated 3% lowest threshold with experimental data where the detection of the perception threshold was measured. These 3% of fibers are likely located at the edges of the electrodes, since the current density is highest there. The selection of lowest thresholds in this research is seen in Figure 4.5 and remain higher compared to the results reported by Morch et al. [1]. The shape of the data seems to show similarities, meaning an increase of threshold for larger electrodes and Aδ threshold becoming lower compared to Aβ for smaller electrodes for percentages of lowest threshold ≤ 3%. Notable is that Morch et al. [1] reports for the 3% (and 1%, 0.3% and 0.1%) lowest threshold that Aδ is below the threshold of Aβ for electrode diameters of 4 mm and less. Whereas for the results in this research it only occurs for electrode sizes of 2 mm in diameter and less. The selection of the lowest threshold values does not reveal the differences in threshold data compared to Morch et al. [1].

As mentioned earlier there is an impedance mismatch, which could result in a lower extracellular potential generated by the FE model, meaning a higher stimulation current is needed to elicit an AP. The fact that a higher stimulation current is needed is exactly observed in the data, yet suggests that the FE model is not correct. The validation steps however, indicate that the FE model is correct. Besides a slight difference in peak values for the activation function, possibly caused by a different shape function and above all gives a higher potential instead of lower, an agreement in current density and activation function is maintained. Thus the difference in result for the mean threshold cannot be explained by the FE model, since the properties used by Morch et al. [1] are implemented correctly, and current density and activation function match. The difference in impedance is unexpected, since there is no clear source for the mismatch. The membrane dynamics and morphology of the branching nerve fibers are also correctly implemented. Despite the variation possible in fiber placement, branching and termination point, the mean threshold with SEM for simulations with different population sizes of fibers, shown in Figure 4.9, indicates that the variation possible cannot account for the difference seen in thres-

hold values since the variation between the populations appear minimal with respect to mean threshold.

This means there is no clear explanation as to why the results of the mean threshold of this research differs compared to Morch et al. [1], leaving the options of a possible error in the mathematical model presented in this research or in the article presented by Morch et al. [1]. Therefore the effect on the results of parameters that are not described in detail or not described at all are discussed in the next section.

5.2 Model Assumptions

Certain assumptions are made and chosen for the mathematical model to represent reality. What the effect of these choices on the data is and whether these assumptions are justified is discussed below.

5.2.1 Parameter Adjustments

As discussed and shown before, the results of the calculated mean threshold of the fibers deviated from what is described by Morch et al. [1]. No clear source was found. Therefore in this section adjustments to the model presented in section 4.2.7 are discussed and it is argued whether the reasoning behind it is justified to attempt a replication of the results described in the article [1].

AP Detection

Due to the model's passive fiber characteristic, it is said that an action potential occurs when the membrane depolarises and exceeds a difference of $20\,mV$ from resting membrane potential $V_r = -70\,mV$. However, a significant amount of hyperpolarisation occurs at the nodes closest to the lower boundary of the hypodermis, seen in Figure 4.15. Therefore the effect on the mean threshold when a hyperpolarisation of the membrane can also account for an AP is tested, where $U_{crit} = -50$ and $-90\ mV$. Figure 4.18 gives the result of the mean threshold for a population of 200 fibers and shows a decrease of mean threshold values for both Aβ and Aδ around a factor 1.4, meaning the extreme hyperpolarisation of the membrane lowers the mean threshold. Yet, including hyperpolarisation in the detection of action potentials is not the (sole) answer to replicating the results by Morch et al. [1], despite it bringing the threshold values down. Therefore more options were explored where a factor is introduced, adjusting certain model properties to replicate the article's [1] results.

Axoplasm Conductivity

The adjustment of the *axoplasm conductivity* (σ_i) from 9.1e-4 S/mm to 9.1 S/mm (a factor 10^4 larger) resembled the results presented by Morch et al. [1] the most. Figure 4.17.B. shows the mean threshold with SEM of both 50 Aβ- and 50 Aδ-fibers with the altered σ_i. Mean threshold values of 0.41 to $0.54\ mA$ for Aβ and 0.51 to $0.65\ mA$ for Aδ, depending on electrode size were obtained. The effect of increasing the axoplasm conductivity is that electrical signals are transported faster on the axon, due to a better conduction, which results in a lower threshold. Regardless of the results of the mean threshold with the σ_i error being almost identical (only $\sim 0.1\ mA$ off) to the results presented by Morch et al. [1], a factor 10^4 is a large mistake that is not easily explainable as a unit error.

5.2.2 Hyperpolarisation of the Membrane

Due to the chosen parameters of the model there is hyperpolarisation visible at the lowest node(s) closest to the hypodermis border and it is suspected that the hyperpolarisation has an effect on the depolarisation at the other end of the fiber (nodes closest to the electrode). The effect being a decrease in depolarisation of the membrane due to the amount of hyperpolarisation at the origin of the fiber. As a way to minimize the hyperpolarisation, the hypodermis layer is increased from 5 mm to 50 mm. Less hyperpolarisation is observed (a factor 3.6 reduced) in Figure 4.15b, yet it is not completely counteracted, meaning there is still a hyperpolarisation visible. The depolarisation however, did not increase. In fact the maximum depolarisation decreased with a factor 1.5 when the same stimulation current was applied. This effect is also seen with the convergence studies where hypodermis thickness was varied. The slope of the external potential changed after $z = -800\,\mu m$, which is in the dermis skin layer where Aβ-fibers terminate. This leaves the question if a hypodermis thickness of 5 mm is justified.

Therefore going back to Morch et al. [1], the radial extent of the FE model reported in the article is justified and based on the evidence of the external potential at the dermo-epidermal junction remaining the same for $r \geq 50\,mm$. Yet no reason is given as to why the hypodermis thickness is set to 5 mm.

Poulsen et al. [15] used model parameters based on the FE model presented in Morch et al. [1] and investigated whether a hypodermis thickness of 5 mm is justified. They reported that the external potential is altered inside the region of interest ($z = [0, -3]\,mm$) when the hypodermis layer increased, yet concluded that this was not large enough to affect the nerve fiber models. In this research however, an increasing hypodermis thickness resulted in a change in membrane potential (decrease of hyperpolarisation and depolarisation), which directly translates to threshold value, questioning if a hypodermis thickness of 5 mm is correct.

5.2.3 Dermo-epidermal junction

Aδ-fibers cross the dermo-epidermal junction and continue as unmyelinated fibers, terminating in the epidermis. Several options on how to model the cross-over are explored, the results seen in Subsection 4.2.6. Currently it is modelled as option E, described in Figure 3.3. There is a slight effect visible on the threshold values when the fibers are located underneath the electrode ($3.9mA$ vs $4.3mA$), where the internode length seems to have the greatest influence. The cross-over from dermis to epidermis only affects Aδ-fibers however, since Aβ terminates in the dermis skin layer. So despite the small effect in threshold value, the various cross-over options for the dermo-epidermal junction cannot explain the differences in the data compared to Morch et al. [1], considering that the mean threshold deviation is seen for both Aδ- and Aβ-fibers.

5.2.4 Nerve-ending Density and Distribution

A simulation with 2300 Aβ- and 1000 Aδ-fibers resulted in a nerve-ending density of 24.4 and 25.19 endings per mm^2 for Aβ and Aδ respectively. This is a significant difference, especially for Aδ, compared to the densities Morch et al. [1] reports which are 59 ± 0.1 per mm^2 Aβ and 153 ± 1.2 per mm^2 Aδ nerve-endings. The possibility to branch for a nerve fiber is set to 10% at each node in the dermis (and also epidermis for Aδ). For Aβ, considering the dermis skin layer together with the internode length and termination point, a branching possibility on only one or two nodes can be achieved. The observation is therefore that Aβ fibers rarely branch, making the nerve ending density reported by Morch et al. [1] particularly high compared to branching anatomy in combination with amount of fibers simulated.

Moreover, the nerve-endings of the 2300 Aβ- and 1000 Aδ-fibers, depicted in Figure 4.7, where a higher density of nerve-endings is seen in the center compared to the nerve-endings at the edges of the chosen skin area, indicating a normal distribution. On top of that, the Aβ-fibers terminate higher up or lower in the dermis, creating two separate layers where Aβ nerve-endings are located. So the fibers' termination points do not show a uniform distribution, but seem normally distributed. This implicates that the fibers are not distributed evenly as is found in glabrous skin biopsies, not resembling reality [22].

The difference in nerve-ending density and the observed normal distribution cannot explain the deviation in threshold results, yet it raises the question how Morch et al. [1] calculated the amount of simulated fibers in order to generate a specific nerve ending density, but more importantly how they were able to generate these densities with their mathematical model.

5.2.5 Electrode sizes

A skin area of 10 by 10 mm was chosen where the fibers originate at random with a uniform distribution. Electrodes with a diameter of 10 mm and higher have as a consequence that all the fibers are more or less located underneath the electrode. Thus no fibers located near the edges where the current density is highest, especially for the 20 mm diameter electrode. An electrode with 20 mm diameter on a skin model with a thickness of 6.389 mm leaves questions as well, since the electrode is more than two times larger than the total FE model thickness. The FE model thickness and selection in electrode diameters is a study design choice made by Morch et al. [1], it however does not resemble reality, since an electrode with diameter of 20 mm will have fibers at the edges and beyond.

5.3 Summary

Sections 5.1 and 5.2 provided an analysis of the mathematical model presented in this research in order to find an explanation for the deviating Aβ and Aδ mean thresholds compared to the mean thresholds reported by Morch et al. [1]. A short summation of the discussed steps is given.

Validation of the model:

- Volume-conduction model
  - Current Density agreed with Morch et al. [1]
  - Activation Function showed slight difference at the peaks, possibly due to a different choice in shape function, yet implies a higher U_e
  - Skin-electrode impedance for an SC of $29\,\mu m$ deviated from the impedance reported by Morch et al. [1], where no clear source was found
- Stochastic branching nerve fiber model
  - Membrane dynamics for a simple myelinated fiber agreed with McNeal et al. [4]
  - Fiber Morphology, including fiber diameter, internode length, placement, branching and origin and termination, agreed with the properties described by Morch et al. [1]
- Volume-conduction model and stochastic fiber model combined gives the mathematical model where a deviating mean threshold of a factor 7 and 12 for Aβ and Aδ respectively, was obtained,
  - Cannot be explained by the impedance mismatch because the FE model seems correct
  - Activation function cannot explain it either because a higher U_e would result in a higher U_m, decreasing the fiber's mean threshold.

Assumptions of the model that required further investigation:

- Adjustment of σ_i (S/mm) with a factor 10^4 closely resembles the mean threshold values reported by Morch et al. [1], however no unit error can describe it
- Choice of hypodermis thickness (5 mm) leads to hyperpolarisation on the nodes closest to the lower boundary, questioning this model design.
- Cross-over of Aδ dermo-epidermal junction was not described in detail, which lead to several model options having an effect on the threshold (only for Aδ)
- Density of simulated nerve-endings did not resemble the densities reported by Morch et al. [1] when simulating an identical amount of fibers and a normal instead of uniform distribution of nerve-endings was observed

Concluding remark: No clear source was found for the deviation of the mean threshold for Aβ and Aδ-fibers compared to the results presented by Morch et al. [1]. Which raises the question whether an error remains in the mathematical model or an inaccuracy in the article by Morch et al. [1].

5.4 IES electrode

As discussed above the results of the validation of the mathematical model were not as expected, leaving the model used for the simulations with the IES electrode to investigate penetration depth not validated yet. The results of the simulations are discussed here and compared with literature, and a critical look is given to the chosen fiber properties and the termination points of the Aδ- and Aβ-fibers.

5.4.1 Preferential A-Delta Activation

The results of the simulations with the needle electrode produced a threshold for Aδ that is lower compared to Aβ, reported in Subsection 4.3.3. The IES electrode's principle is based on a needle that protrudes the epidermis, stimulating the fiber endings that reside there [16]. Two particular needle depths that were simulated are located in the epidermis and produced the following mean thresholds: For $d_n = 0.04\,mm$, where the needle tip is located in the superficial part of the epidermis, a mean threshold of $0.33 \pm 0.06\,mA$ for Aδ and $0.60 \pm 0.02\,mA$ for Aβ was found. And for $d_n = 0.08\,mm$, where the needle almost completely protrudes the epidermis, a mean threshold of $0.43 \pm 0.07\,mA$ for Aδ and $0.62 \pm 0.01\,mA$ for Aβ was found. Moreaux et al. [13] reports that Aδ fibers can be selectively activated with an IES electrode when stimulation currents lower than twice the perceptual threshold are used. Whereas Inui et al. [16] carried out experiments with a single needle electrode protruding the epidermis and were able to selectively activate Aδ-fibers with a mean stimulation current of $0.19 \pm 0.08\,mA$ and $0.22 \pm 0.06\,mA$ (mean $\pm$ SD), depending on location of the hand or upper arm respectively. To compare, non-painful stimuli were measured on the same locations, which resulted in 1.5 to 2 times higher thresholds for the hand and 2 to 3 times higher thresholds on the upper arm. The mean Aδ thresholds for the needle electrode found in this research are higher compared to the thresholds reported by Inui et al. [16]. However, a larger pulse width ($0.5\,ms$) and a different needle geometry were used in their research. Both Moreaux et al. [13] and Inui et al. [16] concluded roughly a factor 2 higher for non-painful Aβ stimulation, which is approximately seen in the data of this research. The threshold values from the needle electrode show similarities to what is reported in literature [13, 16], especially the observation of Aδ threshold below Aβ, which suggest the model can predict preferential stimulation of nociceptive Aδ-fibers.

5.4.2 Termination Point Fibers

The termination points of Aδ and Aβ, seen in Figure 4.21, appear to show a uniform distribution, unlike the termination points depicted in Figure 4.7 which was discussed in Subsection 5.2.4. For the simulations with the IES electrode, the z-coordinate at the origin point was not fixed, but randomly chosen between the lower boundary of the hypodermis and a single internode length of the specific fiber type up. The results showed an evenly distribution of nerve-endings over the defined skin layer, deeming this a more suitable method to choose fiber origin point in order to create the random morphology of fiber termination that is found in reality [22, 35].

5.4.3 Penetration Depth Needle

The depth of the needle in the skin seems to have an effect on the mean threshold, seen in Figure 4.22, and on the threshold values of Aδ depicted in the boxplots of Figure 4.23. When the needle barely protrudes the stratum corneum ($d_n = 0.005\ mm$) a mean threshold of $0.4 \pm 0.059\ mA$ is seen, whereas for $d_n = 0.01\ mm$ the mean threshold decreased and became $0.27 \pm 0.052\ mA$. Then after, the Aδ mean threshold increased with increasing needle depth, where for a maximum needle depth of $d_n = 0.2\ mm$ (needle tip located in the dermis), a mean threshold of $0.59 \pm 0.073\ mA$ is found, matching the mean threshold found for Aβ, which is $0.59 \pm 0.014\ mA$. However, for the various fiber populations several Aδ fibers terminated in the dermis, seen in Figure 4.21b to 4.21i. This is due to the addition of a constant check when the nerve fibers are built to see whether the next node of the fiber is inside the needle boundaries or not. Whenever this happens, the last node outside the needle boundary becomes the fiber's termination point to ensure no interference with the needle in the volume-conduction model. Especially for the maximum needle depth Aδ fibers seem to terminate more frequently in the dermis. It is hard to say what the effect of the early termination of a few fibers is on the (mean) Aδ threshold values and therefore requires more research, possibly excluding these fibers from the results.

5.4.4 Fiber Properties

The fiber properties such as origin point and fiber angle, were chosen to maximize fiber growth towards the needle electrode, because the IES electrode has a concentrated potential field as literature suggests [13, 18, 19]. Due to the stochastic nature of the fibers, variation is possible in fiber design, which could result in Aδ fibers growing away from the needle after branching, as seen in Figure 4.21a. As previous simulations proved, the Aδ threshold is particularly sensitive to location, seen in the spread of threshold values for Aδ in the boxplots of Figure 4.23, where a larger spread of Aδ threshold values is noticed compared to Aβ. An option to counter this is to use a single fiber design as Poulsen et al. [19] describe in their research to optimize electrode properties for increased nociceptive fiber activation. A single fiber model allows optimal Aδ placement near the needle electrode, possibly resulting in lower threshold values, however disregards the variation in fiber population found in reality [22].

5.5 Summary

Section 5.4 provided a discussion of the results from the simulations with the FE model of the needle electrode. Taken together with the discussion in Sections 5.1 and 5.2 a short summation is given.

Validation penetration depth needle:

- Preferential activation of Aδ fibers where Aβ threshold is 1.4 to 1.8 times higher when the needle tip resides in the epidermis, closely resembling what is found in literature [13, 16]
- An increasing threshold for Aδ fibers for increasing needle depth in the skin is noticed
- Early termination of Aδ resulted in (less) than a handful of nerve-endings in the dermis, where the effect on the mean threshold needs to be investigated.

Validation of the mathematical model:

- Compared to Morch et al. [1] deviating results in mean threshold of roughly a factor 7 and 12 higher for Aβ and Aδ respectively where no clear explanation was found
- Simulations with the needle electrode show preferential activation of Aδ where the results are comparable with literature [13, 16].

Concluding remark: Various methods to validate a model are possible, yet these contradictory results with respect to the validation of the mathematical model leave the question what is correct.

6 CONCLUSION AND RECOMMENDATIONS

This research aimed at validating a mathematical model of the electrocutaneous interface of the hairless skin containing Aβ and Aδ nerve fibers, with use of the article by Morch et al. [1]. Such a mathematical model would make it possible to calculate activation profiles for various electrode types to asses the effect on Aβ- and Aδ-fibers.

The model consisted of two parts, the volume-conduction model created in COMSOL Multiphysics 5.4 and the stochastic fiber model in MATLAB 2018b. While all the steps described in Morch et al. [1] were precisely followed and implemented, the results for the mean threshold of Aβ and Aδ fibers calculated in this research did not agree with the article's results. Further investigation into the model's properties revealed no specific source as to where the cause of discrepancy between mean threshold came from. Model options that were not described (in detail) in the article (e.g. model thickness, crossing of the dermo-epidermal junction of Aδ) were also explored. In addition this gave no rise to a clear answer as to why the results differed. No specific cause of differences in the mean threshold for Aβ- and Aδ-fibers could be found after extensive research. This raises the question there could still be a possible mistake in the model presented in this research, which has yet to be found, or leaving doubts about the results presented by Morch et al. [1].

The second aim of this research was to investigate whether the penetration depth of a single needle of the IES electrode constructed by the BSS-NSP group at the University of Twente has an effect on the activation of Aδ- and Aβ-fibers. The results of the simulations showed a (mean) threshold of Aδ lower than Aβ for all needle depths, suggesting selective activation of the nociceptive system with the needle electrode. As for the effect of the penetration depth of the needle, an increase in threshold for Aδ was observed with increasing needle depth.

The findings for the simulations with the needle electrode seem to coincide with literature, whereas the results of the mathematical model in comparison with Morch et al. [1] clearly differed. These contradictory results raise the question whether it can be decided that the mathematical model is valid or not. Therefore it is concluded that further investigation is required, including other validation methods.

Thus the first step recommended for future research is to contact and discuss with the researchers of the article [1] to find a possible source for the differences in outcome. Another validation step to take could be comparing the results of the simulations with the mathematical model with experimental data obtained by measuring the perception threshold on subjects.
Furthermore, FE models of various electrode types as done by Poulsen et al. [15] can be simulated, similarly a 3D model of the 5 needle IES electrode designed by the NSP-BSS group [17]. Another option is expanding the stochastic fiber model to model temperature sensitive C-fibers. Which could be useful due to the density of C-fibers being four times higher compared to Aδ [52]. And last, the already existing toolbox can be used to simulate active nerve fibers instead of passive, with the use of the model presented by Wesselink et al. [37].

Bibliography

[1] C. D. Mørch, K. Hennings, and O. K. Andersen, "Estimating nerve excitation thresholds to cutaneous electrical stimulation by finite element modeling combined with a stochastic branching nerve fiber model," *Medical & biological engineering & computing*, vol. 49, no. 4, pp. 385–395, 2011.

[2] D. Purves, *Neuroscience*. Oxford University Press, 2012. [Online]. Available: https://books.google.nl/books?id=B5YXRAAACAAJ

[3] E. M. Izhikevich, *Dynamical Systems in Neuroscience*. MIT Press, 2007.

[4] D. R. McNeal, "Analysis of a model for excitation of myelinated nerve," *IEEE Transactions on Biomedical Engineering*, no. 4, pp. 329–337, 1976.

[5] H. Breivik, E. Eisenberg, and T. O'Brien, "The individual and societal burden of chronic pain in europe: the case for strategic prioritisation and action to improve knowledge and availability of appropriate care," *BMC public health*, vol. 13, no. 1, pp. 1–14, 2013.

[6] H. E. Merskey, "Classification of chronic pain: Descriptions of chronic pain syndromes and definitions of pain terms." *Pain*, 1986.

[7] A. V. Apkarian, M. N. Baliki, and P. Y. Geha, "Towards a theory of chronic pain," *Progress in neurobiology*, vol. 87, no. 2, pp. 81–97, 2009.

[8] J. D. Loeser and R. Melzack, "Pain: an overview," *The lancet*, vol. 353, no. 9164, pp. 1607–1609, 1999.

[9] D. Fornasari, "Pain mechanisms in patients with chronic pain," *Clinical drug investigation*, vol. 32, no. 1, pp. 45–52, 2012.

[10] R.-D. Treede, J. Lorenz, and U. Baumgärtner, "Clinical usefulness of laser-evoked potentials," *Neurophysiologie Clinique/Clinical Neurophysiology*, vol. 33, no. 6, pp. 303–314, 2003.

[11] C. Perchet, M. Frot, A. Charmarty, C. Flores, S. Mazza, M. Magnin, and L. Garcia-Larrea, "Do we activate specifically somatosensory thin fibres with the concentric planar electrode? a scalp and intracranial eeg study," *Pain*, vol. 153, no. 6, pp. 1244–1252, 2012.

[12] K. S. Frahm, C. D. Mørch, W. M. Grill, N. B. Lubock, K. Hennings, and O. K. Andersen, "Activation of peripheral nerve fibers by electrical stimulation in the sole of the foot," *BMC neuroscience*, vol. 14, no. 1, p. 116, 2013.

[13] A. Mouraux, G. D. Iannetti, and L. Plaghki, "Low intensity intra-epidermal electrical stimulation can activate aδ-nociceptors selectively," *Pain*, vol. 150, no. 1, pp. 199–207, 2010.

[14] R. Hugosdottir, C. D. Mørch, O. K. Andersen, T. Helgason, and L. Arendt-Nielsen, "Preferential activation of small cutaneous fibers through small pin electrode also depends on the shape of a long duration electrical current," *BMC neuroscience*, vol. 20, no. 1, p. 48, 2019.

[15] A. H. Poulsen, J. Tigerholm, S. Meijs, O. K. Andersen, and C. D. Mørch, “Comparison of existing electrode designs for preferential activation of cutaneous nociceptors,” *Journal of Neural Engineering*, 2020.

[16] K. Inui, T. D. Tran, M. Hoshiyama, and R. Kakigi, “Preferential stimulation of aδ fibers by intra-epidermal needle electrode in humans,” *Pain*, vol. 96, no. 3, pp. 247–252, 2002.

[17] B. van den Berg and J. R. Buitenweg, “Observation of nociceptive processing: effect of intra-epidermal electric stimulus properties on detection probability and evoked potentials,” *Brain topography*, vol. 34, no. 2, pp. 139–153, 2021.

[18] J. Motogi, Y. Sugiyama, I. Laakso, A. Hirata, K. Inui, M. Tamura, and Y. Muragaki, “Why intra-epidermal electrical stimulation achieves stimulation of small fibres selectively: a simulation study,” *Physics in Medicine & Biology*, vol. 61, no. 12, p. 4479, 2016.

[19] A. H. Poulsen, J. Tigerholm, O. K. Andersen, and C. D. Mørch, “Increased preferential activation of small cutaneous nerve fibers by optimization of electrode design parameters,” *Journal of Neural Engineering*, vol. 18, no. 1, p. 016020, 2021.

[20] J. Tigerholm, A. H. Poulsen, O. K. Andersen, and C. D. Mørch, “from perception threshold to ion channels—a computational study,” *Biophysical journal*, vol. 117, no. 2, pp. 281–295, 2019.

[21] E. Marieb and K. Hoehn, *Human Anatomy & Physiology*. Pearson, 2013. [Online]. Available: https://books.google.nl/books?id=MythtQAACAAJ

[22] V. Provitera, M. Nolano, A. Pagano, G. Caporaso, A. Stancanelli, and L. Santoro, “Myelinated nerve endings in human skin,” *Muscle & Nerve: Official Journal of the American Association of Electrodiagnostic Medicine*, vol. 35, no. 6, pp. 767–775, 2007.

[23] B. Frankenhaeuser and A. Huxley, “The action potential in the myelinated nerve fibre of xenopus laevis as computed on the basis of voltage clamp data,” *The Journal of Physiology*, vol. 171, no. 2, pp. 302–315, 1964.

[24] R.-D. Treede, “Gain control mechanisms in the nociceptive system,” *Pain*, vol. 157, no. 6, pp. 1199–1204, 2016.

[25] L. Plaghki and A. Mouraux, “How do we selectively activate skin nociceptors with a high power infrared laser? physiology and biophysics of laser stimulation,” *Neurophysiologie Clinique/Clinical Neurophysiology*, vol. 33, no. 6, pp. 269–277, 2003.

[26] E. Iannilli, C. Del Gratta, J. Gerber, G. Romani, and T. Hummel, “Trigeminal activation using chemical, electrical, and mechanical stimuli,” *Pain*, vol. 139, no. 2, pp. 376–388, 2008.

[27] J. A. B. Manresa, C. D. Mørch, and O. K. Andersen, “Long-term facilitation of nociceptive withdrawal reflexes following low-frequency conditioning electrical stimulation: a new model for central sensitization in humans,” *European journal of pain*, vol. 14, no. 8, pp. 822–831, 2010.

[28] R. Hugosdottir, C. D. Mørch, C. K. Jørgensen, C. W. Nielsen, M. V. Olsen, M. J. Pedersen, and J. Tigerholm, “Altered excitability of small cutaneous nerve fibers during cooling assessed with the perception threshold tracking technique,” *BMC neuroscience*, vol. 20, no. 1, p. 47, 2019.

[29] H. Kaube, Z. Katsarava, T. Käufer, H.-C. Diener, and J. Ellrich, “A new method to increase nociception specificity of the human blink reflex,” *Clinical Neurophysiology*, vol. 111, no. 3, pp. 413–416, 2000.

[30] W. M. Grill and J. T. Mortimer, “Stimulus waveforms for selective neural stimulation,” *IEEE Engineering in Medicine and Biology Magazine*, vol. 14, no. 4, pp. 375–385, 1995.

[31] P. Steenbergen, J. R. Buitenweg, E. van der Heide, and P. H. Veltink, “Characterization of a bimodal electrocutaneous stimulation device,” in *4th European Conference of the International Federation for Medical and Biological Engineering*. Springer, 2009, pp. 230–234.

[32] P. Steenbergen, J. R. Buitenweg, J. Trojan, E. M. van der Heide, T. van den Heuvel, H. Flor, and P. H. Veltink, “A system for inducing concurrent tactile and nociceptive sensations at the same site using electrocutaneous stimulation,” *Behavior research methods*, vol. 44, no. 4, pp. 924–933, 2012.

[33] C. Support, “Understanding, and changing, the element order,” 2021, last accessed 21 september 2021. [Online]. Available: https://www.comsol.com/support/knowledgebase/1270

[34] S. Tanaka, J. Gomez-Tames, T. Wasaka, K. Inui, S. Ueno, and A. Hirata, “Electrical characterisation of aδ-fibres based on human in vivo electrostimulation threshold,” *Frontiers in neuroscience*, vol. 14, p. 1305, 2021.

[35] M. Nolano, V. Provitera, C. Crisci, A. Stancanelli, G. Wendelschafer-Crabb, W. R. Kennedy, and L. Santoro, “Quantification of myelinated endings and mechanoreceptors in human digital skin,” *Annals of neurology*, vol. 54, no. 2, pp. 197–205, 2003.

[36] A. L. Hodgkin and A. F. Huxley, “A quantitative description of membrane current and its application to conduction and excitation in nerve,” *The Journal of physiology*, vol. 117, no. 4, pp. 500–544, 1952.

[37] W. Wesselink, J. Holsheimer, and H. Boom, “A model of the electrical behaviour of myelinated sensory nerve fibres based on human data,” *Medical & biological engineering & computing*, vol. 37, no. 2, pp. 228–235, 1999.

[38] B. D. Fornage, M. H. McGavran, M. Duvic, and C. A. Waldron, “Imaging of the skin with 20-mhz us.” *Radiology*, vol. 189, no. 1, pp. 69–76, 1993.

[39] S. Gabriel, R. Lau, and C. Gabriel, “The dielectric properties of biological tissues: Ii. measurements in the frequency range 10 hz to 20 ghz,” *Physics in medicine & biology*, vol. 41, no. 11, p. 2251, 1996.

[40] C. Gabriel, S. Gabriel, and y. E. Corthout, “The dielectric properties of biological tissues: I. literature survey,” *Physics in medicine & biology*, vol. 41, no. 11, p. 2231, 1996.

[41] C. Gabriel, A. Peyman, and E. H. Grant, “Electrical conductivity of tissue at frequencies below 1 mhz,” *Physics in medicine & biology*, vol. 54, no. 16, p. 4863, 2009.

[42] P. Krackowizer and E. Brenner, “Thickness of the human skin,” *Phlebologie*, vol. 37, no. 02, pp. 83–92, 2008.

[43] S. Neerken, G. W. Lucassen, M. A. Bisschop, E. Lenderink, and T. A. Nuijs, “Characterization of age-related effects in human skin: A comparative study that applies confocal laser scanning microscopy and optical coherence tomography,” *Journal of biomedical optics*, vol. 9, no. 2, pp. 274–281, 2004.

[44] J. Sandby-Moller, T. Poulsen, and H. C. Wulf, “Epidermal thickness at different body sites: relationship to age, gender, pigmentation, blood content, skin type and smoking habits,” *Acta Dermato Venereologica*, vol. 83, no. 6, pp. 410–413, 2003.

[45] A. Tavernier, M. Dierickx, and M. Hinsenkamp, “Tensors of dielectric permittivity and conductivity of in vitro human dermis and epidermis,” *Bioelectrochemistry and bioenergetics*, vol. 30, pp. 65–72, 1993.

[46] T. Yamamoto and Y. Yamamoto, “Electrical properties of the epidermal stratum corneum,” *Medical and biological engineering*, vol. 14, no. 2, pp. 151–158, 1976.

[47] G. J. Ebenezer, P. Hauer, C. Gibbons, J. C. McArthur, and M. Polydefkis, “Assessment of epidermal nerve fibers: a new diagnostic and predictive tool for peripheral neuropathies,” *Journal of Neuropathology & Experimental Neurology*, vol. 66, no. 12, pp. 1059–1073, 2007.

[48] A. Iggo and K. Andres, “Morphology of cutaneous receptors,” *Annual review of neuroscience*, vol. 5, no. 1, pp. 1–31, 1982.

[49] D. Reilly, D. Ferdinando, C. Johnston, C. Shaw, K. Buchanan, and M. Green, “The epidermal nerve fibre network: characterization of nerve fibres in human skin by confocal microscopy and assessment of racial variations,” *British Journal of Dermatology*, vol. 137, no. 2, pp. 163–170, 1997.

[50] L. F. Shampine and M. W. Reichelt, “The matlab ode suite,” *SIAM journal on scientific computing*, vol. 18, no. 1, pp. 1–22, 1997.

[51] F. Rattay, “Analysis of models for external stimulation of axons,” *IEEE transactions on biomedical engineering*, no. 10, pp. 974–977, 1986.

[52] J. Ochoa and W. Mair, “The normal sural nerve in man,” *Acta neuropathologica*, vol. 13, no. 3, pp. 217–239, 1969.

A COMSOL MODELS

A.1 FE Model Details

A.1.1 Mesh properties for the Convergence Studies

Mesh properties	"Fine" Setting	"Extra Fine" Setting	"Extremely Fine" Setting	Poulsen2020	Present model
Max. Element Size [mm]	2.65	1	0.5	1.5	{0.04, 0.01, 0.04, 0.1}
Min. Element Size [mm]	0.015	3.75e-3	1e-3	1e-3	1e-4
Max. Element Growth Rate	1.3	1.2	1.1	1.1	1.1
Curvature Factor	0.3	0.25	0.2	0.2	0.2
Resolution of Narrow Regions	1	1	1	1	1

Figure A.1: Mesh Element Size Parameters. Mesh is built for each individual skin layer.

A.2 Potential field

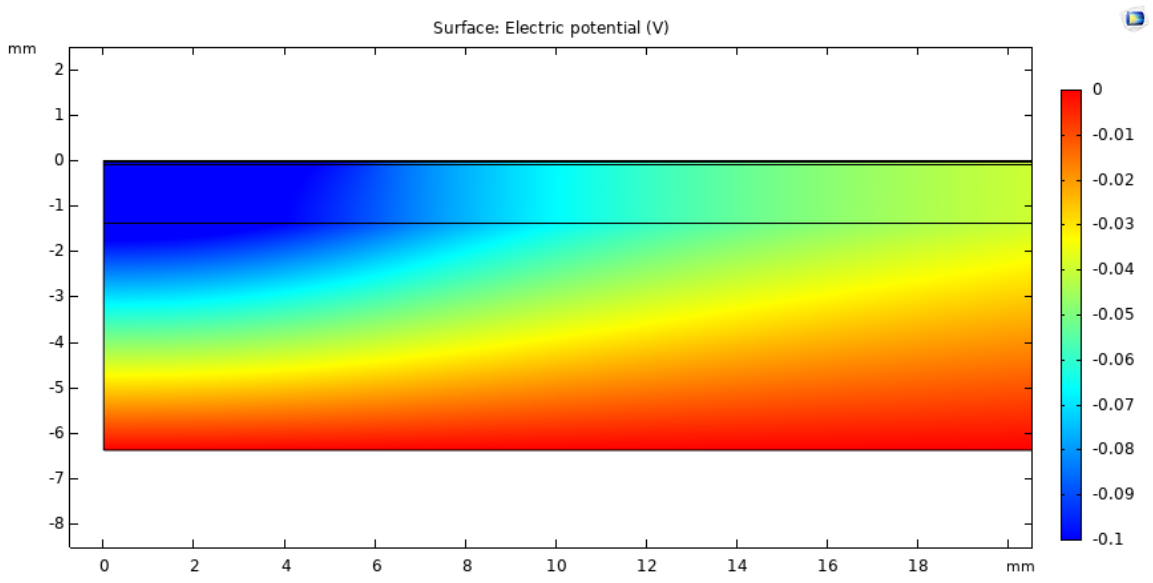

Figure A.2: Potential field in [V] generated by the COMSOL model with a cathode of 12 mm in diameter

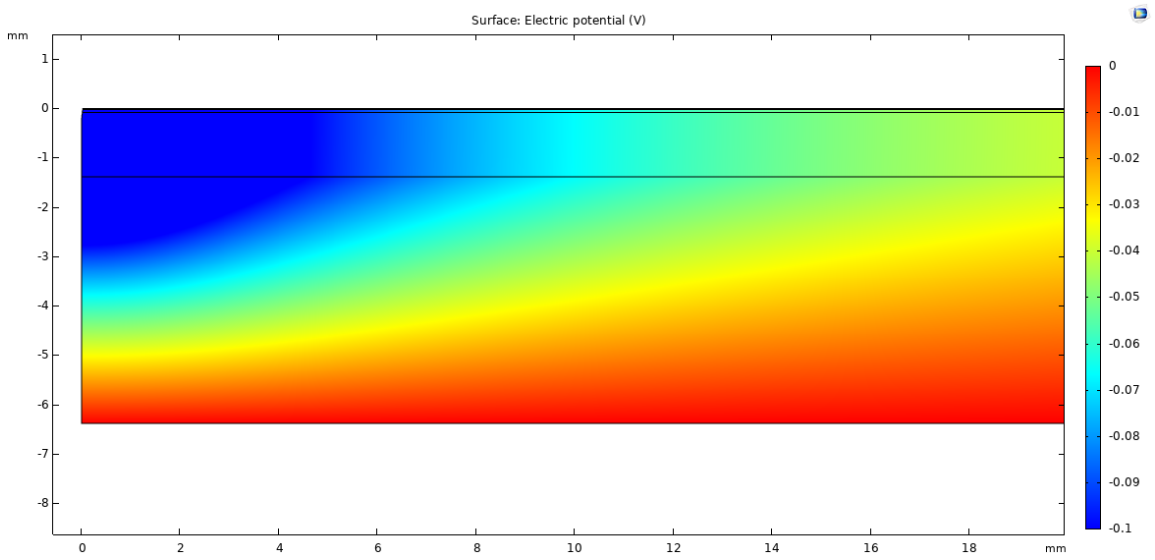

Figure A.3: Potential field in [V] generated by the COMSOL model of an IES electrode with a single needle with $d_{n,max} = 0.2\,mm$

A.3 Electrical Potential

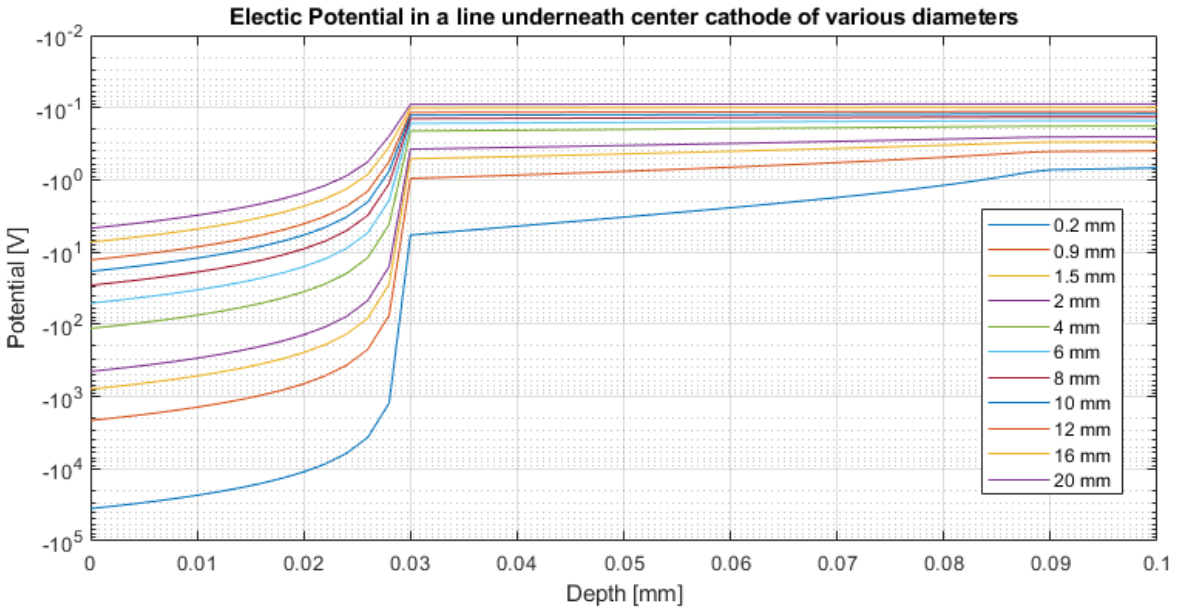

Figure A.4: Electrical Potential [V] in a straight line underneath the center of the cathode for various electrode diameters. The transition from the stratum corneum to epidermis at a depth of 0.029 mm is clearly visible

B SIMULATIONS

B.1 Membrane Potential and Current

B.1.1 A-Delta

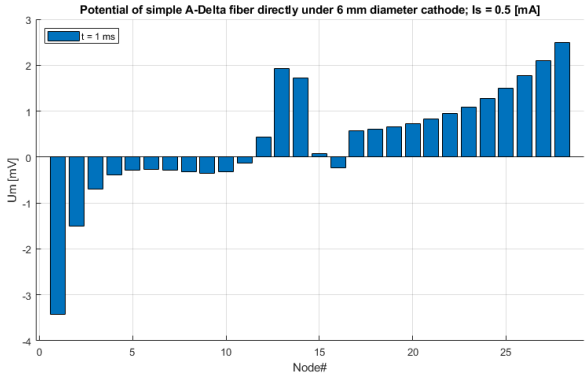

(a) U_m at $t = 1\,ms$

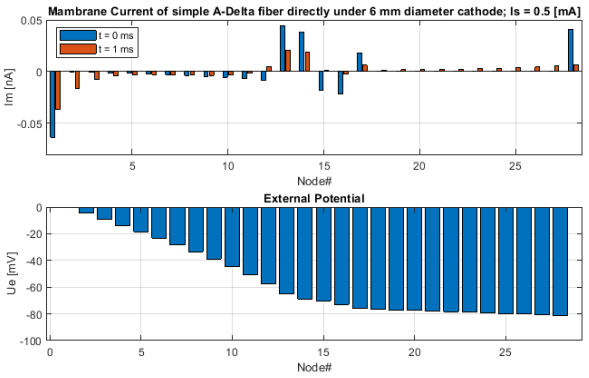

(b) I_m and U_e

Figure B.1: Simple Aδ directly under center of 6 mm electrode ($r = 0\,mm$); Stimulation current of 0.5 mA

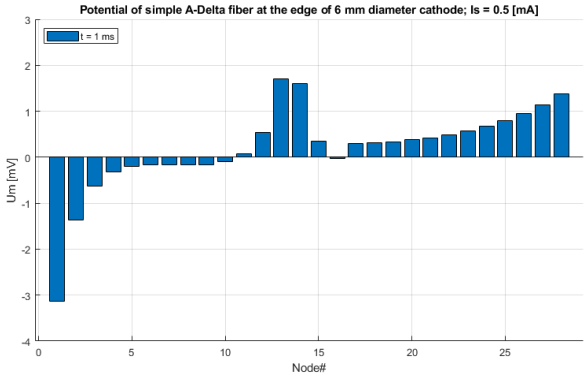

(a) U_m at $t = 1\,ms$

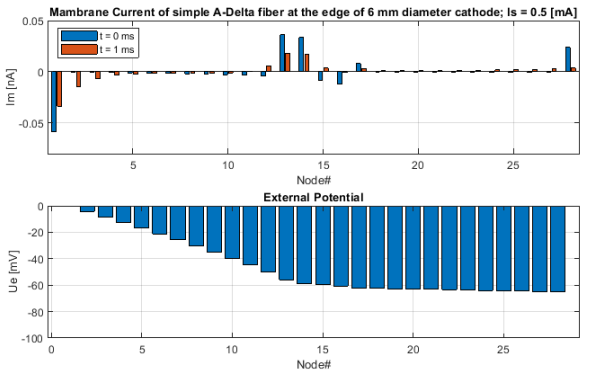

(b) I_m and U_e

Figure B.2: Simple Aδ at the edge of 6 mm electrode ($r = 3\,mm$); Stimulation current of 0.5 mA

B.1.2 A-Beta

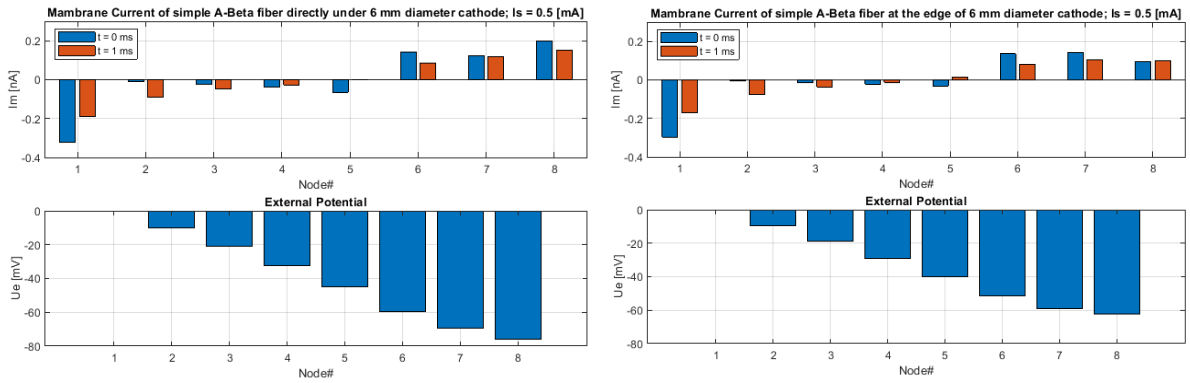

(a) Center (b) Edge

Figure B.3: I_m and U_e for simple Aβ directly under center of 6 mm electrode ($r = 0\,mm$) and at the edge ($r = 3\,mm$); Stimulation current of 0.5 mA

B.2 Mean Threshold

B.2.1 Pulse Width

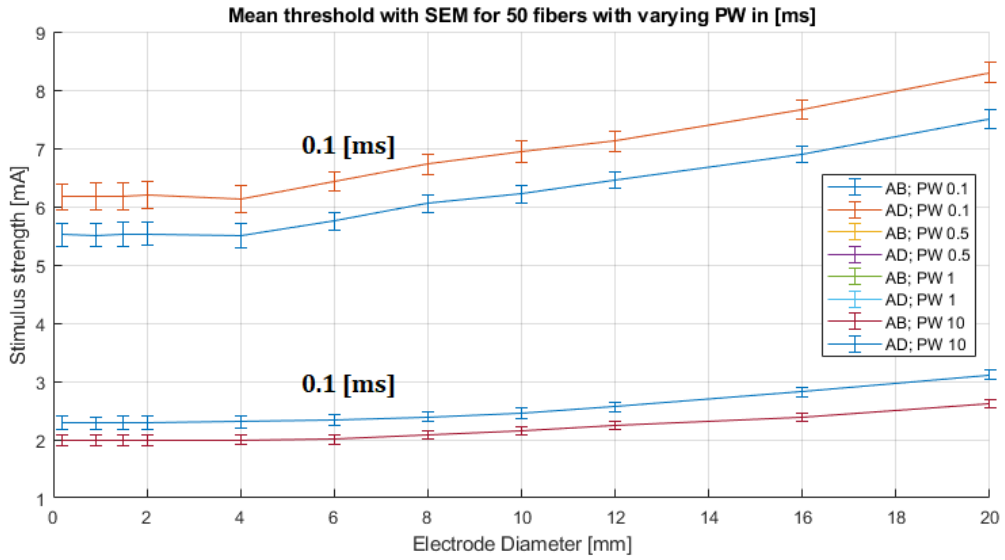

Figure B.4: Mean threshold with SEM of same population of 50 fibers with varying pulse width of the stimulus. Aβ and Aδ show a higher mean threshold for a PW of 0.1 ms compared to the other pulse widths. The same mean threshold is seen for the duration of 0.5, 1 and 10 ms

B.2.2 Stratum Corneum Thickness

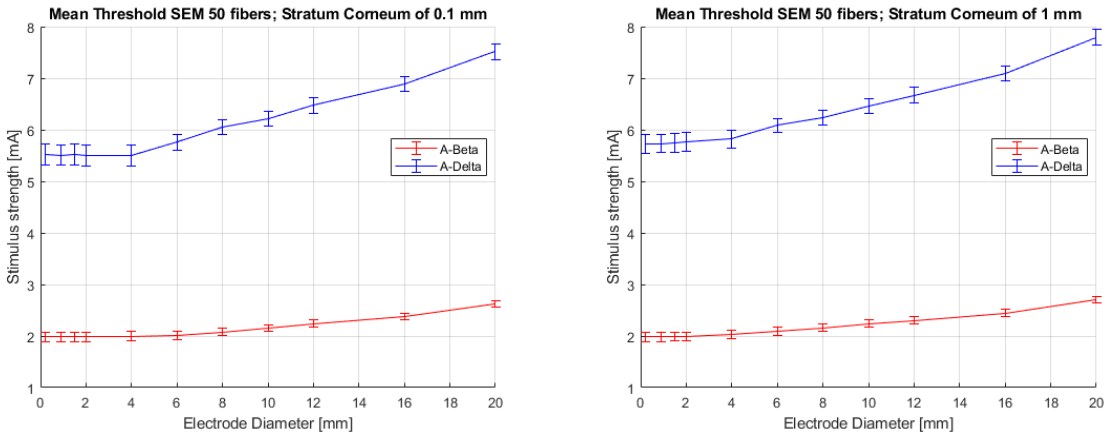

(a) SC = 0.1 mm (b) SC = 1.0 mm

Figure B.5: Mean threshold with SEM for a population of 50 Aβ and 50 Aδ fibers with a stratum corneum thickness of 0.1 mm and 1.0 mm. The mean threshold of Aβ seems to remain the same whereas the mean threshold of Aδ becomes slightly higher (factor 1.05) for larger SC thickness

B.3 Origin and Termination Points Fibers

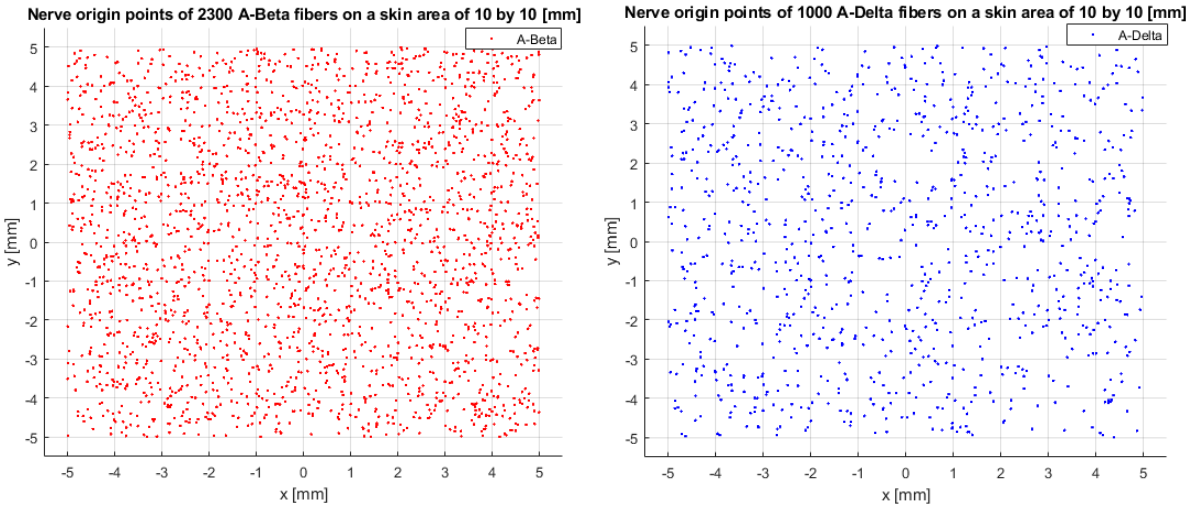

(a) Aβ (b) Aδ

Figure B.6: Origin xy-coordinates of 2300 Aβ (red) and 1000 Aδ (blue) fibers. The fibers appear uniformly distributed over a skin area of $100\ mm^2$

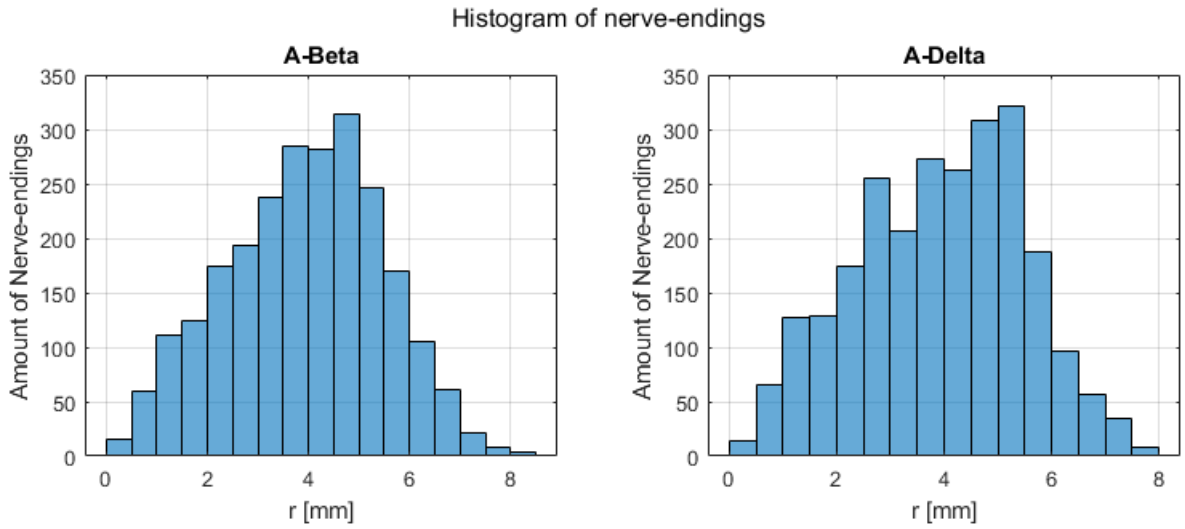

Figure B.7: Histograms of the r-coordinates of the nerve-endings from 2300 Aβ and 1000 Aδ fibers. A normal distribution with a negative skewness is observed

B.4 Boxplots

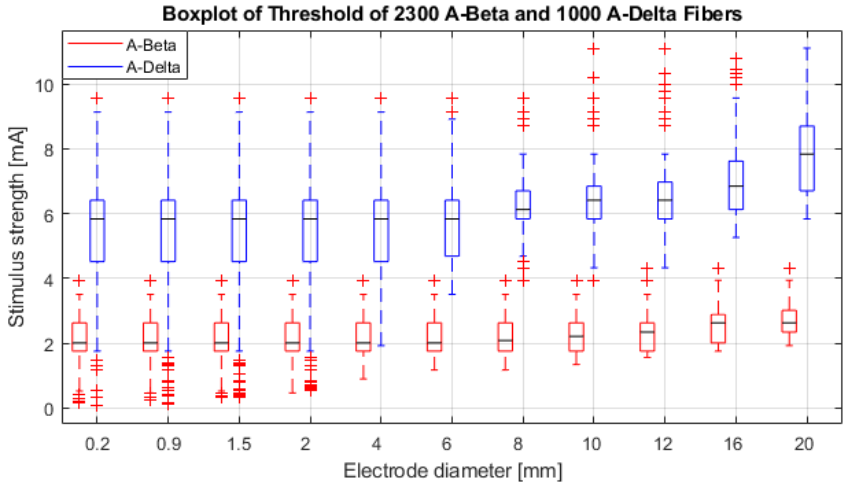

Figure B.8: Boxplot of the threshold of 2300 Aβ (red) and 1000 Aδ (blue) fibers for various electrode diameters

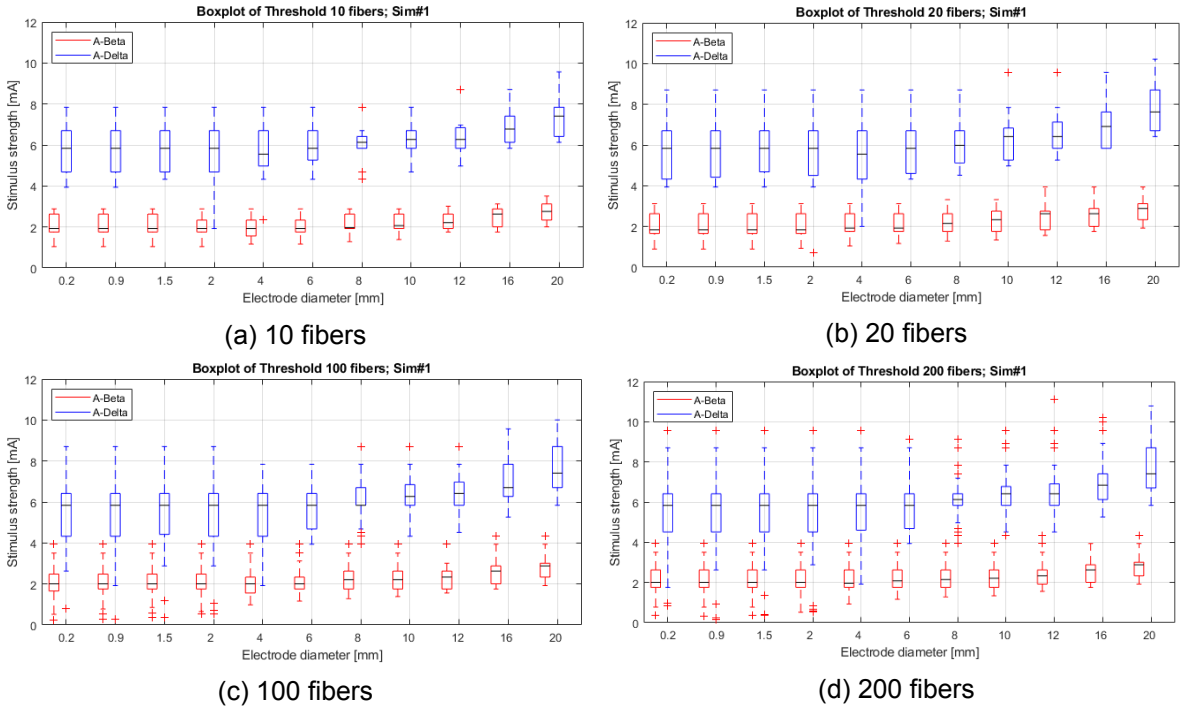

(a) 10 fibers (b) 20 fibers

(c) 100 fibers (d) 200 fibers

Figure B.9: Boxplots of the threshold of Aβ (red) and Aδ (blue) fibers for various electrode diameters, with populations of 10, 20, 100 and 200

B.5 Erroneous Values

B.5.1 Membrane capacitance and conductance

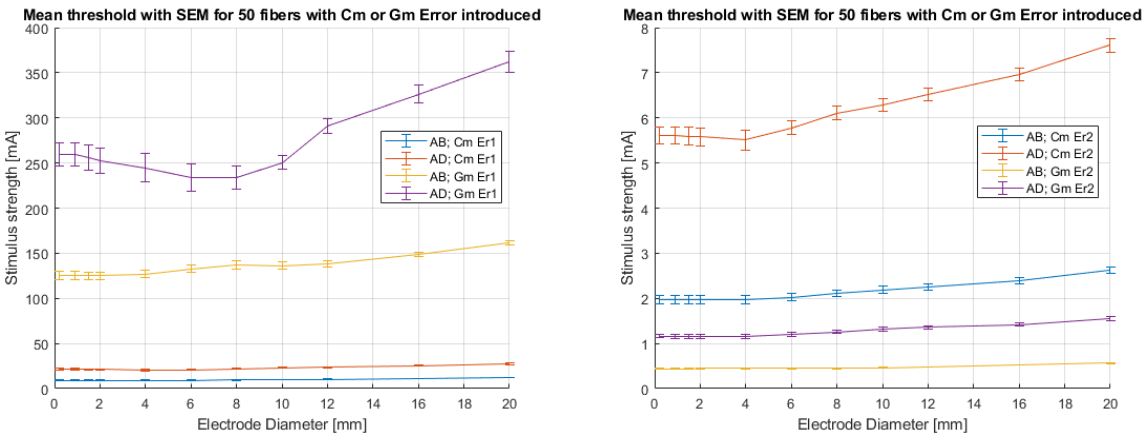

(a) Error 1 $c_m = 2e-4\ F/cm^2$ and $g_m = 30.4e-1\ S/cm^2$

(b) Error 2 $c_m = 2e-8\ F/cm^2$ and $g_m = 30.4e-5\ S/cm^2$

Figure B.10: Mean threshold with SEM for a population of 50 Aβ and 50 Aδ fibers with an error introduced in membrane capacitance per unit area ($c_m = 2e-6\ F/cm^2$) and membrane conductance per unit area ($g_m = 30.4e-3\ S/cm^2$). Increasing the membrane capacitance and conductance by a factor 100 results in higher threshold values seen in (a). Decreasing these values by a factor 1/100 results in lower threshold values as seen in (b)